



RETURNING MATERIALS:
Place in book drop to
remove this checkout from
your record. FINES will
be charged if book is
returned after the date
stamped below.

MSU LIBRARIES

RETURN USE ONLY

THE EFFECT OF INHOMOGENEOUS INFLATION OF A SUBLOBAR
LUNG SEGMENT ON COLLATERAL CHANNEL RESISTANCE

By

Steven Douglas Fuller

AN ABSTRACT OF A DISSERTATION

Submitted to
Michigan State University
in partial fulfillment of the requirements
for the degree of

DOCTOR OF PHILOSOPHY

Department of Physiology

1984

ABSTRACT

THE EFFECT OF INHOMOGENEOUS INFLATION OF A SUBLOBAR LUNG SEGMENT ON COLLATERAL CHANNEL RESISTANCE

By

Steven Douglas Fuller

Inhomogeneous inflation of a sublobar lung segment occurs when the segment is inflated to a different distending pressure than the remainder of the lobe. The effect of inhomogeneity on collateral channel resistance (R_{coll}) was studied in left cranial, left caudal, and right caudal lobes of excised dogs' lungs. A double lumen catheter was advanced through the trachea and wedged in a small bronchus supplying a sublobar segment. Helium (He), air, or sulfurhexafluoride (SF_6) flowed into the outer lumen of the catheter (\dot{V}_{coll}) while segment pressure (P_{ct}) was measured at the tip of the inner lumen. Transpulmonary pressure (P_{ao}) was measured either at the trachea or lobar bronchus as the lobe was inflated with air. At constant P_{ao} , raising \dot{V}_{coll} inflated the segment by increasing $P_{ct}-P_{ao}$, thereby creating inhomogeneity. Collateral channel resistance was calculated as $R_{coll} = (P_{ct}-P_{ao})/\dot{V}_{coll}$. Lobar inflation (i.e., raising P_{ao} at constant $P_{ct}-P_{ao}$) decreased R_{coll} . In contrast, segment inflation (i.e., raising $P_{ct}-P_{ao}$ at constant P_{ao}) increased R_{coll} . Similar results occurred in the lungs of closed chest anesthetized dogs. In excised lungs, the increase in R_{coll} during segment inflation was accentuated when the segment gas flow regime was turbulent and

eliminated when the flow regime was laminar. The fact that R_{coll} failed to decrease during segment inflation, even when flow was laminar, suggests that segment inflation and lobar inflation may have different effects on segment airway geometry. In additional studies designed to determine the arrangement of airways in the segment-lobar interface, corrosion casts of excised dogs' lungs showed that the interface contains bronchi coursing within and parallel to the interface and providing branches to both the segment and lobe. Also, examination of casts of parenchymal tissue from the interface revealed interdigitation of segment and lobar acini. This airway arrangement suggests three possible routes followed by gas flowing out of an obstructed segment, and each route is likely influenced by tissue distortion at the segment-lobar interface occurring during measurements of R_{coll} . Further studies in excised dogs' lungs suggests that most of the gas leaving a segment enters the bronchi in the interface and flows directly out of the lobe without entering the remainder of the lobe.

ACKNOWLEDGMENTS

A most significant and special person in my life during the past eight years has been Dr. Norman Edward Robinson. As my major advisor, he has successfully guided me through M.S. and Ph.D. degrees and has thus played a critical role in my formative academic years. He uniquely blends discipline, intellect, and compassion which allows him to consistently demonstrate academic and research excellence as well as kindness and understanding. He demands high performance but is always supportive and caring during times of frustration and disappointment. It is my hope to emulate these and his many other positive qualities, and I look forward to an enduring friendship and frequent reunions.

I also express my gratitude to Dr. S. Richard Heisey whose thorough critique of this dissertation resulted in its significant improvement. We have also shared a friendship these past eight years which has been very meaningful to me, and I'll miss our long conversations and his frequent attempts at humor. To this day, I still feel just a little guilty for what I did to him on the racquetball court!

The other members of my guidance committee--Dr. Jack Hoffert, Dr. John Chimosky, and Dr. Robert Echt--have also had important duties in guiding my academic progress and critiquing this dissertation. To them, I extend my sincere appreciation, and I wish them well in all future endeavors.

Last, but not at all least, is Roberta Milar who has aided me, directly and indirectly, in every experiment I have ever performed during my graduate school career. For me she has been technician extraordinaire, graphic artist, occasional taxi, and always an understanding and loyal friend. I will miss her greatly.

TABLE OF CONTENTS

	Page
LIST OF TABLES	vi
LIST OF FIGURES	vii
LIST OF ABBREVIATIONS	xi
LIST OF DEFINITIONS	xii
 CHAPTER	
I. GENERAL INTRODUCTION AND LITERATURE REVIEW	1
General Introduction	1
Introduction to Literature Review	6
Anatomy of Collateral Pathways	9
Interalveolar Pores	9
Bronchiolealveolar Canals	12
Interbronchiolar Respiratory Bronchioles	13
Interacinar Ducts	14
Methods Used to Study Collateral Ventilation	15
Pressure-Flow Relationships	24
Basic Concepts of Fluid Mechanics	24
Pressure-Flow Relationships in a Branched System	30
Problems of analysis	30
Rohrer's equation	32
Modification of Rohrer's equations	33
Moody diagram	36
Pressure-Flow Relationships in a Sublobar Lung Segment	40
Segment-Lobar Inhomogeneity	41
Purpose of the Present Studies	43
List of References	45
II. THE EFFECT OF REGIONAL INHOMOGENEITY ON COLLATERAL AIRWAY RESISTANCE	52
Introduction	52
Methods	54
Results	59

CHAPTER	Page
Discussion	73
List of References	81
III. MECHANISM OF INCREASED COLLATERAL AIRWAY RESISTANCE DURING NONHOMOGENEOUS SEGMENT INFLATION	83
Introduction	83
Methods	84
Results	91
Discussion	99
List of References	116
IV. PATHWAYS CONNECTING OBSTRUCTED AND NONOBSTRUCTED SUBLOBAR REGIONS IN THE DOG LUNG	118
Introduction	118
Methods	119
Series One	119
Series Two	120
Series Three: Distribution of Gas Leaving an Obstructed Segment	121
Results	125
Series One	125
Series Two	128
Series Three: Distribution of Gas Leaving an Obstructed Segment	133
Discussion	139
List of References	145
V. DISCUSSION AND SUMMARY	146
List of References	151
VI. CONCLUSIONS	152
APPENDICES	
A. MEAN (\pm SEM) VALUES OF COLLATERAL RESISTANCE FOR CHAPTER II DATA	155
B. RELATIONSHIP OF SEGMENT AIRWAY DIAMETER TO LOBAR VOLUME DURING LOBAR INFLATION FOR CHAPTER III DATA	158

LIST OF TABLES

Table	Page
1-1. Synopsis of literature describing anatomy of collateral channels	16
2-1. Protocols for series one, series two, and series three experiments	58
2-2. Values of Reynolds' number (Re) for each series of experiments	75
3-1. Physical properties of gases [helium (He), air, and sulfurhexafluoride (SF_6)] used in calculation of collateral resistance	89
3-2. Intrasegmental airway resistance (R_s) expressed as a fraction of collateral resistance (R_{coll}) (R_s/R_{coll} , $\bar{x} \pm SEM$) as the segment was inflated to a segment-lobar pressure difference ($P_{ct}-P_{ao}$) = 1-7 cm H_2O at transpulmonary pressure (P_{ao}) = 2-6 cm H_2O in the left caudal lobes of excised dogs' lungs	96
A-1. Data points used in Figures 2-1, 2-2, and 2-3 in Chapter II showing collateral resistance [R_{coll} ; cm H_2O /(ml/sec); $\bar{x} \pm SEM$] in left cranial and right caudal lobes in series one (excised lungs with the segment inflated relative to the lobe), series two (lungs of closed chest anesthetized dogs), and series three (excised lungs with the segment deflated relative to the lobe)	155
B-1. Relationship of segment airway diameter to lobar volume when the curves in each panel of Figure 3-5 are forced to approximate a single curve	164

LIST OF FIGURES

Figure	Page
1-1. Photograph of excised lung showing inhomogeneously inflated sublobar segment (i.e., a segment which is inflated to a relatively greater volume than the remaining lobe) at extreme left	3
1-2. Scanning electron micrograph of a portion of the segment-lobar interface from an excised left caudal lobe of dog lung.	5
1-3. Schematic diagram illustrating three different types of collateral channels (interbronchiolar respiratory bronchiole, bronchiole-alveolar canal, and inter-alveolar pore) connecting two adjacent sublobar lung segments	11
1-4. Schematic diagram illustrating Hilpert's technique (22) for calculating collateral channel resistance (R_{coll})	20
1-5. Pressure-flow characteristics in a straight smooth circular tube	27
1-6. Schematic illustration of Moody diagram where the logarithm of the normalized pressure drop ($\text{Log } P_n$; ordinate) is plotted against the logarithm of Reynold's number ($\text{Log } Re$; abscissa)	38
2-1A. Effect of transpulmonary pressure (P_{ao} ; $\text{cm H}_2\text{O}$); abscissa) on collateral resistance [R_{coll} ; $\text{cm H}_2\text{O}/(\text{ml}/\text{sec})$; ordinate] in left cranial lobes (left panel) and right caudal lobes (right panel) at different levels of segment pressure (P_{ct} ; $\text{cm H}_2\text{O}$) in five excised dogs' lungs ventilated with air	61
2-1B. Same data as in Figure 2-1A showing effect of segment-lobar pressure difference ($P_{ct}-P_{ao}$; $\text{cm H}_2\text{O}$; abscissa) on collateral resistance [R_{coll} ; $\text{cm H}_2\text{O}/(\text{ml}/\text{sec})$; ordinate] at different values of transpulmonary pressure (p_{ao} ; $\text{cm H}_2\text{O}$) in five excised dogs' lungs.	63

Figure	Page
2-2A. Effect of transpulmonary pressure (P_{tp} ; cm H_2O ; abscissa) on collateral resistance [R_{coll} ; cm H_2O /(ml/sec); ordinate] in seven left cranial lobes (left panel) and six right caudal lobes (right panel) at different levels of segment pressure (P_{ct} ; cm H_2O) in lungs from closed chest dogs ventilated with air . . .	66
2-2B. Same data as Figure 2-2A showing effect of segment-lobar pressure difference ($P_{ct}-P_{ao}$; cm H_2O ; abscissa) on collateral resistance [R_{coll} ; cm H_2O /(ml/sec); ordinate] at different values of transpulmonary pressure (P_{tp} ; cm H_2O) in lungs from closed chest dogs	68
2-3A. Effect of transpulmonary pressure (P_{ao} ; cm H_2O ; abscissa) on collateral resistance [R_{coll} ; cm H_2O /(ml/sec); ordinate] in five left cranial lobes (left panel) and six right caudal lobes (right panel) at different levels of segment pressure (P_{ct} ; cm H_2O) when the segment was deflated relative to the lobe in excised dogs' lungs ventilated with air	70
2-3B. Same data as in Figure 2-3A showing effect of segment-lobar pressure difference ($P_{ao}-P_{ct}$; cm H_2O ; abscissa) on collateral resistance [R_{coll} ; cm H_2O /(ml/sec); ordinate] at different values of transpulmonary pressure (P_{ao} ; cm H_2O) in excised dogs' lungs when the segment was deflated relative to the lobe	72
3-1. Illustration of left caudal lobe from an excised dog lung showing double lumen catheter wedged in a bronchus supplying a sublobar segment	87
3-2. Effect of segment inflation by raising the segment-lobar pressure gradient ($P_{ct}-P_{ao}$; cm H_2O ; abscissa) on total collateral resistance [R_{coll} ; cm H_2O /(ml/sec); ordinate], top panel; intrasegmental airway resistance [R_s ; cm H_2O /(ml/sec); ordinate], middle panel, and intersegmental airway resistance [R_i ; cm H_2O /(ml/sec), ordinate], bottom panel, at five transpulmonary pressures ($P_{ao} = 2-6$ cm H_2O)	93
3-3. Same data as Figure 3-2 showing the effect of transpulmonary pressure (P_{ao} ; cm H_2O ; abscissa) on total collateral resistance [R_{coll} ; cm H_2O /(ml/sec), ordinate], top panel; intrasegmental airway resistance [R_s ; cm H_2O /(ml/sec), ordinate], middle panel; and	

Figure	Page
intersegmental airway resistance [R_i ; cm H ₂ O/ (ml/sec), ordinate], bottom panel; as the segment- lobar pressure gradient was held constant at seven values ($P_{ct}-P_{ao} = 1-7$ cm H ₂ O)	95
3-4. The logarithm of the normalized pressure drop (Log P _n ; ordinate) is shown as a function of the logarithm of Reynolds' number (Log Re; abscissa) and is referred to as a Moody diagram (Figure 1-6)	98
3-5. The logarithm of the normalized pressure drop (Log P _n ; ordinate) is shown as a function of the logarithm of Reynolds' number (Log Re; abscissa) and is referred to as a Moody diagram (Figure 1-6)	101
3-6. Effect of scaling segment airway diameter to cube root of lobar volume on data in the Moody diagrams illustrated in Figure 3-5	109
3-7. Effect of scaling segment airway diameter to transpulmonary pressure (P _{ao}) on data in the Moody diagrams illustrated in Figure 3-5	111
3-8. Comparison of the effect of raising lobar volume [plotted as percent vital capacity (VC); abscissa] on the following five resistances (cm H ₂ O/LPS, where LPS = liters per second): homogeneous collateral resistance [R_{coll} (homogeneous) obtained by extrap- olating the curves at each P _{ao} in the center panel of Figure 3-2 to the ordinate]; total lung resistance (R_L) and central (R_c) and peripheral (R_p) airway resistance in vagally intact dogs as reported by Macklem and Mead (5); and R_L in vagotomized dogs as reported by Macklem et al. (6)	115
4-1. Schematic diagram of excised left caudal lobe suspended by lobar bronchus in an airtight box	123
4-2. Corrosion cast of individual bronchopulmonary segment (Figure 4-2A; red) and subsegmental segment (Figure 4-2B; white)	127
4-3A. Corrosion cast of three adjacent subsegmental segments	130

Figure	Page
4-3B. The large arrow points to a large airway, which I term "interface" airway, coursing within and parallel to the red-blue interface and which provides branches into both red and blue segments	130
4-4A. Corrosion cast of three adjacent bronchopulmonary segments	132
4-4B. At the extreme left a blue nonrespiratory bronchiole branches into a blue respiratory bronchiole which further divides into red and blue respiratory bronchioles	132
4-4C. A portion of the interface from another corrosion cast	132
4-4D. A different view of the same specimen from Figure 4-4C	132
4-5. Distribution of outflow of gas leaving an obstructed bronchopulmonary segment (as a percent of total inflow volume, \bar{x} with SEM bars) as a function of inflow segment, inflow rate (low = 1 liter/minute, high = 2 liters/minute), and transpulmonary pressure (Ptp; cm H ₂ O) in six excised left caudal lobes	135
4-6. Model illustrating possible course of resin or gas flow through an obstructed segment and interface airway	140
B-1. Attempt to forcibly approximate the curves in each panel of Figure 3-5 into a single smooth curve	161
B-2. Attempt to forcibly approximate the curves in each panel of Figure 3-5 into a single smooth curve	163

LIST OF ABBREVIATIONS

He	Helium.
ρ	Gas density (gm/ml).
Pao	Pressure (cm H ₂ O) at airway opening of the trachea or lobar bronchus, equivalent to transpulmonary pressure in the excised lungs of Chapters II and III.
Pct	Pressure (cm H ₂ O) in an obstructed segment measured at the tip of the wedged catheter or bronchoscope.
Pn	Normalized pressure drop; i.e., the ratio of the static pressure drop to dynamic pressure.
Ppl	Intrapleural pressure (cm H ₂ O).
Ps	Pressure (cm H ₂ O) in the segment subpleural alveoli in excised lungs.
Ptp	Transpulmonary pressure (cm H ₂ O) in the lungs of closed chest anesthetized dogs (Chapter II). In Chapter IV, in which measurements were taken in excised lungs suspended in an airtight box, Ptp represents the difference between box pressure and atmospheric pressure.
Rcoll	Collateral channel resistance [cm H ₂ O/(ml/sec)] (equation 1-1).
Re	Reynolds' number (equation 1-11).
Ri	Airflow resistance [cm H ₂ O/(ml/sec)] in airways between the segment subpleural alveoli and the airway opening.
Rs	Airflow resistance [cm H ₂ O/(ml/sec)] in airways between the tip of the wedged catheter and the segment subpleural alveoli.
SF ₆	Sulfurhexafluoride.
μ	Gas viscosity [gm/(sec · cm)].
\dot{V} coll	Flow (ml/sec) of gas through the wedged catheter and into the obstructed segment.

LIST OF DEFINITIONS

Acinus All the respiratory bronchioles, alveolar ducts, and alveoli distal to a terminal bronchiole.

Airways Refers to the series of bronchi and bronchioles leading from the trachea to the alveolar ducts.

Collateral Channel A pathway connecting acini originating from two different airways.

Flow Regime The predominant pattern of flow in a system (i.e., whether flow is laminar, transitional, or turbulent).

Laminar Flow Fluid flow having the following characteristics: (1) flow in all parts of the stream is constant and occurs in parallel laminae which slide over one another; (2) the profile of the leading edge of flow is parabolic, the axial velocity of flow being twice as fast as the average velocity.

Transitional Flow Fluid flow having characteristics of both laminar and turbulent flow.

Turbulent Flow Fluid flow having the following characteristics: (1) the velocity of flow at any point in the stream fluctuates vigorously and randomly in both magnitude and direction; (2) the profile of the leading edge of flow is only slightly curved, the axial velocity of flow being 1.2 times the average velocity.

CHAPTER I

GENERAL INTRODUCTION AND LITERATURE REVIEW

General Introduction

Inhomogeneous inflation of a sublobar lung segment occurs when the segment is inflated to a relatively different distending pressure than the remainder of the lobe. Inhomogeneity may be created by flowing gas into a sublobar segment through a catheter obstructing the bronchus supplying the segment (Figure 1-1). The incoming gas inflates the segment to a relatively greater volume than the lobe, then exits the segment via collateral channels to flow out of the lobe.

Inhomogeneity creates an area of tissue distortion at the segment-lobar parenchymal interface. This is demonstrated in Figure 1-2 which shows a scanning electron micrograph of a section of the interface from an inhomogeneously inflated air-dried left caudal lobe of dog lung. Parenchyma from the relatively inflated segment is on the right of the figure, and parenchyma from the relatively deflated lobe is on the left. The interface is observed as a thin line of distorted, compressed parenchymal tissue in the center of the figure.

Collateral channels serving as connections between the segment and the lobe may also be distorted during inhomogeneity, for they not only pass through the zone of parenchymal tissue distortion at the interface but they also are subjected to abrupt changes in distending pressure as they pass from the segment to the lobe. Distortion of

Figure 1-1. Photograph of excised lung showing inhomogeneously inflated sublobar segment (i.e., a segment which is inflated to a relatively greater volume than the remaining lobe) at extreme left.

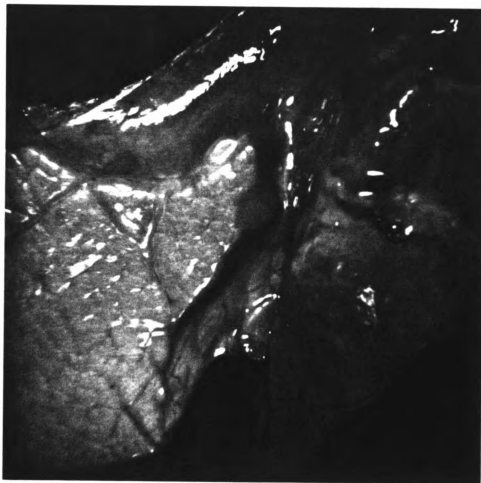


Figure 1-1

Figure 1-2. Scanning electron micrograph of a portion of the segment-lobe interface from an excised left caudal lobe of dog lung. The lobe was air-dried as the segment was inflated inhomogeneously within the lobe (i.e., the segment was inflated to a relatively greater volume than the lobe). Segment tissue is on the right, lobar tissue is on the left. The solid bar (bottom of figure) is a scale representing 1000.0 μm .

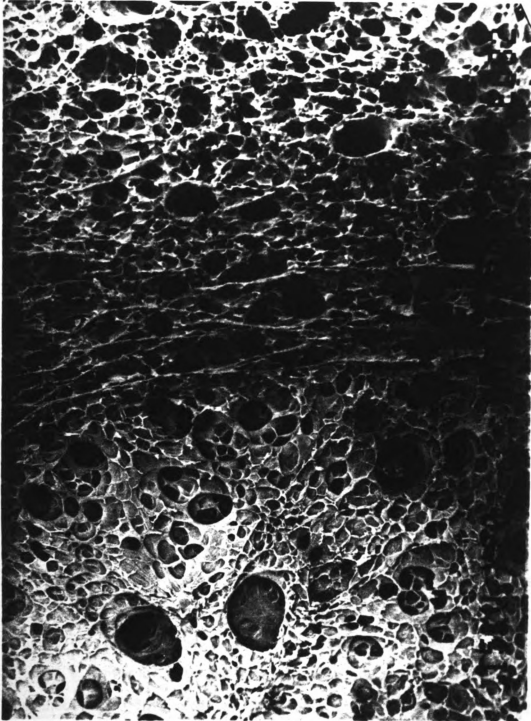


Figure 1-2

collateral channels should affect collateral airflow resistance (R_{coll}), but there are few reports describing the effect of inhomogeneity is reported to increase R_{coll} , decrease R_{coll} , or have no effect on R_{coll} . In addition, these studies used several methods to measure R_{coll} in three animal species, and measurements were made over a restricted range of inhomogeneities. Thus, these studies are difficult to compare.

The major purpose of this dissertation is to provide a systematic examination of the effect of inhomogeneity on R_{coll} . Chapter II documents the effect, and two hypotheses are proposed to explain the mechanism. Chapter III reports testing of the hypotheses. In Chapter IV, the arrangement of the airways in the segment-lobar interface is determined, so that the function of the airways discussed in Chapters II and III may be correlated with anatomy. Chapter I describes the known anatomy of the collateral channels, discusses the various methods used to measure R_{coll} , and provides background information needed to appreciate the hypotheses proposed in Chapter II and tested in Chapter III.

Introduction to Literature Review

The tracheobronchial tree is an irregularly dichotomous branching system of airways, beginning at the trachea, branching into the bronchi, bronchioles, and alveolar ducts, and terminating in the alveolar sacs and alveoli. Prior to 1930 these airways were considered to be a series of dead-end tubes because there were no known interconnections. This model of the lung explained the common clinical observation that obstruction of a lobar bronchus produced atelectasis,

because the gas trapped inside the segment was absorbed by the blood. In 1930, however, using this concept of the lung, VanAllen, Lindskog, and colleagues (78, 80, 82) were unable to explain why atelectasis failed to occur in the dog lung in which a segmental bronchus had been experimentally obstructed. In addition, they were able to flow India ink through the airways of the obstructed segment and into the lobe. They reasoned that the airways, rather than being isolated from one another, were interconnected by collateral channels through which air could enter an obstructed segment from the surrounding lobe and prevent segmental collapse. They termed this phenomenon "collateral respiration" and concluded that the collateral channels must be interalveolar pores since these were the only known potential segment-lobar connections.

During the next 35 years these investigators studied collateral respiration (more recently referred to as collateral "ventilation") in a series of simple and direct experiments using the lungs of a variety of species (2, 7, 38-40, 77-84). They cannulated two portions of an excised lung lobe from humans, dogs, cats, and rabbits: one cannula was ligated in a segmental bronchus, and a second cannula was ligated in the lobar bronchus leading to the remaining segments. When air was gently blown into either of the cannulas, it escaped from the other (81, 82). In excised rabbit lungs, air could be passed between cannulas ligated in the lobar bronchi of adjacent lobes, indicating incomplete separation of the lobes (83). In the lungs of closed-chested anesthetized dogs, segmental bronchi were obstructed by a

variety of means. At autopsy performed three hours to one-and-one-half months following the obstruction, none of the obstructed segments were collapsed, indicating they had been ventilated collaterally (80).

Collateral ventilation was not found in all species investigated, for when a cannula obstructed an airway in calf and pig lungs, air flowing into the cannula only inflated the obstructed segment (83). To explain their results, VanAllen and Lindskog observed that the lobes of pig and calf lungs are divided into many small lobules by connective tissue septae [which extend from the visceral pleura down to the airways (67)]. They concluded that collateral channels do not penetrate the septae, thus preventing collateral ventilation. In contrast, the septae are incomplete in human lungs and are totally absent in dog and cat lungs, accounting for the presence of collateral ventilation in these species.

VanAllen, Lindskog, and colleagues also demonstrated the functional importance of collateral ventilation. They sampled gas from an obstructed lung segment of a healthy anesthetized dog and found that the O_2 and CO_2 tensions closely correlated with those of arterial blood (39), demonstrating that segmental bronchial obstruction does not impair the gas exchange function of the segment. They showed that the mechanical behavior of collateral channels and airways is similar because the pressure required for gas flow in the channels varies inversely with lung volume (82) as does airway resistance (46). They demonstrated that the volume of an obstructed segment's collaterally respired gas is inversely proportional to respiratory frequency (7),

and that an atelectatic segment can be inflated through collateral channels (84). In addition, pulmonary artery ligation or the injection of histamine or curare into the pulmonary artery decreases collateral ventilation (2, 7) while serotonin has no effect (7), indicating that collateral channels must have smooth muscle capable of reacting with vasoactive compounds. These experiments provided the framework for future investigators of collateral ventilation and were remarkable in that the majority of the subsequent research, although more sophisticated and detailed, is primarily a confirmation of VanAllen and Lindskog's original findings.

Anatomy of Collateral Pathways

Collateral channels connect acini originating from different parent airways. The majority of research on collateral channels centers on their function rather than anatomy, and the few investigators who have attempted anatomical studies have succeeded in describing channels which are only theoretically or indirectly linked with a collateral ventilatory function.

Interalveolar Pores

Interalveolar pores (Figure 1-3) are round or oval openings in alveolar walls. Pore diameter is 2-10 μ (47) although the exact dimension depends on the lung fixation technique. The number of pores per alveolus may be as high as 50 (44), and they have been found in every mammalian species investigated including the bat, dog, rabbit, pig, cat, human, monkey, rat, guinea pig, orangutan, chimpanzee,

Figure 1-3. Schematic diagram illustrating three different types of collateral channels (interbronchiolar respiratory bronchiole, bronchiole-alveolar canal, and interalveolar pore) connecting two adjacent sublobar lung segments.

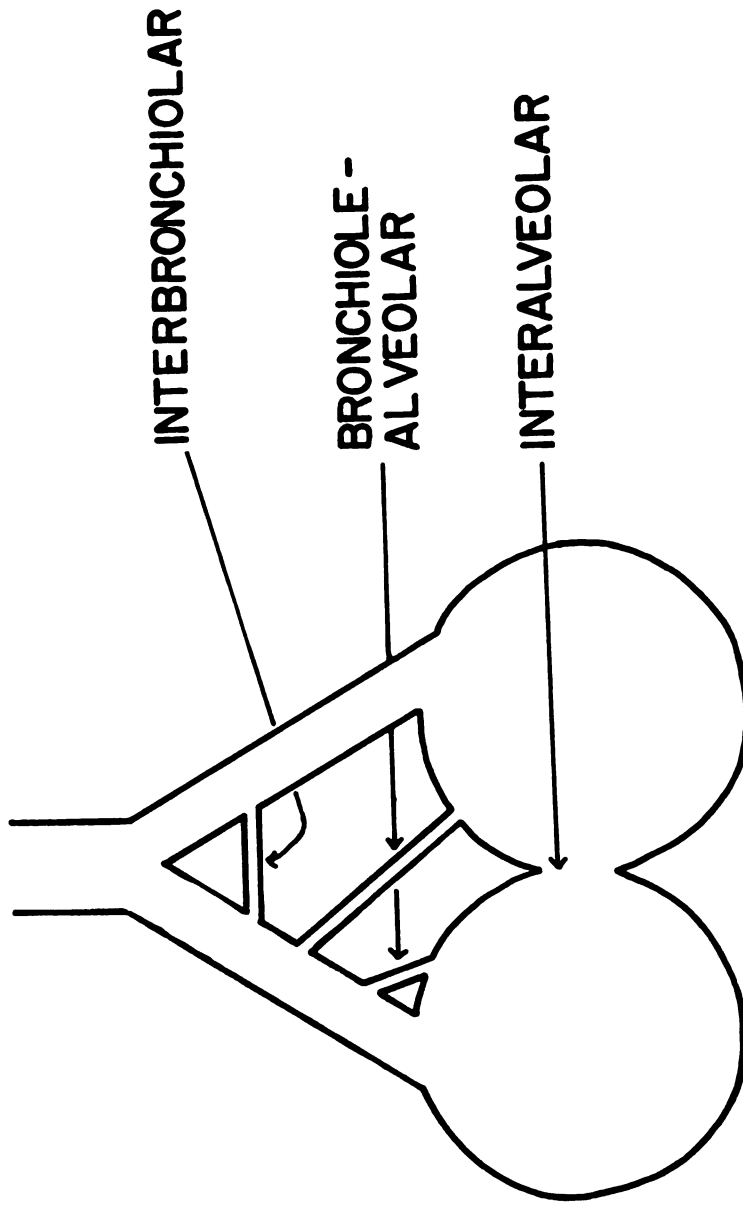


Figure 1-3

baboon, mouse, mole, hedgehog, horse, ox, sheep, goat, opossum, and manatee (43, 44).

Interalveolar pores were first described in 1847 (1) and were well characterized anatomically by the time of the original investigations of collateral ventilation by VanAllen, Lindskog, and colleagues (2, 7, 38-40, 77-84) nearly 100 years later. These investigators reported that obstruction of sublobar airways in humans, dogs, cats, and rabbits did not produce atelectasis, so they reasoned that the obstructed segment must be ventilated by the surrounding normal lung tissue through some type of collateral channel. Since the interalveolar pore was the only known anatomical structure which could theoretically provide such a connection, the pore was assigned the function of a collateral channel. Later reports suggest that pores offer much too high a resistance to participate in collateral ventilation. Martin (48) calculated that the opening pressure of a collateral pore would be 192 cm H₂O, and Sasaki et al. (73) reported that airflow resistance through pores may exceed 4000 cm H₂O/l/sec. Both investigators conclude that larger pathways must participate in collateral ventilation.

Bronchioalveolar Canals

Bronchioalveolar canals (BAC) (Figure 1-3), first described by Lambert (34) and later by others (5, 13, 19, 33, 65), are connections between a bronchiole (nonterminal, terminal, or respiratory) and the immediately surrounding alveoli. They are either a single interruption in a bronchiolar wall which opens into an adjacent alveolar sac or a tubule connecting the bronchiole with the sac. The BAC is 30 μ in

diameter and has been found in humans of all ages, cats, rabbits, rats, and sheep. They are more numerous in the lungs of patients with emphysema and in certain cystic lung diseases, such as honeycomb lungs (37).

The BAC cannot be ascribed a route for collateral flow merely because of its presence within the lung. Indeed, the following arguments suggest only a minor role of the BAC in collateral ventilation: (1) the BAC connects alveoli, via recurrent airways, with their parent bronchiole. Thus, there is no evidence demonstrating that the BAC connects acini having different parent airways. (2) Collateral ventilation still occurs when obstruction is found in airways much more proximal than the bronchiole (i.e., bronchi), and this would not occur if the BAC only connects alveoli with their parent bronchiole. The BAC is therefore not required for collateral ventilation.

Interbronchiolar Respiratory Bronchioles

An interbronchiolar respiratory bronchiole (Figure 1-3) is a respiratory bronchiole which connects two terminal bronchioles. In 1966 Martin (48) cannulated the first two bronchial branches in left upper lobes of excised dogs' lungs. In one series of experiments a suspension of polystyrene spheres having diameters from 60 to 710 μ were made to flow through one cannula and were collected from the other cannula. Examination of the outflow revealed that the largest sphere which passed between the two obstructed segments was 120 μ in diameter. In a second series of experiments he caused aerosolized India ink to flow into the lobe through one of the cannulas. After fixing the lobe

in the inflated state with formaldehyde, he dissected out the segment-lobar parenchymal interface, embedded it in paraffin, and made serial sections. He found India ink deposited on a respiratory bronchiole which connected two terminal bronchioles each lying on opposite sides of the interface. Martin concluded that respiratory bronchioles are the pathways for collateral ventilation. He also concluded that alveolar pores are not collateral channels since India ink was rarely deposited within alveoli in the segment-lobar interface.

Martin's conclusions may not be justified, however, because his serial sections simply identify a respiratory bronchiole passing from one bronchiole towards another. At no point does he demonstrate the respiratory bronchiole opening into the two bronchioles which it supposedly connects, and yet this is the crucial evidence needed to consider the respiratory bronchiole as a collateral pathway.

Interacinar Ducts

In 1968 Henderson et al. (21) cannulated two segmental bronchi in disease free post mortem human lung lobes. They used a similar perfusion pressure as Martin (48) to flow a suspension of polystyrene spheres into one cannula and collected the effluent from the other, and they found that 90 percent of the spheres had a diameter of less than 64 μ . In addition, they made resin casts of the lungs by pouring a different colored resin down each cannula. After the resin cured and tissue was dissolved away, the cast was dissected along the segment-lobar interface, revealing collateral airway connections between alveolar ducts originating from two acini supplied by different

airways. Boyden (6) described a similar interacinar pathway in a plastic reconstruction of an acinus from a child.

In 1975 Raskin and Herman (66) used a micropuncture technique to inject a radio-opaque silicone rubber into subpleural acini of inflated and fixed human lungs. The flow and distribution of the rubber was studied by cinematography. A frame-by-frame analysis of the motion pictures revealed ducts having a diameter approximately 200μ connecting acini separated by interlobular septae. The much larger size of these ducts in comparison to those described by Henderson et al. (21) may be related to the state of lung inflation: Raskin and Herman fixed the lungs at 25 cm H₂O, whereas Henderson et al. perfused deflated lungs with a driving pressure of 5 cm H₂O.

Table 1-1 is a synopsis of the anatomical literature described above.

Methods Used to Study Collateral Ventilation

Collateral ventilation was first assessed by measuring the pressure required to initiate collateral flow in excised dog lungs. VanAllen et al. (82) placed a freshly excised lung lobe in an air-tight chamber, cannulated the lobar and one segmental bronchus with separate cannulas, and connected the cannulas to the chamber's exterior with tubes. The lobe was inflated by reducing chamber pressure, following which the tip of one tube was submerged in water while air was blown into the other tube. When pressure in the inflow tube equalled one cm H₂O, the initiation of collateral airflow was indicated by bubbling in the water at the tip of the submerged tube. When the lobe was

Table 1-1. Synopsis of literature describing anatomy of collateral channels

Collateral Channel	Species ^a			Reference	Dates ^b
	Human	Dog	Others		
Interalveolar pore	Yes	Yes	All mammals	57a	1847
Bronchioloalveolar canal	Yes	No	cats, rats, rabbits, sheep	5, 13, 19, 33, 34, 37, 65	1953
Interbronchiolar respiratory bronchiole	No	Yes	No	48	1966
Interacinar duct	Yes	No	No	6, 21, 66	1968

^aMost research on collateral channels uses the lungs of humans and dogs. Therefore, for ease of comparison, these species are listed separately from other mammalian species.

^bDates of first investigation.

completely deflated, six cm H₂O was required to initiate collateral flow and two cm H₂O to maintain it. Thus, the pressure required to initiate collateral flow was inversely proportional to lung volume.

A similar method was used to measure collateral gas flow in the lungs of closed chested anesthetized dogs. A cannula was passed through the trachea and into a segmental bronchus of the right lower lobe where the cannula tip was dilated to form a leak-proof seal (76, 82). The proximal end of the cannula was attached to glass tubing whose tip was submerged in water. Each time the spontaneously breathing dog exhaled, gas escaped the obstructed segment through the cannula, causing bubbling at the submerged tip of glass tubing. In other experiments, exhaled gas from the segment was collected in a Krogh spirometer attached to the proximal port of the cannula, and the volume of gas collected was directly proportional to lung volume (39). VanAllen and colleagues used these methods to study collateral ventilation in the excised and intact lungs of a variety of species, and they determined how collateral channels respond to changes in lung volume (39), histamine and serotonin (7), isoproterenol and CO₂ (31), rate and depth of respiration, pulmonary artery ligation, pulmonary embolism, and pulmonary venous ligation (7). These early experiments were landmarks in the history of collateral ventilation because they not only provided much of the current knowledge of the function and behavior of the collateral pathways, but they also provided the basic method used in virtually all subsequent research: namely, obstructing an airway with a catheter or bronchoscope which was used to flow gas into or collect gas from the obstructed segment.

More recently, airflow resistance through collateral channels (R_{coll}) was measured by Hilpert (22) who used a variation of the methods of VanAllen and colleagues (Figure 1-4). In Hilpert's technique, a double lumen catheter is inserted into the trachea and advanced until it becomes wedged in a small bronchus supplying a sublobar segment. A constant flow of gas (\dot{V}_{coll}), injected into the segment through the outer lumen of the catheter, inflates the segment and exits the segment via collateral channels. Segment pressure (P_{ct}) is measured by the inner lumen of the catheter while transpulmonary pressure (P_{ao}) is measured at the trachea. Collateral channel resistance is calculated as:

$$R_{coll} = \frac{P_{ct} - P_{ao}}{\dot{V}_{coll}} \quad (1-1)$$

This method has been used to confirm many of the original findings of VanAllen and colleagues as well as measure vagal influences on R_{coll} (59) and the effect of ozone on R_{coll} (20). Also, segment gas may be withdrawn through the catheter, allowing analysis of segment gas exchange (16, 17, 55). In addition, the resistance through collateral channels could be compared to airway resistance, for the route having the lower resistance is the one through which an unobstructed segment receives the majority of its tidal volume. Subsequent reports have shown that R_{coll} in excised dogs' lungs is greater than airway resistance (52, 54), demonstrating that a segment in the healthy dog is likely ventilated primarily by airways.

Figure 1-4. Schematic diagram illustrating Hilpert's technique (22) for calculating collateral channel resistance (R_{coll}). A double lumen catheter is inserted into the trachea and advanced until it becomes wedged in a small bronchus supplying a sublobar segment. A constant flow of gas (\dot{V}_{coll} ; ml/sec), made to flow into the outer lumen of the catheter, inflates the segment and exits the segment via collateral channels. Segment pressure (P_{ct} ; cm H₂O) is measured by the inner lumen of the catheter while transpulmonary pressure (P_{ao} ; cm H₂O) is measured at the trachea. Collateral resistance is calculated as $R_{coll} = (P_{ct} - P_{ao})/\dot{V}_{coll}$.

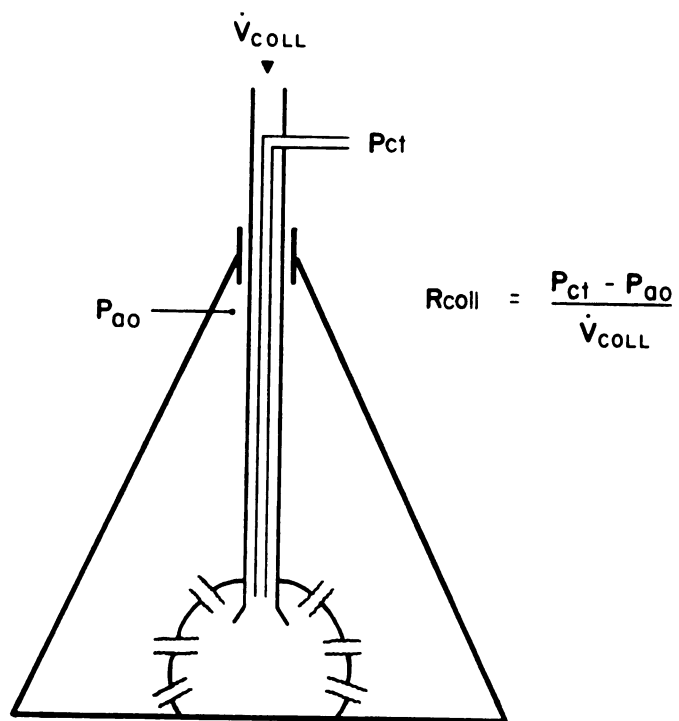


Figure 1-4

Several investigators have attempted to partition R_{coll} into various components. Hogg et al. (23) cannulated the trachea of excised human lungs. A double lumen catheter was inserted through a side-arm in the tracheal cannula and ligated in the lower lobe bronchus beyond the first branch to the superior segment. Air which flowed into the bronchial catheter entered the basal segments and flowed through collateral pathways into the superior segment and out of the lobe. The inner lumen of the catheter measured pressure at the catheter tip. Alveolar pressure in the basal and superior segments was obtained by inserting a catheter through the pleural surface on either side of the superior-basal segment interface and ligating the two catheters to the visceral pleura. The following resistances were calculated:

$$R_{base} = \frac{P_{ct} - P_{alv} (base)}{\dot{V}_{coll}} \quad (1-2)$$

$$R_{coll} = \frac{P_{alv} (base) - P_{alv} (sup)}{\dot{V}_{coll}} \quad (1-3)$$

$$R_{sup} = \frac{P_{alv} (sup) - P_{ao}}{\dot{V}_{coll}} \quad (1-4)$$

where R_{base} = airway resistance in basal segments, R_{coll} = resistance in collateral pathways between basal and superior segments, R_{sup} = airway resistance of superior segment airways, P_{ct} = pressure at the tip of the bronchial catheter, $P_{alv} (base)$ = alveolar pressure in the basal segments, $P_{alv} (sup)$ = alveolar pressure in the superior segment,

P_{ao} = tracheal pressure, and \dot{V}_{coll} = rate of gas flow into the bronchial catheter. Hogg et al. (23) found that in health lungs R_{coll} greatly exceeded R_{base} and that R_{sup} was zero ($R_{coll} > R_{base} > R_{sup}$). In emphysematous lungs, however, there was a marked fall in R_{coll} and increase in R_{base} and R_{sup} , such that $R_{base} > R_{sup} > R_{coll}$. They suggested that an obstructed segment is ventilated primarily by airways in healthy lungs but may be ventilated preferentially by collateral pathways in emphysematous lungs.

Menkes and colleagues (8, 54) used Hilpert's technique (equation 1-1) and observed that when the constant \dot{V}_{coll} into the segment was suddenly interrupted causing $P_s - P_{ao}$ to decay to zero, the initial portion of the decay occurred more rapidly than the remaining portion. They attributed the rapid initial drop in $P_s - P_{ao}$ to pressure equilibration (and thus resistance) in the small airways between the tip of the wedged catheter and collateral channels, and the subsequent slower decline to deflation of the obstructed segment through collateral channels. They used this analysis in an attempt to differentiate the response of small airways and collateral channels to methacholine, CO_2 , and variations in lung volume.

Sasaki et al. (73), realizing that R_{coll} measured with Hilpert's technique (72) includes the resistance of small airways and one or more types of collateral channels, attempted to measure airflow resistance through interalveolar pores only. The first measured R_{coll} using Hilpert's technique in the excised lower lobes of dogs' lungs. Then they glued 2 small capsules to the segment's

pleural surface and a third capsule to the lobar pleural surface, and the pleural surface under each capsule received 30 small punctures. A silicone rubber solution, having an experimentally adjusted viscosity, was poured into the lobar bronchus, and following vulcanization of the rubber, lobar airways were obstructed to the bronchiolar level. Segment airways were prevented by the wedged catheter from receiving the rubber. Sasaki et al. (73) reasoned that when air flowed into one of the segment capsules and was collected from the lobar capsule, the only collateral pathways available would be interalveolar pores. The resistance through the pores was often greater than 100 times higher than R_{coll} measured by Hilpert's technique, so they concluded that collateral ventilation does not normally occur through interalveolar pores.

The time constant for collateral ventilation (T_{coll}) provided another assessment of the mechanical behavior of collateral channels. When a constant \dot{V}_{coll} into a segment was suddenly interrupted, Hilpert found that $P_s - P_{ao}$ decayed exponentially to zero, and T_{coll} was calculated as the time required for $P_s - P_{ao}$ to decrease to 37 percent of its initial value. The shorter the T_{coll} , the more readily collateral ventilation occurs. Woolcock and Macklem used two other methods to measure T_{coll} (87). In the first method, a small volume of air was injected into the outer lumen of a double lumen catheter which obstructed an airway. The pressure in the obstructed segment, measured by the inner lumen of the catheter, initially rose, and T_{coll} was estimated as the pressure fell back to baseline. In the second method, an excised lung was oscillated sinusoidally at different frequencies (f) through a tracheal cannula attached via a loud speaker

powered by a variable frequency wave generator. Simultaneously, pressure in an obstructed segment (P_s) was measured by the inner lumen of a wedged catheter. The phase angle (θ) by which P_s lagged behind transpulmonary pressure was given by: $\theta = \tan^{-1} 2\pi f T_{coll}$. The equation was rearranged as: $T_{coll} = \tan\theta/(2\pi f)$. The T_{coll} calculated by this method was in close agreement with that measured by Hilpert (22).

All these methods revealed that T_{coll} in the dog lung was inversely proportional to lung volume. Also, increasing the size of the segment increased T_{coll} in the dog but not in the human (87). In addition, it has recently been determined that T_{coll} is dependent on lobar anatomy. Robinson and Milar (70) found in excised dogs' lungs that T_{coll} was longest in the right middle and left cranial lobes and shortest in the right and left caudal lobes.

Pressure-Flow Relationships

Basic Concepts of Fluid Mechanics

The pressure required to cause gas to flow through a tube is dependent on flow rate, geometry of the tube, density and viscosity of the gas, and flow regime (i.e., whether flow is laminar, transitional, or turbulent). If the tube is straight, smooth, and circular, the flow regime at low flow rates is laminar (64) having the following characteristics: (1) flow in all parts of the stream is constant and occurs in parallel laminae which slide over one another, and (2) the profile of the leading edge of flow is parabolic, the axial velocity of flow being twice as fast as the average velocity. At high flow

rates, the flow regime becomes turbulent (64) having the following characteristics: (1) the velocity at any point in the stream fluctuates vigorously and randomly in both magnitude and direction, and (2) the flow profile is only slightly rounded, so the axial velocity is only 1.2 times the average velocity. At moderate flow rates, flow is said to be transitional having characteristics of both laminar and turbulent flow.

These $P-\dot{V}$ characteristics are illustrated in Figure 1-5 which shows the formation of a fully developed laminar flow profile in sections A-C. Gas enters the tube from the left through a smoothly rounded orifice which introduces no disturbances into the flow. Every molecule entering the tube has the same velocity, so the velocity profile at the entrance is virtually flat. At this point (Figure 1-5A), pressure and flow are related as:

$$P = K_1 \rho \dot{V}^2 \quad (1-5)$$

where P is the driving pressure, \dot{V} is flow, ρ is gas density, and K in equation 1-5 and in the equations that follow is a constant which includes the geometry of the system (45). It takes a finite distance and time for the gas to establish the parabolic flow profile normally associated with the laminar flow regime, and during this distance (entrance length, Figure 1-5 A-C) unequal amounts of shearing force are present between adjacent gas laminae (58). The gas in contact with the wall adheres to the wall, so that the relative velocity of the gas and solid is zero (the "no slip" condition) (64). The laminae near the

Figure 1-5. Pressure-flow characteristics in a straight smooth circular tube. The driving pressure for flow (P ; cm H₂O) is related to the geometry of the tube contained in a constant (K), gas density (ρ ; gm/ml), and gas viscosity [μ ; gm/(sec cm)]. The exponent x is a number between -1 and 0 (it is -1 if flow is laminar and 0 if flow is orifice flow). Gas flow entering from the left progresses from entrance flow (A), boundary layer growth (B), laminar flow (C), transitional flow (D), and fully developed turbulent flow (E).

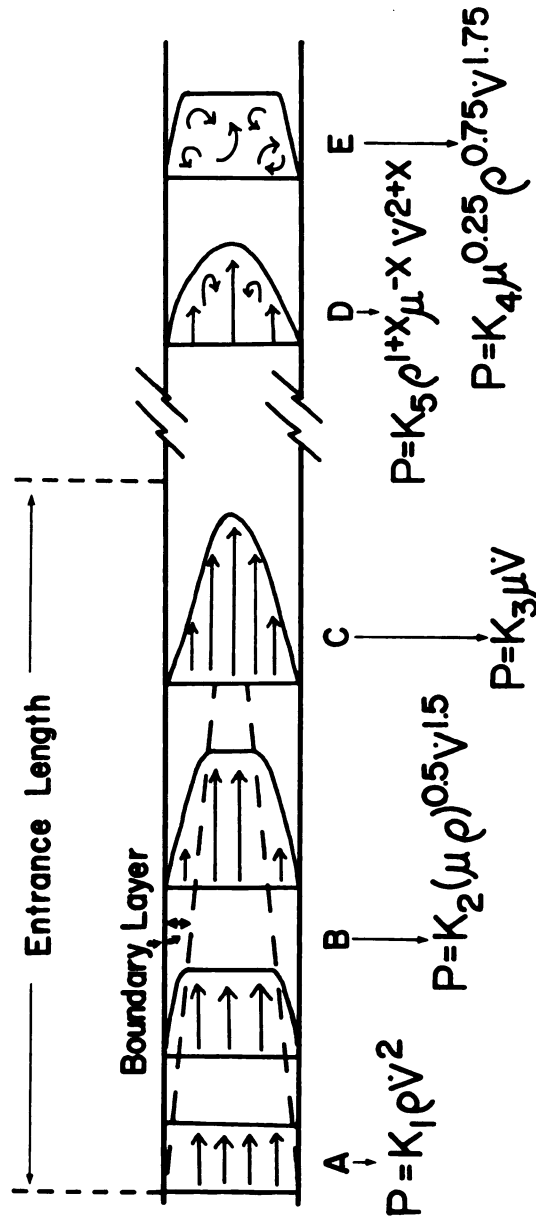


Figure 1-5

no slip layer experience a high shearing force which causes them to decelerate to decrease this shear. The laminae near the center of the tube have less shearing force which causes them to accelerate to increase their shear. This occurs until the gas has established an optimum distribution of shear between the laminae. Thus, in the entrance length, the flow profile changes from flat to parabolic.

There is a thin region adjacent to the wall in which the velocity rises from zero to its value over most of the cross section (i.e., core value), \bar{v} . This region is called the boundary layer (see Figure 1-5), and the central region where the flow profile is flat is called the core. The thickness of the boundary layer is defined as the distance across which the velocity rises from zero to a value indistinguishable from its core value (\bar{v}). As the flow profile becomes progressively more parabolic in the entrance length, the boundary layer grows in thickness. Pressure (P) and flow (\dot{V}) are related as follows during this period of boundary layer growth (45):

$$P = K_2(\mu\rho)^{0.5} \dot{V}^{1.5} \quad (1-6)$$

where μ is gas viscosity.

When the entrance length has been established, laminar flow is fully developed. The P- \dot{V} characteristics for laminar flow were first described by Poiseuille as:

$$P = \frac{8\mu l}{\pi r^4} \dot{V} \quad (1-7)$$

where l is the tube length and r is the radius. When the dimensions of the tube are held constant, then pressure is directly proportional to flow and viscosity:

$$P = K_3 \mu \dot{V} \quad (1-8)$$

When the flow profile is parabolic and the flow rate is increased, the flow profile gradually departs from a parabola, first by becoming transitional where elements from adjacent laminae occasionally mix with one another (Figure 1-5D). When this occurs, pressure and flow are related as follows (11):

$$P = K_5 \rho^{1+x} \mu^{-x} \dot{V}^{2+x} \quad (1-9)$$

where x is a number between -1 and 0 (it is -1 if flow is laminar and 0 if flow is orifice flow). As flow rate continues to increase, the flow regime becomes turbulent (Figure 1-5E), at which point P is proportional to gas density and flow (86):

$$P = K_4 \mu^{0.25} \rho^{0.75} \dot{V}^{1.75} \quad (1-10)$$

Reynolds (68) was the first to show that the transition from laminar to turbulent flow in a tube always occurs at the same value of the following dimensionless number:

$$Re = \frac{2\rho}{\pi\mu r} \dot{V} \quad (1-11)$$

This has been confirmed with a wide range of tube diameters, flow rates, and fluid properties. Laminar flow occurs when Re is less than 2300,

and turbulent flow occurs when Re is greater than 3000 (61). Transitional flow occurs when Re is between 2300 and 3000. The entrance conditions of the tube play an important role in determining the critical Re (64). If there are no disturbances in the fluid before entering the tube, and if the inlet is constructed in a smooth curve, the critical Re at which turbulence develops may reach 40,000. If the incoming fluid has disturbances, then the critical Re may be reduced to 2000, but not below.

Pressure-Flow Relationships in a Branched System

Problems of analysis. The lung poses a unique challenge in the analysis of its $P-\dot{V}$ characteristics because it is far from being the single circular conduit of uniform dimensions described above. Rather, the lung is a complex geometrical structure consisting of irregularly shaped airways branching dichotomously and asymmetrically over twenty or more generations. The total cross sectional area of the combined airways increases from the trachea to the alveoli [it is estimated that the total cross sectional area of the bronchioles is more than one thousand times larger than that of the trachea (30)] while the radius of the individual airways from the trachea to the bronchioles decreases. This not only causes flow velocity to decrease toward the periphery [such that if the velocity in the trachea is 100 cm/sec, then the velocity in the small bronchi would be less than 0.1 cm/sec (30)], but Re decreases as well (49a). In addition, there is very little development of the flow profile until after the fifth order

bronchi (58). This is because eddies which form at each bifurcation are carried away from the site of their formation to disturb the flow downstream (30). The distance over which this flow disturbance occurs (the length of transition), is longer than the length of the trachea and large bronchi. Eddies thus prevent the establishment of the laminar parabolic flow profile in the trachea and large airways (10, 85). The length of transition is shorter than the length of the small bronchi, however, so that laminar flow may be established in these small airways. Thus, the driving pressure for flow through all the airways is significantly determined by the entrance effects in the upper airways (63), and the greatest resistive pressure drop is found in these large airways due to the smaller total cross sectional area of these airways and because of the predominance of entrance length flow where the exponent for flow is greater than 1.0 as opposed to the fully developed laminar flow profile in small airways where the exponent for flow equals 1.0 (see Figure 1-5).

Other factors contribute to the complexity of the $P-\dot{V}$ relationship in the lung. First, the airways are not consistently cylindrical but rather cylindrical in their proximal portion and elliptical near the branch points (24). Secondly, the dimensions of the airways change throughout the respiratory cycle, dilating during inspiration and constricting during expiration (80). Third, the flow rate in the airways varies not only in time as a result of the cyclical nature of breathing but also in space because of the increase in cross-sectional area resulting from airway branching.

Fourth, the airways are lined by a viscous liquid (mucus), and gas flow down the airways may cause the formation of waves on the liquid resulting in a roughened surface (9). This phenomenon of two-phase gas-liquid flow becomes significant at higher flow rates in healthy lungs or at normal flow rates in diseased lungs. Fifth, the geometry of the airway bifurcations varies throughout the lung (64). Thus, as a result of its complex geometry, the lung likely contains many Re, and turbulence may be found at a critical Re which is much lower than the value of 2300 found in a straight, smooth, cylindrical tube. The variations in Re which occur during cyclic respiration support the theory that the flow regime in the lung undergoes a progressive metamorphosis as flow rate varies from low to high values (30).

Rohrer's equation. Rohrer (72) was the first investigator to attempt to describe the pressure-flow relationships in the lung. He believed that the lung contained both turbulent and laminar flow which were related as follows:

$$P = K_6 \mu \dot{V} + K_7 \rho \dot{V}^2 \quad (1-12)$$

where K_6 and K_7 are constants. The term $K_6 \mu \dot{V}$ describes the laminar flow component in the lung, and the term $K_7 \rho \dot{V}^2$ describes the turbulent flow component. The constant K_6 contains the geometry of that portion of the airways where flow is laminar, and K_7 contains the geometry of the airways where flow is turbulent. In 1955 McIlroy et al. (49) pointed out that Rohrer's equation provided an excellent curve fitting equation for pulmonary pressure-flow curves. However, breathing helium

would be expected to result in a reduction of K_7 due to a decrease in gas density and a slight increase in K_6 due to an increase in gas viscosity. In fact, 100 percent helium reduced K_6 . In contrast, ethane, which is only one-half as viscous as air and should have reduced K_6 , produced little change in this value. McIlroy et al. (49) also pointed out that the "constants" K_6 and K_7 change as the distribution of turbulence within the lung changes. As flow rate increases and turbulence increases with it, K_7 should increase and K_6 should diminish because more of the airways contain turbulent flow and fewer airways contain laminar flow. Similarly, because changing gas physical properties alters the distribution of Re , it also alters the distribution of flow regimes. Therefore, K_6 and K_7 should be different when gases of different physical properties are breathed. In contrast, K_6 and K_7 would remain constant only when the physical properties of the gas were changed such that the kinematic viscosity (viscosity divided by density) remained constant. Thus, even though Rohrer's equation fits experimentally determined pressure-flow curves quite well, it does not account for the site and nature of the gas flow regime in the lung.

Modification of Rohrer's equations. Several investigators have attempted to modify Rohrer's equation to better account for the pressure-flow relationships in the lung and thus provide a better estimation of the flow regime. Using rigid models of human airways, Pedley, Schroter, and Sudlow (62, 63) showed that most of the resistance to air flow is located in the large airways. Since the flow profile through large airways is undeveloped, these investigators

proposed that P , \dot{V} , and gas physical properties could be related as in equation 1-6 for boundary layer growth. They assume that flow regimes other than boundary layer growth contribute such a small percentage to the total resistance to flow that they may be ignored. Wood et al. (86), however, found that this is not the case in dogs breathing air because peripheral airways with fully developed laminar flow contribute 33 percent or more of the total lower pulmonary resistance. They conclude that the equation for boundary layer growth does not describe the P - \dot{V} relationships for the lower airways because other P - \dot{V} regimes contribute substantially to the resistance. Thus, Wood et al. (86) propose the following equation which is designed to take into account the metamorphosis in space and time of the flow regimes:

$$P = K\rho^{a-1} \mu^{2-a} \dot{V}^a \quad (1-13)$$

The exponent 'a' varies between 1 and 2. When flow is laminar through all the airways, $a = 1$, and the equation simplifies to the Poiseuille equation (equation 1-8). When the flow profile is undeveloped, $a = 2$, and the equation simplifies to that describing orifice flow (equation 1-5). When the flow regime is different in different parts of the airway, the value of 'a' will be between 1 and 2. If there is fully developed laminar flow in those airways that contribute most to resistance, 'a' will be close to 1, whereas if there is orifice flow in those airways that contribute most to resistance, 'a' will be closer to 2. Thus, the flow regime in the lung may be predicted by the value of 'a'.

This equation proposed by Wood et al. (86) fails in several respects to accurately describe the $P-\dot{V}$ relationships in the lung. First, since the spatial and temporal variation in Re determines the spatial and temporal variation in flow regimes which in turn determines the value of 'a', 'a' itself should be a function of Re only. However, Lisboa et al. (41) found that the relationship between 'a' and Re is quite different during breathing 80 percent He-20 percent O_2 than it is for air, suggesting that factors other than Re influence 'a'. Second, the equation predicts that when flow is laminar (i.e., $a = 1$) and resistance is viscosity dependent, the pressure required to produce a unit of flow with He/ O_2 should be greater than with air because He/ O_2 is more viscous. In contrast, when flow is orifice flow ($a = 2$) and resistance is density dependent, the pressure required to produce a unit of flow should be less on He/ O_2 than with air because He/ O_2 is less dense. Lisboa et al. (41), however, found no consistent relationship between resistance with He/ O_2 and air and the value of 'a'. Thus, equation 1-14 does not account for the effect of gas physical properties. Third, equation 1-14 contains the same general inadequacies as Rohrer's equation (equation 1-12): that is, since the distribution of Re and thus the flow regime changes with the flow rate and gas physical properties, the geometry of the airways containing laminar and turbulent flow also changes. As a result, the constant K which contains this geometry also changes (i.e., the 'constant' is not constant). It is evident, therefore, that the pressure-flow relationships in the lung are very complicated, especially considering that the flow pattern undergoes a progressive metamorphosis as flow

rate varies from low to high values (30). This relationship cannot be expressed by any single algebraic equation.

Moody diagram. Another method used to describe the flow regime through the lung makes use of a unique relationship between the degree of turbulence as indicated by the Re and the ratio of the static pressure drop to dynamic pressure within the lung (i.e., the normalized pressure drop). This normalized pressure drop (Pn) is expressed as follows:

$$P_n = \frac{\Delta P}{0.5\rho v^2} \quad (1-14)$$

where ΔP is the static pressure drop, and v is the velocity of gas flow. When $\text{Log } P_n$ is plotted against $\text{Log } Re$ (Figure 1-6), a Moody diagram (56) results, the slope of which indicates the flow regime. Three regions may be identified in the Moody diagram. At the extreme left, Re is low and flow is laminar. The slope of the curve is -1 , so that pressure and flow are related as follows:

$$\text{Log } \frac{\Delta P}{0.5\rho v^2} = -\text{Log } \frac{\rho dv}{\mu} \quad (1-15)$$

At the extreme right of the Moody diagram the high Re indicates that flow is fully turbulent. The slope of the curve is 0 , so pressure and flow are related as:

$$\text{Log } \frac{\Delta P}{0.5\rho v^2} = C \quad (1-17)$$

Figure 1-6. Schematic illustration of Moody diagram where the logarithm of the normalized pressure drop ($\text{Log } P_n$; ordinate) is plotted against the logarithm of Reynolds' number ($\text{Log } Re$; abscissa). The slope of the curve is determined by the gas flow regime: if the slope = -1, the flow regime is laminar (extreme left); if the slope = 0, the flow regime is turbulent (extreme right); if the slope is between -1 and 0, the flow regime is transitional (center). In the equations, ΔP = static pressure drop (cm H_2O) from the trachea to the alveoli; ρ = gas density (gm/ml); μ = gas viscosity [gm/(sec \cdot cm)]; v = gas velocity (cm/sec); and d = a reference cross sectional area (cm^2).

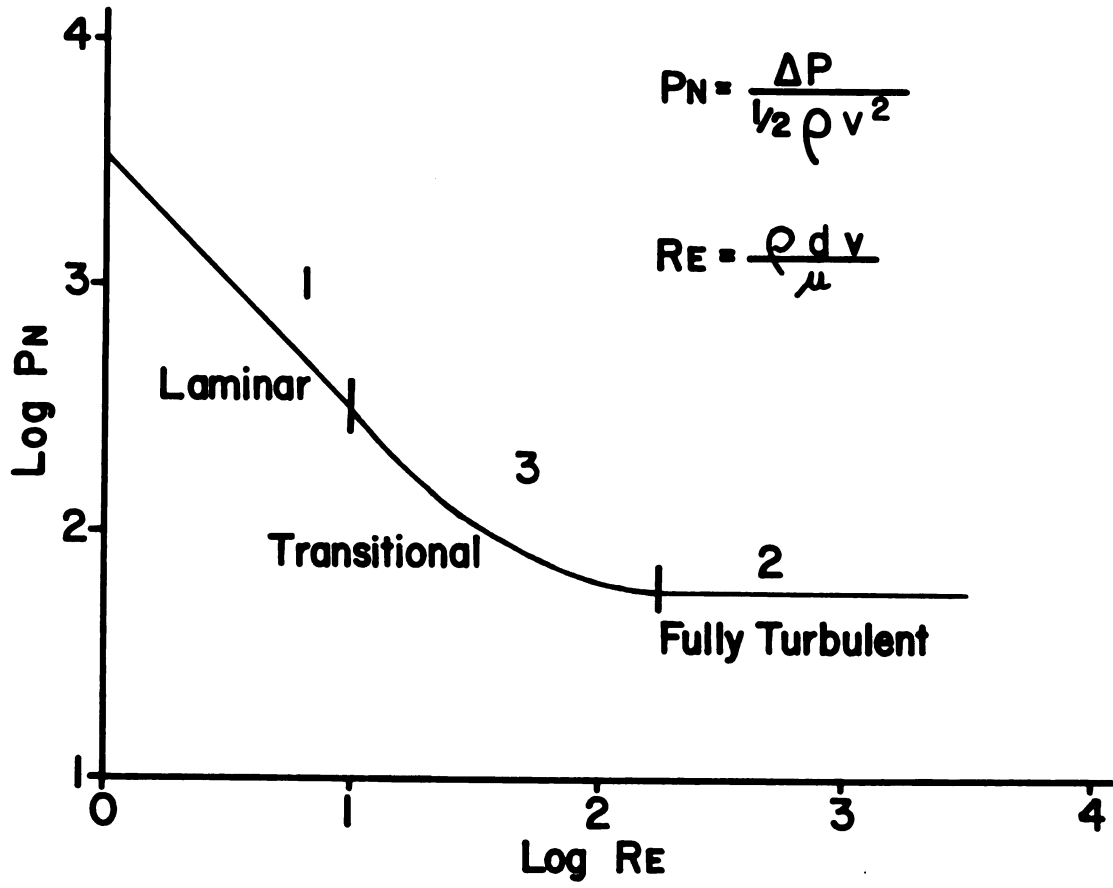


Figure 1-6

where C is a constant. Between these two extremes the slope changes from -1 to 0. The intermediate Re's indicate that flow is transitional, and pressure and flow are related as:

$$\text{Log } \frac{\Delta P}{0.5\rho v^2} = x \text{ Log } \frac{\rho d v}{\mu} \quad (1-18)$$

This equation applies only to a small section of the curve where x (the slope of the curve in log-log coordinates) can be considered constant (11). The Moody diagram is a classical fluid dynamic approach for characterizing the flow regime in a single conduit (56). This graphical method assumes that when geometry is constant, the change in Pn with \dot{V} is a function of Re only.

A Moody diagram may be determined experimentally for a single conduit or for more complex systems such as the branching system of airways (11, 27-30, 42, 58, 60, 74). In the latter case, what is measured is the predominant flow regime through the lung as a whole rather than a single specific flow regime through any particular airway. In other words, the entire lung is considered as a single rough tube (11). This method finds that the critical Re (indicating the loss of laminar flow) in the lung differs greatly from that determined for a straight, smooth, circular tube. Slutsky et al. (74) found that the predominant flow in a model of the human lung was laminar at Re less than 500, transitional between Re of 500 and 5000, and turbulent when Re exceeds 5000. Isaby and Chang (27), using a similar model, found laminar flow at Re less than 200, transitional flow at Re between 500 and 1500, and turbulent flow at Re greater than 4000. These critical

Re of 200 (27) and 500 (74) for models of the human lung would tend to be even lower in the living lung where two-phase gas-liquid flow predisposes to turbulence (9).

Pressure-Flow Relationships in a Sublobar Lung Segment

Collateral channel resistance (R_{coll}) is measured in sublobar lung segments (22) by advancing a polyethylene catheter having a flared tip through the trachea or lobar bronchus until it becomes wedged in a small bronchus (Figure 1-4). This procedure obstructs a sublobar segment which is the only region which inflates when gas is blown through the catheter. The gas which inflates the segment escapes by flowing through collateral pathways which direct the gas to airways outside the segment. When both the driving pressure for gas flow and the flow rate are known under a variety of conditions, the $P-\dot{V}$ relationships (and thus the predominant flow regime) in the segment can be estimated. Olson et al. (60) recently pointed out that the segment flow regime may be an important determinant of R_{coll} . To explain why segment inflation increases R_{coll} and excised lungs (71) but may decrease R_{coll} in intact lungs (32, 35, 36), Olson et al. (60) theorize that the higher gas flow rates used to inflate segments in excised lungs may result in a turbulent flow regime which increases R_{coll} . They used a Moody analysis to characterize the segment flow regime in anesthetized vagotomized dogs under the following conditions: transpulmonary pressure (P_{tp}) = 0 (functional residual capacity), 2, and 4 cm H_2O while segment pressure (P_s) exceeded P_{tp} by 3 cm H_2O . They repeated their measurements using gases having different physical properties. This allowed them to vary

gas density, viscosity, and flow rates while maintaining P_s 3 cm H_2O greater than P_{tp} . They concluded that when Re is less than approximately 100, flow through the segment is laminar, and when Re is between 100 and 1000, their data indicate that flow is nonlaminar (transitional, but not fully turbulent). In addition, they estimated Re for excised and intact dogs' lungs using published data and found that Re ranged from 140 to 600 in excised lungs and from 30 to 100 in intact lungs. They suggest that the different Re in excised and intact lungs may be due to differences in the flow regime.

Segment-Lobar Inhomogeneity

The most important determinant of airway resistance is airway diameter which in turn is determined primarily by the compliance of the surrounding lung parenchyma which exerts radial traction on the airways (57). Since collateral channels connect an obstructed segment with the lobe, it follows that R_{coll} is strongly influenced by both segment compliance (C_S) and lobar compliance (C_L). Although $C_S = C_L$ during homogeneous lobar inflation (i.e., when lobar distention pressure is distributed uniformly throughout the segment and lobe), C_S is less than C_L during inhomogeneity (i.e., when the segment distention pressure is greater than lobar distention pressure) (18, 50, 51, 53, 69, 70, 75, 87). The latter occurs during measurement of R_{coll} using Hilpert's technique (22) (Figure 1-4) because of interdependence in which tissue attachments common to the segment and lobe tend to prevent segment expansion, causing a smaller increase in segment volume per unit

increase in segment pressure. Thus, since inhomogeneity influences C_S and C_L , inhomogeneity should likewise influence R_{coll} .

A second mechanism by which inhomogeneity may influence R_{coll} is by distortion of collateral channels as they pass through the zone of parenchymal tissue distortion at the segment-lobar interface (Figure 1-2). Blood vessels in the interface are also likely distorted, and the resultant increased vascular resistance has been suggested as a cause of the decreased segment blood flow measured during inhomogeneity (14, 15).

The effect of inhomogeneity on collateral ventilation is uncertain. Woolcock and Macklem (87) propose that inhomogeneity enhances collateral ventilation because the reduced C_S would also reduce the time constant for collateral ventilation ($T_{coll} = R_{coll} \cdot C_S$). Direct measurements, however, indicate that T_{coll} changes little during inhomogeneity (71). Other studies have measured the effect of inhomogeneity on R_{coll} and have yielded conflicting results. Using Hilpert's technique (Figure 1-4), Robinson and Sorenson (71) reported that inhomogeneity increased R_{coll} in excised dogs' and horses' lungs while Kaplan et al. (32) calculated a decrease in R_{coll} in intact dogs' lungs. In contrast, Baker and Daly (4) measured the volume of collateral gas flow during inhomogeneity and found that the volume was directly related to the intersegmental pressure gradient, suggesting that R_{coll} remained constant as inhomogeneity increased. Baarsema and Dirken (3) obtained similar findings in intact rabbits' lungs. Thus, the studies describing

the effect of inhomogeneity on collateral channels provide inconsistent results and demonstrate the need for further investigation.

Since R_{coll} is influenced by the mechanical behavior of both the segment and the lobe, it is of interest to know which region influences R_{coll} more. In the only report on this issue, Kaplan et al. (32) found that R_{coll} fell more during lobar inflation than during inhomogeneous segment inflation, suggesting R_{coll} was influenced more by the lobe than by the segment. This study was not well controlled, however, because comparisons were not made at equal degrees of inhomogeneity during each mode of inflation. Also, a narrow range of lobar and segment inflation pressures were used. Other data suggest that the lobe has a stronger influence because raising lobar volume undisputedly decreases R_{coll} (23, 25, 52, 71, 82, 87), whereas the evidence for the effect of segment volume on R_{coll} is inconclusive. Well controlled studies are needed which make direct comparisons of segment and lobar influences on R_{coll} .

Purpose of the Present Studies

Much of the knowledge of the characteristics and function of collateral channels has been obtained using Hilpert's technique (22) where an obstructed sublobar lung segment is inflated inhomogeneously within a lobe. The effect of inhomogeneity on R_{coll} is uncertain, however. The purpose of Chapter II is to determine the effect of inhomogeneity on R_{coll} under a variety of measurement conditions commonly employed by Hilpert's technique, and also to determine whether the segment of the lobe has the stronger influence on R_{coll} .

The purpose of Chapter III is to determine the mechanism of the effect of inhomogeneity on R_{coll} . Chapter IV presents findings on the anatomy of the airways in the segment-lobar interface and also describes the route for collateral gas flow.

LIST OF REFERENCES

Chapter I

1. Adriani, quoted from Miller, W. S. *The Lung*. Springfield, Ill.: Thomas, 1937, pp. 64-68.
2. Alley, R. D. and G. E. Lindskog. Pharmacological factors influencing collateral respiration; possible relation to the etiology of pulmonary complications. Ann. Surg. 128: 497-508.
3. Baarsema, P. R. and M. N. J. Dirken. Collateral ventilation. J. Thoracic Surg. 17: 238-251, 1948.
4. Baker, D. H. and W. J. Daly. Collateral ventilation demonstrated by helium transfer. J. Appl. Physiol. 26: 321-325, 1969.
5. Boyden, E. A. Notes on the development of the lung in infancy and early childhood. Am. J. Physiol. 121: 749-762, 1967.
6. Boyden, E. A. The structure of the pulmonary acinus in a child of six years and eight months. Am. J. Physiol. 132: 275-300, 1971.
7. Call, E. P., Jr., G. E. Lindskog, and A. A. Liebow. Some physiologic and pharmacologic aspects of collateral ventilation. J. Thoracic Cardiovas. Surg. 49: 1015-1025, 1965.
8. Chang, H. K. and J. P. Mortola. Fluid dynamic factors in tracheal pressure measurement. J. Appl. Physiol.: Respirat. Environ. Exercise Physiol. 51: 218-225, 1981.
9. Clark, S. W., J. G. Jones, and D. R. Oliver. Resistance to two-phase gas-liquid flow in airways. J. Appl. Physiol. 29: 464-471, 1970.
10. Dekker, E. Transition between laminar and turbulent flow in the human trachea. J. Appl. Physiol. 16: 1060-1064, 1961.
11. Drazen, J. M., S. H. Loring, and R. H. Ingram, Jr. Distribution of pulmonary resistance: effects of gas density, viscosity, and flow rate. J. Appl. Physiol. 41: 388-395, 1976.

12. Drazen, J. M., S. H. Loring, and R. H. Ingram, Jr. Localization of airway constriction using gases of varying density and viscosity. J. Appl. Physiol. 41: 396-399, 1976.
13. Duguid, J. B. and M. W. Lambert. The pathogenesis of coal miners pneumoconiosis. J. Path. Bact. 88: 389-403, 1964.
14. Enjeti, S., J. T. O'Neil, P. B. Terry, H. A. Menkes, and R. J. Traystman. Sublobar atelectasis and regional blood flow. J. Appl. Physiol.: Respirat. Environ. Exercise Physiol. 47: 1245-1250, 1979.
15. Enjeti, S., P. B. Terry, H. A. Menkes, and R. J. Traystman. Mechanical factors and the regulation of perfusion through atelectatic lung. J. Appl. Physiol.: Respirat. Environ. Exercise Physiol. 52: 647-654, 1982.
16. Flenley, D. C., J. Picken, L. Welchel, F. Rufff, P. M. Corry, and P. T. Macklem. Blood gas transfer after small airways obstruction in the dog and minipig. Resp. Physiol. 15: 39-51, 1972.
17. Flenley, D. C., L. Welchel, and P. T. Macklem. Factors affecting gas exchange by collateral ventilation in the dog. Resp. Physiol. 15: 52-69, 1972.
18. Ford, G. T., C. A. Bradley, and N. R. Anthonisen. Forces involved in lobar atelectasis in intact dogs. J. Appl. Physiol.: Respirat. Environ. Exercise Physiol. 48: 22-33, 1980.
19. Gamsu, G., W. M. Thurlbeck, P. T. Macklem, and R. G. Fraser. Peripheral bronchographic morphology in the normal human lung. Invest. Radiol. 6: 161-170, 1971.
20. Gertner, A., B. Bromberger-Barnea, L. Kelly, R. Traystman, and H. A. Menkes. Local vagal reflexes in the lung periphery (abstract). Fed. Proc. 42: 1094, 1983.
21. Henderson, R., K. Horsfield, and G. Cumming. Intersegmental collateral ventilation in the human lung. Resp. Physiol. 6: 128-134, 1968/1969.
22. Hilpert, P. Collaterale Ventilation Habilitationsschrift. Ans der Medizinischen (Thesis). Tubingen: Universitatsklinik, 1970.
23. Hogg, J. C., P. T. Macklem, and W. M. Thurlbeck. The resistance of collateral channels in excised human lungs. J. Clin. Invest. 48: 421-431, 1969.

24. Horsfield, K., G. Dart, D. E. Olson, G. F. Filley, and G. Cumming. Models of the human bronchial tree. J. Appl. Physiol. 31: 207-217, 1971.
25. Inners, C. R., P. B. Terry, R. J. Traystman, and H. A. Menkes. Collateral ventilation and the middle lobe syndrome. Am. Rev. Resp. Dis. 118: 305-310, 1978.
26. Inners, C. R., P. B. Terry, R. J. Traystman, and H. A. Menkes. Lung volume and resistance to collateral ventilation in man (abstract). Fed. Proc. 37: 927, 1978.
27. Isaby, D. and H. K. Chang. Steady and unsteady pressure-flow relationships in central airways. J. Appl. Physiol.: Respirat. Environ. Exercise Physiol. 51: 1338-1348, 1981.
28. Jaffrin, M. Y. and P. Kesic. Airway resistance; a fluid mechanical approach. J. Appl. Physiol. 36: 254-361, 1974.
29. Jaeger, M. J. and H. Matthys. The pattern of flow in the upper human airways. Resp. Physiol. 6: 113-127, 1968.
30. Jaeger, M. J. and H. Matthys. The pressure flow characteristics of the human airways. In Airway Dynamics, Physiology and Pharmacology, edited by A. Bouhuys. Springfield, Ill.: Thomas, 1970, pp. 21-32.
31. Johnson, R. M. and G. E. Lindskog. Further studies on factors influencing collateral ventilation. J. Thoracic Surg. 62: 321-329, 1971.
32. Kaplan, J., R. C. Koehler, P. B. Terry, H. A. Menkes, and R. J. Traystman. Effect of lung volume on collateral ventilation in the dog. J. Appl. Physiol.: Respirat. Environ. Exercise Physiol. 49: 9-15, 1980.
33. Krahl, V. E. Microscopic anatomy of the lungs. Am. Rev. Resp. Dis. 80: 24-44, 1959.
34. Lambert, M. W. Accessory bronchiole-alveolar communications. J. Path. Bact. 70: 311-314, 1955.
35. Levy, H. L. and L. D. H. Wood. Effect of gas physical properties on resistance to collateral ventilation (abstract). Fed. Proc. 35: 231, 1976.
36. Levy, H. L. and L. D. H. Wood. Effect of pulmonary interdependence on channels of collateral ventilation (abstract). The Physiologist. 20: 56, 1977.

37. Liebow, A. A. Recent advances in pulmonary anatomy. In Ciba Found. Symp. Pulmonary Structure Function, edited by A. V. S. DeReuck and M. O'Conner. London: Churchill, 1962.
38. Lindskog, G. E. Collateral respiration in the normal and diseased lung. Yale J. Bio. Med. 23: 311-316, 1950/1951.
39. Lindskog, G. E. and H. H. Bradshaw. Collateral respiration. The chemical composition and volume of the collateral respired gases. Am. J. Physiol. 108: 581-592, 1934.
40. Lindskog, G. E. and C. M. VanAllen. The aerodynamics of bronchial obstruction. Arch. Surg. 24: 204-230, 1932.
41. Lisboa, C., W. R. D. Ross, J. Jardim, and P. T. Macklem. Pulmonary pressure-flow curves measured by a data averaging circuit. J. Appl. Physiol.: Respirat. Environ. Exercise Physiol. 47: 621-627, 1979.
42. Lisboa, C., L. D. H. Wood, J. Jardim, and P. T. Macklem. Relation between flow, curvilinearity, and density dependence of pulmonary pressure-flow curves. J. Appl. Physiol.: Respirat. Environ. Exercise Physiol. 48: 878-885, 1980.
43. Loosli, C. G. Inter-alveolar communications in normal and pathologic mammalian lungs. Arch. Path. 24: 743-776, 1937.
44. Macklem, P. T. Airway obstruction and collateral ventilation. Physiol. Rev. 51: 368-436, 1971.
45. Macklem, P. T. The paradoxical nature of pulmonary pressure-flow relationships. Fed. Proc. 39: 2755-2758, 1980.
46. Macklem, P. T., A. J. Woolcock, J. C. Hogg, J. A. Nadel, and N. J. Wilson. Partitioning of pulmonary resistance in the dog. J. Appl. Physiol. 26: 798-805, 1969.
47. Martin, H. B. The effect of aging on the alveolar pores of Kohn in the dog. Am. Rev. Resp. Dis. 88: 773-778, 1963.
48. Martin, H. B. Respiratory bronchioles as the pathway for collateral ventilation. J. Appl. Physiol. 21: 1443-1447, 1966.
49. McIlroy, M. B., J. Mead, N. J. Selverstone, and E. P. Radford. Measurement of lung tissue viscous resistance using gases of equal kinematic viscosity. J. Appl. Physiol. 7: 485-490, 1955.

- 49a. Mead, J. Mechanical properties of lungs. Physiol. Rev. 41: 281-330, 1961.
50. Mead, J., T. Takishima, and D. Leith. Stress distribution in lungs: a model of pulmonary elasticity. J. Appl. Physiol. 28: 596-608, 1970.
51. Menkes, H., G. Gamsu, R. Schroter, and P. T. Macklem. Interdependence of lung units in isolated dog lungs. J. Appl. Physiol. 32: 675-680, 1974.
52. Menkes, H., D. Lindsay, G. Gamsu, L. Wood, A. Muir, and P. T. Macklem. Measurement of sublobar lung volume and collateral flow resistance in dogs. J. Appl. Physiol. 35: 917-921, 1973.
53. Menkes, H., D. Lindsay, L. Wood, A. Muir, and P. T. Macklem. J. Appl. Physiol. 32: 681-686, 1972.
54. Menkes, H. A. and R. J. Traystman. State of the art. Collateral ventilation. Am. Rev. Resp. Dis. 116: 287-309, 1977.
55. Metcalf, J. F., P. D. Wagner, and J. B. West. Effect of local bronchial obstruction on gas exchange in the dog. Am. Rev. Resp. Dis. 117: 85-95, 1978.
56. Moody, L. F. Friction factors for pipe flow. Trans. ASME. 66: 671-678, 1944.
57. Murray, J. F. The Normal Lung. Philadelphia, Pa.: Saunders, 1976, p. 99.
- 57a. Ogawa, C. Contribution to the histology of the respiratory spaces of the vertebrate lungs. Am. J. Anat. 27: 333-393, 1920.
58. Olson, D. E., G. A. Dart, and G. F. Filley. Pressure drop and fluid flow regime of air inspired into the human lung. J. Appl. Physiol. 28: 482-494, 1970.
59. Olson, L. E. and N. E. Robinson. Effect of vagal stimulation on collateral flow resistance in dog lungs. J. Appl. Physiol.: Respirat. Environ. Exercise Physiol. 49: 289-293, 1980.
60. Olson, L. E., J. R. Rodarte, and N. E. Robinson. Pressure-flow relationships in a collaterally ventilating dog lung segment. J. Appl. Physiol.: Respirat. Environ. Exercise Physiol. 54: 956-960, 1983.

61. Patel, V. and M. R. Head. Reversion of turbulent to laminar flow. J. Fluid Mech. 34: 371-392, 1968.
62. Pedley, T. J., R. C. Schroter, and M. F. Sudlow. Energy losses and pressure drop in models of human airways. Resp. Physiol. 9: 371-386, 1970.
63. Pedley, T. J., R. C. Schroter, and M. F. Sudlow. The prediction of pressure drop and variation of resistance within the human bronchial airways. Resp. Physiol. 9: 387-405, 1970.
64. Pedley, T. J., R. C. Schroeter, and M. F. Sudlow. Gas flow and mixing in the airways. In Bioengineering Aspects of the Lung, edited by J. B. West. New York: Marcel Dekker, Inc., 1971, pp. 163-266.
65. Pump, K. K. The morphology of the finer branches of the bronchial tree of the human lung. Dis. Chest. 46: 379-398, 1964.
66. Raskin, S. P. and P. G. Herman. Interacinar pathways in the human lungs. Am. Rev. Resp. Dis. 111: 489-495, 1975.
67. Reid, L. The secondary lobule in the adult human lung, with special reference to its appearance in bronchograms. Thorax. 13: 110-115, 1958.
68. Reynolds, O. An experimental investigation of the circumstances which determine whether the motion of water shall be direct or sinuous, and the law of resistance in parallel channels. Phil. Trans. R. Soc. London. 174: 935-982, 1883.
69. Robinson, N. E. Lobar variations in the mechanics of collateral ventilation in intact dog lungs. Am. Rev. Resp. Dis. 124: 68-71, 1981.
70. Robinson, N. E. and R. Milar. Lobar variation in collateral ventilation in excised dog lungs. Am. Rev. Resp. Dis. 121: 827-834, 1980.
71. Robinson, N. E. and P. R. Sorenson. Collateral flow resistance and time constants in dog and horse lungs. J. Appl. Physiol.: Respirat. Environ. Exercise Physiol. 44: 63-68, 1978.
72. Rohrer, F. Der Stromungswiderstand in den menschlichen Atemwegen. Pflugers Arch. Gesamte. Physiol. 162: 225-259, 1915.
73. Sasaki, H., T. Takishima, and M. Nakamura. Collateral resistance at alveolar level in excised dog lungs. J. Appl. Physiol.: Respirat. Environ. Exercise Physiol. 48: 982-990, 1980.

74. Slutsky, A. S., G. G. Berdine, and J. M. Drazen. Steady flow in a model of human central airways. J. Appl. Physiol.: Respirat. Environ. Exercise Physiol. 49: 417-423, 1980.
75. Sylvester, J. T., H. A. Menkes, and F. Stitik. Lung volume and interdependence in the pig. J. Appl. Physiol. 38: 395-401, 1975.
76. VanAllen, C. M. A dilatable bronchial cannula. Yale J. Bio. Med. 2: 295-296, 1930.
77. VanAllen, C. M. Obstructive pulmonary emphysema and collateral respiration. Surg. Gynecol. Obst. 55: 303-307, 1932.
78. VanAllen, C. M. and F. Adams. The mechanism of obstructive pulmonary atelectasis. Surg. Gynecol. Obst. 50: 385-396, 1930.
79. VanAllen, C. M. and T. S. Jung. Postoperative atelectasis and collateral respiration. J. Thoracic Surg. 1:3-14, 1931.
80. VanAllen, C. M. and G. E. Lindskog. Obstructive pulmonary atelectasis. Problems of pathogenesis and clinical management. Arch. Surg. 21: 1195-1213, 1930.
81. VanAllen, C. M. and G. E. Lindskog. Collateral respiration in the lung. Role in bronchial obstruction to prevent atelectasis and to restore patency. Surg. Gynecol. Obst. 53: 16-21, 1931.
82. VanAllen, C. M., G. E. Lindskog, and H. G. Richter. Gaseous interchange between adjacent lung lobules. Yale J. Bio. Med. 2: 297-300, 1930.
83. VanAllen, C. M., G. E. Lindskog, and H. G. Richter. Collateral respiration. Transfer of air collaterally between pulmonary lobules. J. Clin. Invest. 10: 559-590, 1941.
84. VanAllen, C. M. and Y. C. Soo. Collateral respiration. Spontaneous reinflation of an atelectatic pulmonary lobule by collateral respiration. J. Clin. Invest. 12: 171-179,
85. West, J. B. and P. Hugh-Jones. Patterns of gas flow in the upper bronchial tree. J. Appl. Physiol. 14: 753-759, 1959.
86. Wood, L. D. H., L. A. Engel, P. Griffin, P. Despas, and P. T. Macklem. Effect of gas physical properties and flow on lower pulmonary resistance. J. Appl. Physiol. 41: 234-244, 1976.
87. Woolcock, A. J. and P. T. Macklem. Mechanical factors influencing collateral ventilation in human, dog, and pig lungs. J. Appl. Physiol. 30: 99-115, 1971.

CHAPTER II
THE EFFECT OF REGIONAL INHOMOGENEITY
ON COLLATERAL AIRWAY RESISTANCE

Introduction

Regional inhomogeneity occurs when a sublobar lung segment is inflated to a different relative volume than the remainder of the lobe. The segment has a low compliance due to its interdependence with the adjacent lobar parenchyma (3, 10, 11, 13, 20), and it has been proposed that this low compliance promotes collateral ventilation by reducing the time constant for collateral air flow (20). Blood flow to a segment is not promoted by regional inhomogeneity, however, for Enjeti et al. (2) demonstrated that regional blood flow decreases more when a sublobar than a lobar region is made atelectatic. They theorize that interdependence between the sublobar region and the lobe causes additional mechanical distortion of vessels which is not likely to occur in the case of lobar atelectasis (1, 2). If collateral channels behave like blood vessels, then collateral ventilation may be decreased during regional inhomogeneity rather than increased as previously suggested (20). Indeed, collateral channels passing through the parenchymal interface between the segment and the lobe are subjected to abrupt changes in distending pressure which may distort the channels, and the degree of distortion should be determined by the pressure

difference between the segment (Pct) and the lobe as measured at the airway opening (Pao).

It is generally accepted that when Pct-Pao is held constant, raising transpulmonary pressure decreases collateral resistance (Rcoll) (5, 12). Although this is probably due primarily to the volume-dependency of airway resistance (9), the degree of interface distortion produced by a given Pct-Pao may vary as the lung inflates because of changes in the degree of interdependence with lung inflation (12, 19). Thus, Rcoll and interface distortion resulting from regional inhomogeneity enjoy a complex interrelationship which may depend on both Pct and transpulmonary pressure, and this interrelationship has not been adequately described in the literature.

It has been reported that raising Pct-Pao from two to ten cm H₂O increases Rcoll in excised dog and horse lungs (17). In contrast, raising Pct-Pao from one to three cm H₂O decreases Rcoll in intact dog lungs held at functional residual capacity (8). This latter report did not explore the possibility, however, that larger changes in Pct-Pao using a wider range of transpulmonary pressures may increase Rcoll. In the present study, combinations of Pct and transpulmonary pressures were assembled into a block design so as to produce a variety of Pct and Pct-Pao at several transpulmonary pressures. Experiments were performed in isolated segments in the left cranial and right caudal lobes of excised and intact dogs' lungs to determine if differences in segment geometry or the presence of a chest wall altered the response of the collateral channels to regional inhomogeneity. Data were interpreted on the basis of there being collateral channels and airways

located not only in the body of the segment but also passing through the segment-lobar parenchymal interface, so that changes in R_{coll} are determined by which population of channels changes its resistance in greatest magnitude.

Methods

In experiments using excised lungs, mixed-breed dogs were anesthetized with sodium pentobarbital and exsanguinated. The lungs and attached trachea were removed from the chest cavity, and the pleural surfaces were kept moist with saline throughout the experiment. The lungs were suspended by the trachea which was attached to one arm of a 3-way connector. A second arm of the connector was attached to a variable speed blower which was used to inflate the lungs. The third arm of the connector was used for passage of a double lumen catheter into the tracheobronchial tree. Transpulmonary pressure was tracheal pressure (P_{ao}), measured by a transducer (model no. PM131, Statham, Hato Rey, Puerto Rico) connected to the trachea by means of a polyethylene catheter and needle.

Collateral resistance was calculated by the method of Hilpert (5) (Figure 1-4). A double-lumen catheter (o.d. 3.2 mm) with the distal end flared to an outside diameter of 5 mm was wedged in a bronchus while the lung was inflated to total lung capacity ($P_{ao} = 30 \text{ cm H}_2\text{O}$). When the lung was deflated, gentle traction on the catheter depressed the lobar pleural surface, and considerable force was required to remove the catheter, suggesting the catheter securely obstructed the airway. The inner lumen (o.d. 1.7 mm) of the catheter was connected to one side

of a second differential pressure transducer (model no. PM131, Statham, Hato Rey, Puerto Rico). The other side of the transducer was connected to the trachea with a catheter and needle so that the pressure difference ($P_{ct}-P_{ao}$) between the tip of the wedged catheter (P_{ct}) and the trachea could be measured. A photorecording oscilloscope (Model DR8, Electronics for Medicine, White Plains, New York) was used to record P_{ao} and $P_{s}-P_{ao}$. During measurement of R_{coll} the lobe was inflated to the desired P_{ao} , and air flow from a compressed air tank (\dot{V}_{coll}) was directed through the outer lumen of the wedged catheter and into the isolated segment; it passed through collateral channels and left the lung via the trachea. Flow was adjusted by means of a rotameter (Model 7431T, Matheson, East Rutherford, New Jersey) until the desired steady-state pressure gradient ($P_{ct}-P_{ao}$) was obtained. Collateral resistance was calculated as $(P_{ct}-P_{ao})/\dot{V}_{coll}$. In one series of experiments, gas was withdrawn from the segment at a constant flow rate adjusted by the rotameter connected to a vacuum source. Collateral resistance was calculated as above. A minimum of two sequential R_{coll} measurements were taken at each $P_{ct}-P_{ao}$. The lungs were inflated to total lung capacity preceding each measurement to ensure a constant volume history.

In the experiments using intact lungs, R_{coll} was measured as described by Inners et al. (7) using a bronchoscope instead of a double-lumen catheter. Mixed-breed dogs were anesthetized with sodium pentobarbital (33 mg/kg), and a femoral vein was cannulated for delivery of supplemental anesthetic. A tracheostomy was performed, and the trachea

was connected to one arm of a 3-way connector. A second arm of the connector was attached to a Harvard pump (model 607, Harvard Apparatus, Dover, Massachusetts), frequency and tidal volume being adjusted to maintain the dogs' end-expired CO_2 concentration between 4.5 and 5.0 percent. The dog was placed in sternal recumbency, and the Harvard pump was briefly turned off at end expiration, during which time a bronchoscope of 5 mm o.d. (model BF2, B2, Olympus Corp., New Hyde Park, New York) was passed through the third arm of the connector and wedged in a peripheral airway of either the left cranial or right caudal lobe. A rubber cuff placed around this third connector arm provided a seal to prevent air leaks during ventilation. An esophageal balloon, passed through the nares and into the esophagus, positioned to measure pleural pressure (P_{pl}), was attached to one side of a differential pressure transducer. The other side of this transducer sensed tracheal pressure (P_{ao}), providing a measurement of transpulmonary pressure ($P_{tp} = P_{ao} - P_{pl}$). The esophageal balloon was positioned such that spontaneous breathing against a closed airway produced minimal fluctuations in P_{tp} . This resulted in a P_{tp} of 3 to 4 cm H_2O at functional residual capacity in these dogs. A catheter was inserted into the suction/biopsy part of the bronchoscope and connected to another differential pressure transducer to measure P_{ct} , and the other side of this transducer measured P_{ao} . The remainder of the suction/biopsy channel was connected to a rotameter and a compressed gas source of 95 percent O_2 and 5 percent CO_2 to provide \dot{V}_{coll} into the isolated segment while maintaining a physiologic alveolar CO_2 tension of 5 percent.

I measured R_{coll} at several different P_{tp} . The ventilator was switched off at end-expiration (functional residual capacity), and the lungs were then inflated to the desired P_{tp} with a variable speed blower attached to the expiratory port of the ventilator. The \dot{V}_{coll} was adjusted to provide a constant $P_{ct}-P_{ao}$, and R_{coll} was calculated as: $R_{coll} = (P_{ct}-P_{ao})/\dot{V}_{coll}$. The mean of a minimum of two sequential R_{coll} measurements taken at each $P_{ct}-P_{ao}$ in all experiments were averaged, and the lungs were inflated to total lung capacity before each measurement to ensure a constant volume history.

Three series of experiments, each using a different group of dogs, were performed to determine the effect of regional inhomogeneity on R_{coll} . All measurements were taken in the left cranial and right caudal lobes ventilated with room air, and the specific transpulmonary pressures, P_{ct} , and $P_{ct}-P_{ao}$ used are summarized in Table 2-1. In each series, transpulmonary pressure was held constant while $P_{ct}-P_{ao}$ was raised to the values shown in the table. Specific combinations of $P_{ct}-P_{ao}$ and transpulmonary pressures were chosen to allow P_{ct} to remain constant over a range of transpulmonary pressures. This enabled me to determine not only the effect of P_{ct} on R_{coll} , but also the effect of $P_{ct}-P_{ao}$ on R_{coll} . In series one, the lungs of five dogs were excised. In series two, experiments were performed on the intact lungs of seven closed chest anesthetized dogs. Left cranial lobe data were taken from all seven dogs, and right caudal lobe data were taken from six dogs. In series three, lungs from six dogs were excised, and regional inhomogeneity was created by withdrawing air from the

segment at a constant flow rate, thus deflating the segment relative to the lobe. Left cranial lobe data were taken from five dogs, and right caudal lobe data were taken from six dogs. In this series only, R_{coll} was calculated as $(P_{ao}-P_{ct})/\dot{V}_{coll}$.

The effect of $P_{ct}-P_{ao}$ on R_{coll} in series one and two, $P_{ao}-P_{ct}$ on R_{coll} in series three, and transpulmonary pressure on R_{coll} in series one-three was analyzed using a randomized complete block design analysis of variance, and significant differences between means were tested using the Student-Newman-Keuls' procedure (18). Means were considered significantly different at the $p < .05$ level.

Results

In both excised and intact dogs' lungs, regional inhomogeneity (i.e., increasing $P_{ct}-P_{ao}$) increased R_{coll} at higher P_{ao} and had little effect on R_{coll} at the lowest P_{ao} . Figure 2-1A shows the results of series one experiments in excised lungs. In both the left cranial and right caudal lobes R_{coll} is plotted against P_{ao} at five different levels of P_{ct} . At a constant P_{ct} , raising P_{ao} decreased R_{coll} . In both lobes, all changes occurring at each P_{ct} as P_{ao} was raised were statistically significant. When R_{coll} was plotted as a function of $P_{ct}-P_{ao}$ at several levels of P_{ao} (Figure 2-1B), raising $P_{ct}-P_{ao}$ increased R_{coll} at $P_{ao} = 3, 4, \text{ and } 5 \text{ cm H}_2\text{O}$ but had little effect on R_{coll} at $P_{ao} = 2 \text{ cm H}_2\text{O}$. There was a significant interaction between $P_{ct}-P_{ao}$ and P_{ao} .

In Figure 2-2A the results from series two experiments (closed chest dogs) are shown where R_{coll} is plotted against P_{tp} at several

Figure 2-1A. Effect of transpulmonary pressure (P_{ao} ; cm H₂O; abscissa) on collateral resistance [R_{coll} ; cm H₂O/(ml/sec); ordinate] in left cranial lobes (left panel) and right caudal lobes (right panel) at different levels of segment pressure (P_{ct} ; cm H₂O) in five excised dogs' lungs ventilated with air.

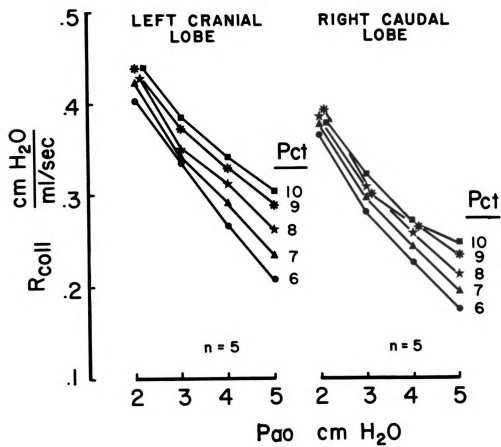


Figure 2-1A

Figure 2-1B. Same data as in Figure 2-1A showing effect of segment-lobar pressure difference (Pct-Pao; cm H₂O; abscissa) on collateral resistance [Rcol; cm H₂O/(ml/sec); ordinate] at different values of transpulmonary pressure (Pao; cm H₂O) in five excised dogs' lungs. All adjacent points when Pao is constant are significantly different except for those marked ns.

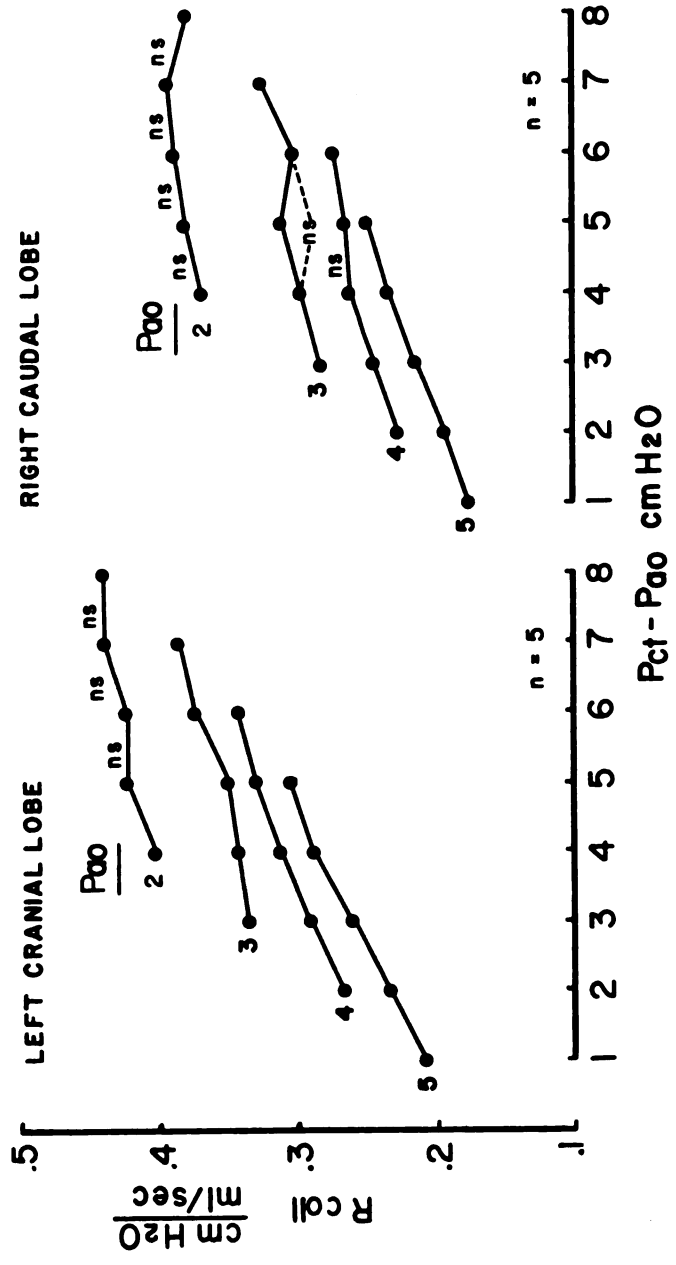


Figure 2-1B

different levels of Pct. Raising Ptp decreased Rcoll at constant Pct. In both lobes, all changes occurring at each Pct as Ptp was raised were statistically significant with one exception noted by the "ns" on the graph. When Rcoll was plotted as a function of Pct-Pao at several levels of Ptp (Figure 2-2B), raising Pct-Pao consistently increased Rcoll at Ptp = 6, 7, and 8 cm H₂O. At Ptp = 5 cm H₂O in both lobes, Rcoll decreased markedly at Pct-Pao = 6 to 7 cm H₂O. This decrease was due primarily to a large decrease in two dogs in the left cranial lobe and in one dog in the right caudal lobe, whereas the other dogs showed little or no change in Rcoll. I suspect, therefore, that Rcoll may be little influenced by increases in Pct-Pao at Ptp = 5 cm H₂O. There was a significant interaction between Pct-Pao and Ptp.

The results from series 3 experiments are shown in Figure 2-3. In Figure 2-3A, Rcoll is plotted against Pao at 3 different levels of Pct. Raising Pao decreased Rcoll at constant Pct in the right caudal lobe, and all but one of the changes were statistically different. In the left cranial lobe, increasing Pao increased Rcoll at Pct = 3 cm H₂O, had no effect on Rcoll at Pct = 2 cm H₂O, and decreased Rcoll between Pao = 4 and 5 cm H₂O at Pct = 1 cm H₂O. Data were replotted in Figure 2-3B as Rcoll versus Pao-Pct at 3 different levels of Pao. In both lobes, raising Pao-Pct caused greater increases in Rcoll than in series 1 and 2 (Figures 2-1B and 2-2B). There was a significant interaction between Pao-Pct and Pao.

Table A-1 tabulates the data with the standard error from Figures 2-1B, 2-2B, and 2-3B to indicate variation in data.

Figure 2-2A. Effect of transpulmonary pressure (P_{tp} ; cm H_2O ; abscissa) on collateral resistance [R_{coll} ; cm H_2O /(ml/sec); ordinate] in seven left cranial lobes (left panel) and six right caudal lobes (right panel) at different levels of segment pressure (P_{ct} ; cm H_2O) in lungs from closed chest dogs ventilated with air.

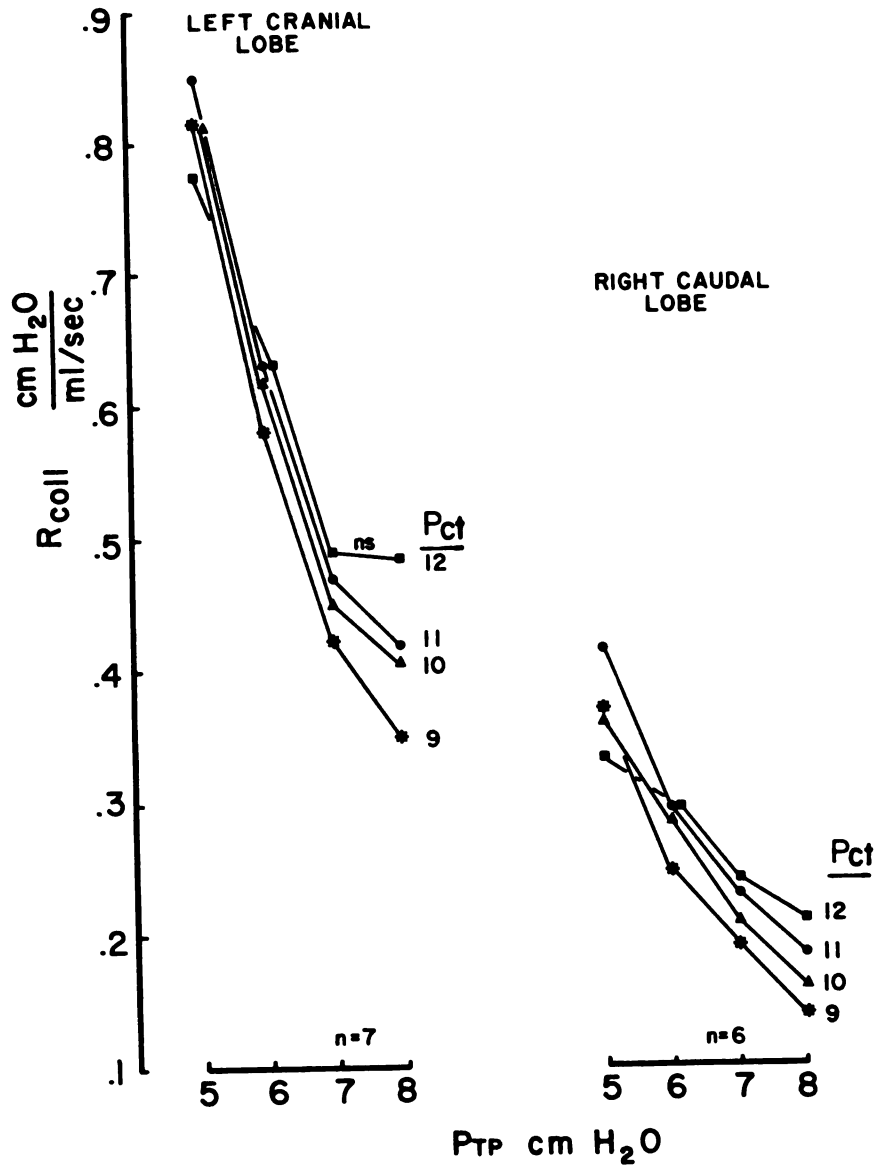


Figure 2-2A

Figure 2-2B. Same data as Figure 2-2A showing effect of segment-lobar pressure difference ($P_{ct}-P_{ao}$; cm H₂O; abscissa) on collateral resistance [R_{coll} ; cm H₂O/(ml/sec); ordinate] at different values of transpulmonary pressure (P_{tp} ; cm H₂O) in lungs from closed chest dogs. All adjacent points when P_{tp} is constant are significantly different except for those marked ns.

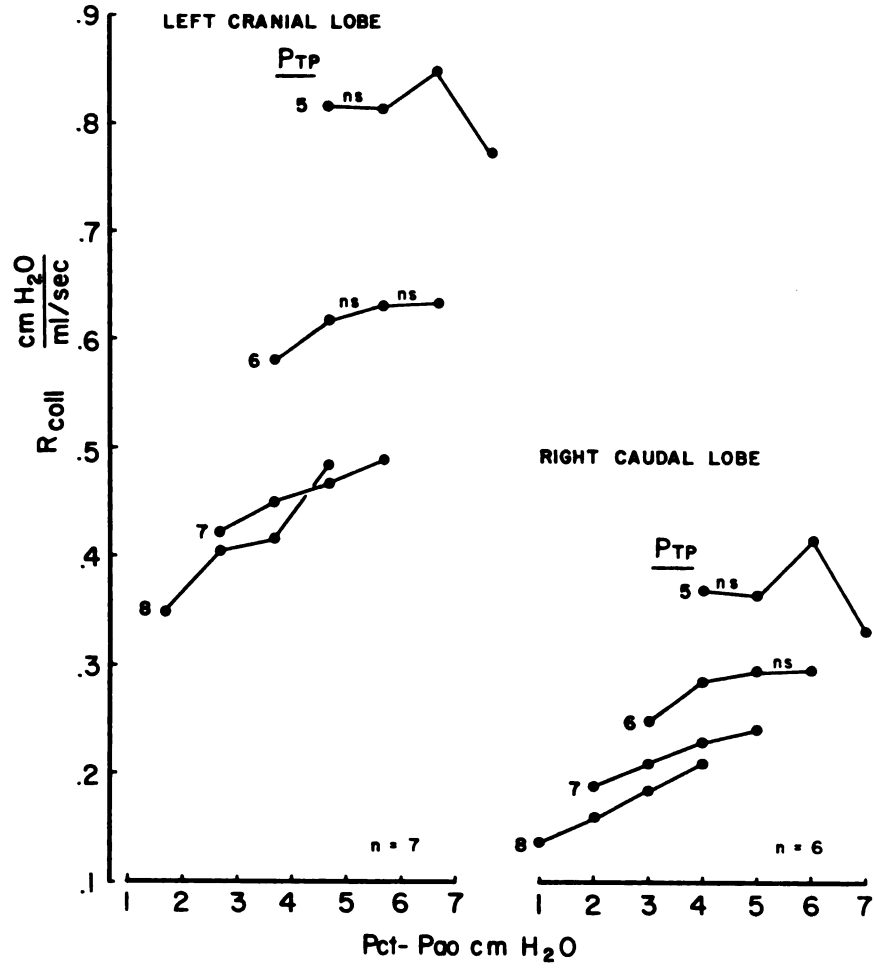


Figure 2-2B

Figure 2-3A. Effect of transpulmonary pressure (P_{ao} ; cm H_2O ; abscissa) on collateral resistance [R_{coll} ; cm H_2O /(ml/sec); ordinate] in five left cranial lobes (left panel) and six right caudal lobes (right panel) at different levels of segment pressure (P_{ct} ; cm H_2O) when the segment was deflated relative to the lobe in excised dogs' lungs ventilated with air.

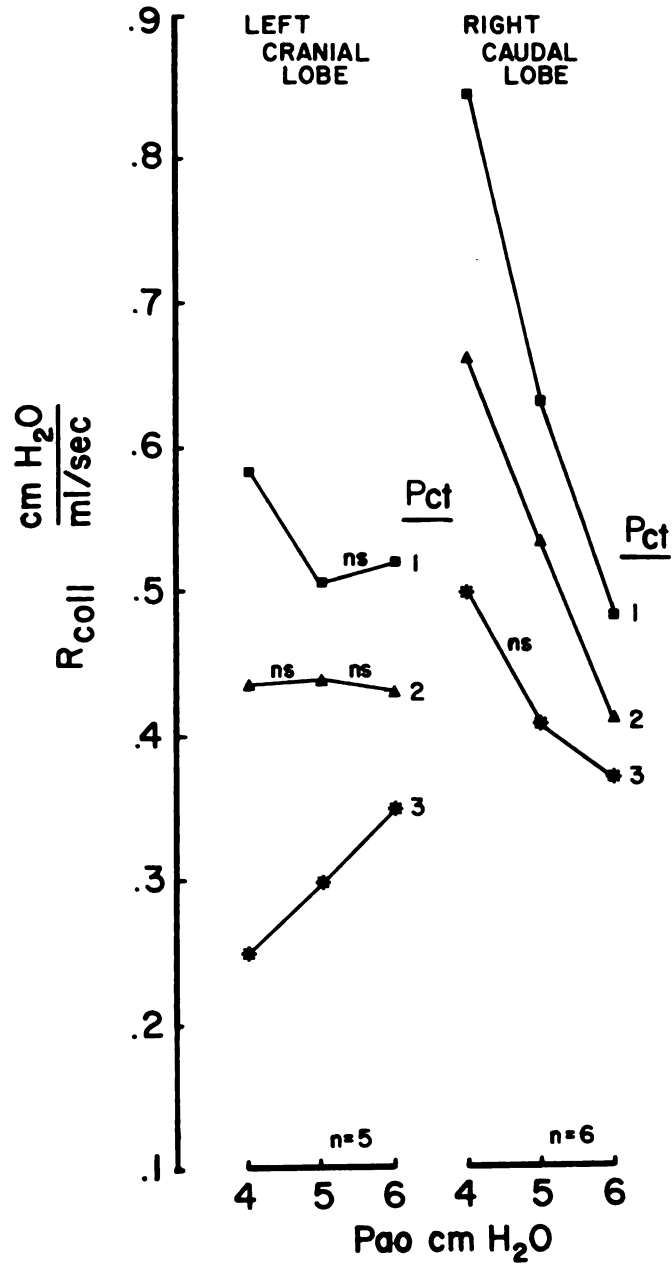


Figure 2-3A

Figure 2-3B. Same data as in Figure 2-3A showing effect of segment-lobar pressure difference ($P_{ao}-P_{ct}$; cm H₂O; abscissa) on collateral resistance [R_{coll} ; cm H₂O/(ml/sec); ordinate] at different values of transpulmonary pressure (P_{ao} ; cm H₂O) in excised dogs' lungs when the segment was deflated relative to the lobe. All adjacent points when P_{ao} is constant are significantly different.

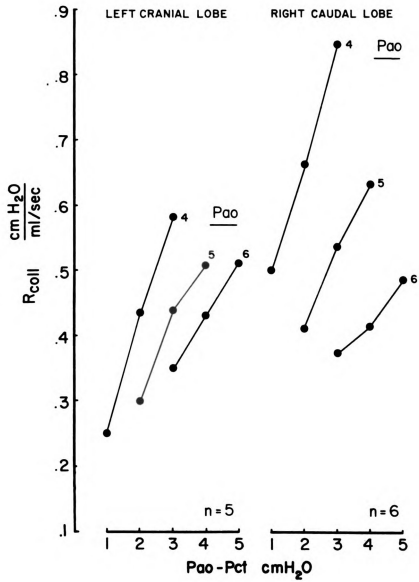


Figure 2-3B

Discussion

Figures 2-1A and 2-2A show that raising transpulmonary pressure decreased R_{coll} when P_{ct} was held constant, while raising P_{ct} increased R_{coll} when transpulmonary pressure was held constant. In addition, R_{coll} changed more when transpulmonary pressure was decreased by 1 cm H_2O at a constant P_{ct} than when P_{ct} was increased by 1 cm H_2O at a constant transpulmonary pressure. Since each of these maneuvers raises $P_{ct}-P_{ao}$ by 1 cm H_2O , transpulmonary pressure was a stronger determinant of R_{coll} than was P_{ct} . Increasing transpulmonary pressure increases both lobar and segment volume (11, 19) which probably accounts for the majority of this effect. In addition, raising transpulmonary pressure at a constant positive P_{ct} tends to restore homogeneity between the segment and the lobe by reducing P_s-P_{ao} and may therefore reduce the tissue distortion caused by the inhomogeneity at the segment-lobe parenchymal interface. Reducing this distortion may contribute to the effect of transpulmonary pressure on R_{coll} .

The increased R_{coll} resulting from increased $P_{ct}-P_{ao}$ at constant transpulmonary pressure (Figures 2-1B and 2-2B) would appear to be at variance with the known effect of lung volume on R_{coll} . If R_{coll} is decreased by raising lobar volume (5, 12), it would seem that R_{coll} should also be decreased by raising $P_{ct}-P_{ao}$ which increases segment volume. Clearly, this does not occur in my preparation. It is possible R_{coll} was overestimated because turbulence was created in the segment by the higher collateral flow rates (\dot{V}_{coll}) necessary to raise $P_{ct}-P_{ao}$. To estimate the degree of turbulence in the segment, Reynolds' number

was calculated according to equation 11 ($Re = \rho dv/\mu$), where ρ is the density of air (1.14×10^{-3} gm/ml), μ is the viscosity of air [1.9×10^{-4} gm/(sec \cdot cm)], d is the diameter of the wedged catheter tip (0.5 cm o.d.), $v = \dot{V}/A$, \dot{V} is the averaged lowest and highest flow rates used in the experiments, and A is the cross-sectional area of the wedged catheter tip. The values of Re are indicated in Table 2-2. In all experiments, Re lies far below the value of 2000 which is required for fully developed turbulent flow to occur in straight, smooth tubes. Olson et al. (15), using dogs' lungs, conclude that when Re is less than 100, flow through the segment is laminar, and when Re is between 100 and 1000, their data indicate that flow is transitional. This suggests my results are not caused by fully developed turbulent flow because Re indicate only laminar and transitional flow. However, Olson et al. (15) took measurements with the segment inflated to $Pct-Pao = 3$ cm H_2O at transpulmonary pressure = 0(FRC), 2, and 4 cm H_2O . The present study uses a wider range of transpulmonary pressures and $Pct-Pao$ in both excised and intact lungs. The Re at which turbulence occurs in the present study may therefore be different than reported by Olson et al. (15). In addition, it is possible that the bronchus in which the catheter was wedged does not represent the smallest cross-sectional area in the isolated segment, and therefore the Re 's may be underestimated. However, if a high degree of turbulence was present, the slopes of Figures 2-1B and 2-2B should be steepest at the higher $Pct-Pao$ where the greatest \dot{V}_{coll} occur. Since none of the curves exhibit

Table 2-2. Values of Reynolds' number (Re) for each series of experiments. Numbers were calculated using the average lowest and highest collateral flows.

Series	Left Cranial Lobe		Right Caudal Lobe	
	Low Flow	High Flow	Low Flow	High Flow
1	73.1	278.1	87.2	332.0
2	44.4	157.6	108.6	322.8
3	61.2	146.9	30.6	157.6

this tendency, it is unlikely that turbulence is the primary cause of these results.

I propose to explain my observations using a hypothesis with three assumptions: (1) calculations of R_{coll} use measurements of the pressure difference between the tip of the wedged catheter (P_{ct}) and the airway opening (P_{ao}), so the pressure gradient $P_{ct}-P_{ao}$ consists of pressure gradients along two distinct populations of airways or channels: those lying within the body of the segment contributing their component of R_{coll} (R_s), and those passing through the parenchymal interface between the segment and the lobe contributing their component of R_{coll} (R_i). The resistance of the lobar airways outside the segment are not considered because this is negligible (6). (2) Regional inhomogeneity creates an area of tissue distortion at the parenchymal

interface between the segment and the lobe. (3) The resistance in the airways and collateral channels within the segment (R_s) decreases as segment volume is raised, correlating with the observation that airway resistance decreases as lung volume is raised (9). Thus, small increases in $P_{ct}-P_{ao}$ should markedly decrease R_s at low transpulmonary pressures while having little effect on R_s at higher transpulmonary pressures.

Assembling these assumptions provides a possible explanation for my data. Regional inhomogeneity created by inflating the segment relative to the lobe has opposing effects on the two populations of collateral channels. The net change in R_{coll} as measured by the wedged catheter technique is determined by the initial magnitudes and relative changes of each component. At low transpulmonary pressures, raising $P_{ct}-P_{ao}$ decreases R_s and increases R_i ; the magnitudes of these changes approximate each other, so R_{coll} remains unchanged. At higher transpulmonary pressures, raising $P_{ct}-P_{ao}$ causes little change in R_s , but interface distortion raises R_i , and R_{coll} increases.

I anticipated that differences in segment geometry affect the interrelationship between R_s and R_i . Raising $P_{ct}-P_{ao}$ should greatly increase segment volume in the excised left cranial lobe, because this segment is very compliant due to its large pleural surface-to-volume ratio and has little interdependence with the surrounding lobe (16). The expected large decrease in R_s must be exceeded by an even larger increase in R_i , however, since raising $P_{ct}-P_{ao}$ increases R_{ao} . This seems plausible because R_i must initially be very high since relatively

few collateral channels would pass through the small parenchymal interface surface available. Tissue distortion resulting from regional inhomogeneity need cause only a small percentage increase in R_i to exceed the large decrease in R_s .

In the right caudal lobe segment, raising Pct-Pao should cause a smaller increase in segment volume, because this segment is less compliant due to its smaller pleural surface-to-volume ratio and its greater interdependence with the surrounding lobe (16). The resulting decrease in R_s must be accompanied by a larger increase in R_i whose initial value is probably low because the large parenchymal surface of this segment likely contains many collateral channels. The initially lower R_i must undergo a larger percentage increase during regional inhomogeneity in order to exceed the decrease in R_s , and this is possible because the larger parenchymal surface provides a greater area in which tissue distortion may occur. Thus, in the right caudal lobe segment, R_i may be initially lower but experience a larger percentage increase during regional inhomogeneity, whereas in the left cranial lobe segment R_i may be initially higher but experiences a smaller percentage increase during regional inhomogeneity.

Three further observations require explanation. First, a comparison of Figures 2-1B and 2-2B shows that raising Pct-Pao increases R_{coll} at a lower transpulmonary pressure in excised than in intact lungs. This may be related to the different relationship between airway resistance and lung volume described for excised and intact lungs (9). During inflation of excised lungs, airway resistance falls steeply to

a minimum at a volume slightly above residual volume and then changes little at higher lung volumes (9). This suggests that airways and collateral channels in the body of the segment represented by R_s are maximally dilated at low lung volumes. When P_{ct-Pao} is raised, therefore, the associated increase in R_i would be unopposed by a concomitant decrease in R_s at low lung volumes. During inflation of intact lungs, however, airway resistance decreases steeply as lung volume initially increases from residual volume, and it continues to decrease, albeit more gradually, at higher lung volumes (9). This suggests that the airways and collateral channels represented by R_s are not fully dilated until higher lung volumes are achieved. Thus, when P_{ct-Pao} is raised, the associated increase in R_i would be opposed by a concomitant decrease in R_s up to higher lung volumes.

Second, R_{coll} in the caudal lobes is lower than in the cranial lobes. This may be related to the geometry of the isolated segments. Caudal lobe segments have a large parenchymal surface (16) through which many intersegmental pathways may pass, resulting in low R_{coll} . Cranial lobe segments have a small parenchymal surface area (16) through which few intersegmental pathways may pass, resulting in higher R_{coll} . This lobar variation, therefore, may be due to differences in the initial magnitudes of R_i .

Third, R_{coll} was greater in intact than in excised lungs, and the difference was greater for the left cranial lobe than for the right caudal lobe. This was unexpected because larger segments were probably isolated in the intact lungs (where the bronchoscope was wedged at FRC

as opposed to the catheter being wedged at TLC in excised lungs), and larger segments are associated with a lower R_{coll} (16). The explanation is not clear but is likely not related to vagal tone since there is no difference in R_{coll} in pre- and post-vagotomy open chest dogs (14). It is doubtful that the presence of perfusion in the intact lungs influenced the difference in R_{coll} between intact and excised lungs. Pulmonary venous pressures would need to exceed 25 mm Hg in excised lungs before affecting R_{coll} at the transpulmonary pressures used in the present study (4).

Several other factors may theoretically contribute to the difference in R_{coll} between intact and excised lungs. Raising $P_{ct}-P_{ao}$ may expand the segment differently in these two preparations because the chest wall may prevent the segment in intact lungs from expanding toward the pleural surface. Raising $P_{ct}-P_{ao}$ would then expand the segment inwardly, causing more distortion at the interface and resulting in an increased R_i and thus R_{coll} . In contrast, the segment in excised lungs may expand toward the pleural surface with only moderate distortion at the interface, resulting in a lower R_{coll} . In addition, because nonhomogeneous segment compliance is less in intact lungs than in excised lungs (11, 13), a given increase in $P_{ct}-P_{ao}$ will cause a smaller increase in segment volume in the former than the latter. This would cause R_s to be greater in intact than in excised lungs and may contribute to the higher R_{coll} in intact lungs.

If segment expansion causes the resistances of the two populations of collateral channels to change in opposite directions, segment deflation should cause different behavior: R_s should increase because

segment volume is reduced (5, 12), and R_i should also increase due to tissue distortion at the interface. Since both resistances should change in the same direction, increasing $P_{ao}-P_{ct}$ should cause a greater increase in R_{coll} than when R_s and R_i change in opposite directions. Series three experiments used a similar range of transpulmonary pressures and $P_{ct}-P_{ao}$ as in series one and two. Data in Figure 2-3A indicate that raising transpulmonary pressure decreased R_{coll} in the right caudal lobe but not in the left cranial lobe. Since raising transpulmonary pressure at a constant negative P_{ct} increases regional inhomogeneity, and since we earlier suggested that R_i is initially very high in the left cranial lobe segment, the failure of R_{coll} to decrease in the left cranial lobe may be caused by a large increase in R_i resulting from the increasing inhomogeneity. In addition, the lack of segment-lobar interdependence results in little increase in segment volume as transpulmonary pressure is raised and therefore probably little decrease in R_s . Data in Figure 2-3B indicate that with deflation, raising $P_{ao}-P_{ct}$ increased R_{coll} much more than inflation of either intact or excised lungs (Figures 2-1 and 2-2). This correlates with our expectation that when intrasegmental and intersegmental airways change their resistances in the same direction, greater changes in measured R_{coll} result.

In conclusion, I have shown that regional inhomogeneity increased R_{coll} in excised and intact dogs' lungs. Although it is possible that turbulent gas flow occurred in the segment, I feel these findings more likely result from distortion of airways at the segment-lobar interface.

LIST OF REFERENCES

Chapter II

1. Enjeti, S., J. T. O'Neill, P. B. Terry, H. A. Menkes, and R. J. Traystman. Sublobar atelectasis and regional blood flow. J. Appl. Physiol.: Respirat. Environ. Exercise Physiol. 47: 1245-1250, 1979.
2. Enjeti, S., P. B. Terry, H. A. Menkes, and R. J. Traystman. Mechanical factors and the regulation of perfusion through atelectatic lung in pigs. J. Appl. Physiol.: Respirat. Environ. Exercise Physiol. 52: 647-654, 1982.
3. Ford, G. T., C. A. Bradley, and N. R. Anthonisen. Forces involved in lobar atelectasis in intact dogs. J. Appl. Physiol.: Respirat. Environ. Exercise Physiol. 48: 29-33, 1980.
4. Fuller, S. D., N. E. Robinson, and J. B. Scott. Effect of pulmonary venous pressure on steady-state collateral resistance. J. Appl. Physiol.: Respirat. Environ. Exercise Physiol. 49: 643-648, 1980.
5. Hilpert, P. Collaterale ventilation Habilitations-schrift, Ans. der Medizinischen (Ph.D. Thesis), pp. 19-20. Tubingen W. Germany: Universitätsklinik, 1970.
6. Hogg, J. C., P. T. Macklem, and W. M. Thurlbeck. The resistance of collateral channels in excised human lungs. J. Clin. Invest. 48: 421-431, 1969.
7. Inners, C. R., P. B. Terry, R. J. Traystman, and H. A. Menkes. Collateral ventilation and the middle lobe syndrome. Am. Rev. Respir. Dis. 118: 305-310, 1978.
8. Kaplan, J., R. C. Koehler, P. B. Terry, H. A. Menkes, and R. J. Traystman. Effect of lung volume on collateral ventilation in the dog. J. Appl. Physiol.: Respirat. Environ. Exercise Physiol. 49: 9-15, 1980.
9. Macklem, P. T., A. J. Woolcock, J. C. Hogg, J. A. Nadel, and N. J. Wilson. Partitioning of pulmonary resistance in the dog. J. Appl. Physiol. 26: 798-805, 1969.

10. Mead, J., T. Takishima, and D. Leith. Stress distribution in lungs: a model of pulmonary elasticity. J. Appl. Physiol. 28: 596-608, 1970.
11. Menkes, H., G. Gamsu, R. Schroter, and P. T. Macklem. Interdependence of lung units in isolated dog lungs. J. Appl. Physiol. 32: 675-680, 1972.
12. Menkes, H., D. Lindsay, G. Gamsu, L. Wood, A. Muir, and P. T. Macklem. Measurement of sublobar lung volume and collateral flow resistance in dogs. J. Appl. Physiol. 35: 917-921, 1973.
13. Menkes, H., D. Lindsay, L. Wood, A. Muir, and P. T. Macklem. Interdependence of lung units in intact dog lungs. J. Appl. Physiol. 32: 681-686, 1972.
14. Olson, L. E. and N. E. Robinson. Effect of vagal stimulation on collateral flow resistance in dog lungs. J. Appl. Physiol.: Respirat. Environ. Exercise Physiol. 49: 287-293, 1980.
15. Olson, L. E., J. R. Rodarte, and N. E. Robinson. Pressure-flow relationships in a collaterally ventilating dog lung segment. J. Appl. Physiol.: Respirat. Environ. Exercise Physiol. 54: 956-960, 1983.
16. Robinson, N. E. and R. Milar. Lobar variations in collateral ventilation in excised dog lungs. Am. Rev. Respir. Dis. 121: 827-834, 1980.
17. Robinson, N. E. and P. R. Sorenson. Collateral flow resistance and time constants in dog and horse lungs. J. Appl. Physiol.: Respirat. Environ. Exercise Physiol. 44: 63-68, 1978.
18. Steel, R. G. D. and J. H. Torrie. Principles and Procedures of Statistics. New York: McGraw-Hill, 1960, pp. 110-111.
19. Sylvester, J. T., H. A. Menkes, and F. Stitik. Lung volume and interdependence in the pig. J. Appl. Physiol. 38: 395-401, 1975.
20. Woolcock, A. J. and P. T. Macklem. Mechanical factors influencing collateral ventilation in human, dog, and pig lungs. J. Appl. Physiol. 30: 99-115, 1971.

CHAPTER III

MECHANISM OF INCREASED COLLATERAL AIRWAY RESISTANCE DURING NONHOMOGENEOUS SEGMENT INFLATION

Introduction

In Chapter II, I reported that inhomogeneous inflation of a sublobar lung segment increases collateral channel resistance (R_{coll}) (2), contrary to the decrease in R_{coll} measured during lobar inflation (2, 3). To explain my findings, I proposed two hypotheses: (1) measurement of R_{coll} during inhomogeneous segment inflation includes the resistances of two populations of airways which are in series: the resistance of intrasegmental airways (R_s) and the resistance of intersegmental airways (R_i) passing through the segment-lobar interface. Inhomogeneous segment inflation increases R_i more than decreasing R_s , causing a net decrease in R_{coll} ; (2) inhomogeneous segment inflation causes nonlaminar gas flow which increases R_{coll} . It is possible that both these mechanisms act simultaneously. The purpose of the present study was to test these hypotheses. After measuring R_{coll} during a variety of inhomogeneities between the segment and the lobe, I analyze the first hypothesis by partitioning R_{coll} into its intrasegmental and intersegmental airway components. I analyze the second hypothesis by comparing R_{coll} measured using air, a low density gas (helium, He), and a high density gas (sulfurhexafluoride, SF_6) to

produce both laminar and nonlaminar gas flow in the segment. A fluid mechanical analysis (8) is used to estimate the segment gas flow regime.

Methods

Mixed-breed dogs were anesthetized with sodium pentobarbital and exsanguinated. The lungs were excised, and the left caudal lobe was used for the experiments. The pleural surface of the excised lobe was kept moist with saline, and the lobe was suspended by the lobar bronchus attached to one arm of a 3-way connector. A second arm of the connector was attached to a variable speed blower which allowed controlled inflation of the lobe. The third arm of the connector was used for passage of a double lumen catheter with a flared tip (4 mm o.d.) into a peripheral airway for calculation of R_{coll} . Transpulmonary pressure (P_{ao}) was measured with a differential pressure transducer (Model PM131, Statham, Hato Rey, Puerto Rico) connected to the lobar bronchus by means of a catheter and needle.

Collateral resistance was calculated by the method of Hilpert (3) (equation 1-1). The double lumen catheter was wedged in a bronchus as the lobe was held at total lobe capacity defined as $P_{ao} = 30 \text{ cm H}_2\text{O}$. With the lobe inflated, the catheter was retracted several millimeters to prevent it from resting against an airway bifurcation. When the lobe was deflated, gentle traction on the catheter depressed the lobar surface, and considerable force was required to remove the catheter, suggesting the catheter securely obstructed the airway. The inner lumen of the catheter was connected to one side of a differential pressure transducer (Model PM131, Statham, Hato Rey, Puerto Rico)

which measured pressure at the catheter tip (Pct) while the other side of the transducer measured Pao, and this allowed measurement of the pressure difference between the catheter tip and the lobar bronchus (Pct-Pao) (see Figure 3-1).

The segment was inflated by directing gas flow from a compressed gas tank into the outer lumen of the wedged catheter as the lobe was held at Pao = 0 cm H₂O. The pleural boundaries of the segment were easily distinguished on the lobar surface. A measurement of the average alveolar pressure in the segment (Ps) was obtained using a modification of the method of Sasaki et al. (10). A 20 gauge needle was used to puncture 20 holes in the segmental pleural surface. The holes were distributed within a 5 mm diameter circle and were approximately 2 mm deep. A fast setting adhesive (Elmer's WonderBond) was used to glue a capsule (10 mm i.d., 17 mm o.d., 10 mm height) to the segment's pleural surface, covering the underlying punctured area (Figure 3-1). A small metal tube (20 gauge, 2 inches in length), which pierced the top of the capsule, was attached to a piece of polyethylene tubing which in turn was connected to one arm of a small 3-way connector. A second arm of this connector was attached via tubing to a differential pressure transducer (Model PM131, Statham, Hato Rey, Puerto Rico) whose other end measured Pct, thus measuring the pressure gradient between the catheter tip and the segmental alveoli (Pct-Ps). The third arm of the 3-way connector was connected by tubing to another differential pressure transducer (Model PM131, Statham, Hato Rey, Puerto Rico) whose other side measured Pao, thus measuring the pressure gradient

Figure 3-1. Illustration of left caudal lobe from an excised dog lung showing double lumen catheter wedged in a bronchus supplying a sublobar segment (shaded area). Helium, air, or sulfurhexafluoride flowed into the outer lumen of the catheter (\dot{V}_{coll}) while the following pressures were measured: pressure at the catheter tip (P_{ct} ; cm H₂O) measured by the inner lumen of the catheter, pressure in the segment subpleural alveoli (P_s ; cm H₂O) measured by a capsule glued over punctures in the segment pleural surface, and transpulmonary pressure (P_{ao} ; cm H₂O) measured at the lobar bronchus. Calculations show collateral resistance [$R_{coll} = (P_{ct} - P_{ao}) / \dot{V}_{coll}$; cm H₂O/(ml/sec)], and its two component resistances: intra²segmental airway resistance [$R_s = (P_{ct} - P_s) / \dot{V}_{coll}$; cm H₂O/(ml/sec)] and intersegmental airway resistance [$R_i = (P_s - P_{ao}) / \dot{V}_{coll}$; cm H₂O/(ml/sec)]. Tracing shows that two capsules on any portion of the segment surface measure the same $P_{ct} - P_s$ pressure drop.

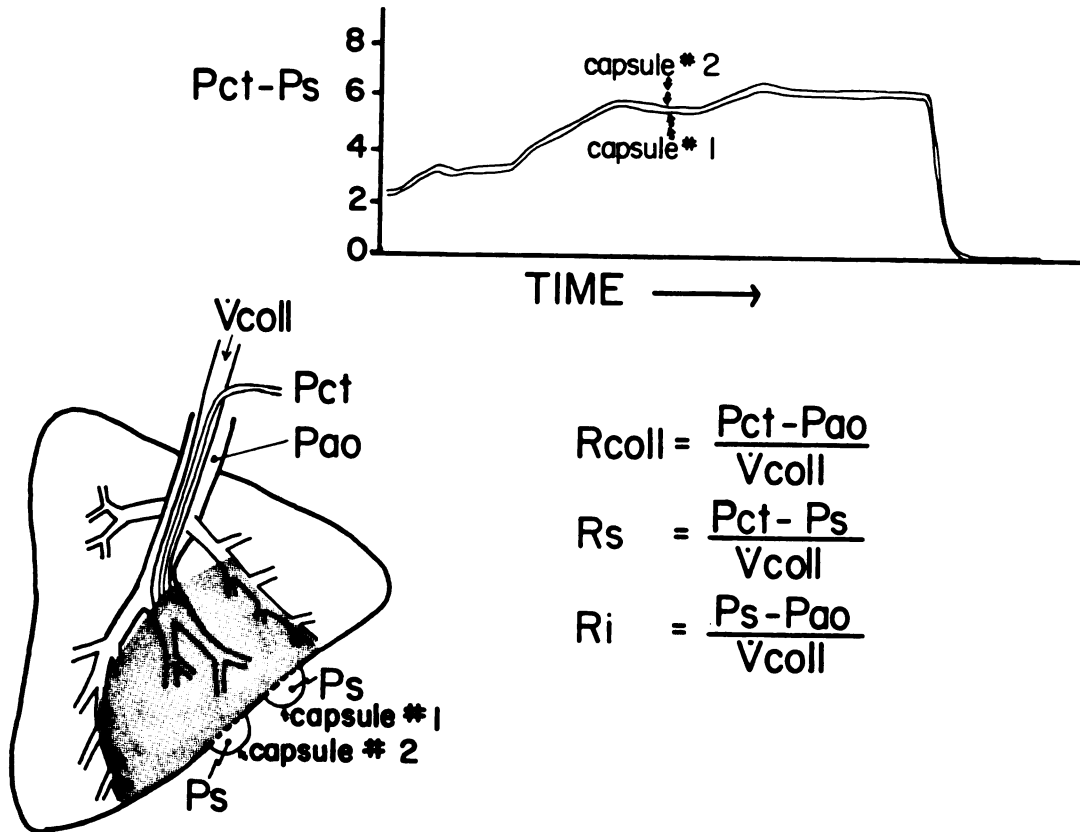


Figure 3-1

between the segmental alveoli and the airway opening ($P_s - P_{ao}$). Gas flow (\dot{V}_{coll}) was adjusted with a rotameter (Model 7431T, Matheson, East Rutherford, New Jersey) until a desired steady state pressure gradient between the catheter tip and the airway opening ($P_{ct} - P_{ao}$) was achieved. The following calculations were then made: resistance through the entire segment [$R_{coll} = (P_{ct} - P_{ao}) / \dot{V}_{coll}$], resistance between the catheter tip and the segmental subpleural alveoli [segment resistance, $R_s = (P_{ct} - P_s) / \dot{V}_{coll}$], and resistance between the segmental subpleural alveoli and the airway opening [interface resistance, $R_i = (P_s - P_{ao}) / \dot{V}_{coll}$]. The position of the capsule on the segment's pleural surface did not influence P_s , for when two capsules were glued to a distended segment and \dot{V}_{coll} was varied, the two $P_{ct} - P_s$ pressure gradients were the same (see Figure 3-1).

Resistances were calculated during inhomogeneous segment inflation to seven different pressures ($P_{ct} - P_{ao} = 1, 2, 3, 4, 5, 6,$ and $7 \text{ cm H}_2\text{O}$), during which the lobe was held at each of 5 different transpulmonary pressures ($P_{ao} = 2, 3, 4, 5,$ and $6 \text{ cm H}_2\text{O}$). This was done in the following manner: the lobe was slowly inflated to $P_{ao} = 30 \text{ cm H}_2\text{O}$ and then deflated to the desired P_{ao} where it remained for approximately one minute. During this time, \dot{V}_{coll} was adjusted to raise $P_{ct} - P_{ao}$ sequentially in step increments to 1, 2, 3, 4, 5, 6, and 7 $\text{cm H}_2\text{O}$, and each \dot{V}_{coll} was maintained for several seconds to obtain steady state conditions. The P_{ao} and $P_{ct} - P_{ao}$ pressure tracings were recorded on a photorecording oscilloscope (Model VR12, Electronics for Medicine, White Plains, New York), and

the \dot{V}_{coll} recorded at each Pct-Pao was used to calculate R_{coll} , R_s , and R_i . Measurements were made in duplicate, and the two values were averaged. During all measurements, air was used to ventilate the lobe. This entire protocol was performed three times, each time using a different gas to inflate the segment (first air, then helium, then SF_6). The physical properties of air, helium, and SF_6 are shown in Table 3-1. When using either helium or SF_6 , the segment was initially flushed with approximately 300 ml of this gas at each Pao before making any measurements, ensuring that the concentration of the gas in the segment was not diluted by the room air used to inflate the lobe. Air and helium data were obtained from six dogs and SF_6 data from five dogs.

Table 3-1. Physical properties of gases [helium (He), air, and sulfurhexafluoride (SF_6)] used in calculation of collateral resistance.

	He	Air	SF_6
μ [gm/(sec · cm)]	1.94×10^{-4}	1.90×10^{-4}	1.33×10^{-4}
ρ (gm/ml)	1.80×10^{-4}	1.14×10^{-3}	6.60×10^{-3}

μ = viscosity.

ρ = density.

The effect of gas physical properties of R_{coll} , R_s , and R_i was initially assessed by comparing these resistances when using the three different gases. The flow regime in the segment was further assessed using a fluid mechanical approach described by Moody (8). This consists of analyzing the pressure-flow relationships in the segment by constructing a diagram (referred to as a Moody diagram, Figure 1-6) of the logarithm of the ratio of the static pressure drop to dynamic pressure (i.e., the normalized pressure drop, equation 1-15) against the logarithm of Reynolds' number [equation 1-11, $Re = (\rho dv)/\mu$], where $\Delta P = P_{ct} - P_{ao}$ (cm H_2O), $v = \dot{V}_{coll}/A$ (cm/sec), ρ is gas density (gm/ml), μ is gas viscosity [gm/(sec · cm)], and d and A are the diameter (cm) and cross sectional area (cm²) of the wedged airway. I assumed that the diameter of the wedged airway equalled the diameter of the flared tip catheter (0.4 cm). The Moody analysis assumes that when the geometry of the airways is constant, P_n is solely a function of Re . Varying Re should result in a single curve with a slope of -1 if flow is laminar, 0 if flow is turbulent, and between -1 and 0 if flow is transitional (see Figure 1-5). I assumed that identical segment geometry resulted when the segment was inflated to the same pressure with each of the three gases.

The effects of increasing $P_{ct} - P_{ao}$ and P_{ao} on R_{coll} , R_s , and R_i , respectively, were analyzed using a randomized complete block analysis of variance (11). Means were compared using the Student-Newman-Keul's procedure, and differences were considered statistically significant at $p < .05$.

Results

Figure 3-2 shows the effect of inhomogeneous segment inflation (raising Pct-Pao at constant Pao) on Rcoll, Rs, and Ri at five different Pao. In general, raising Pct-Pao increased Rcoll, Rs, and Ri measured when air and SF₆ were the inflating gas but had no effect on these resistances measured when helium was used. Figure 3-3 uses the same data as in Figure 3-2 to illustrate the effect of Pao on Rcoll, Rs, and Ri at seven different Pct-Pao. Increasing Pao decreased Rcoll, Rs, and Ri measured with each gas at all Pct-Pao.

Table 3-2 shows Rs expressed as a fraction of Rcoll (Rs/Rcoll). During helium inflation, Rs/Rcoll was unaffected by increasing Pct-Pao. During air inflation, Rs/Rcoll tended to increase with increases in Pct-Pao, but these changes were statistically insignificant at the $p < .05$ level. During SF₆ inflation, however, Rs/Rcoll increased as Pct-Pao increased from 1-7 cm H₂O at a constant Pao. Raising Pao at a constant Pct-Pao caused no significant changes in Rs/Rcoll during both air and helium inflation but decreased Rs/Rcoll during SF₆ inflation.

In Figure 3-4, Log Pn is plotted as a function of Log Re (Moody diagram; see Figure 1-6). Data points obtained when the segment was inflated with He are shown as circles, air as triangles, and SF₆ as squares. Each panel represents data obtained at a constant 2, 3, 4, 5, and 6 cm H₂O. All helium data lie on a line with a slope of -1 indicating laminar flow, all air data lie on a line deviating slightly from a slope of -1 indicating transitional flow, and all SF₆ data lie on a line with a slope closer to 0 indicating transitional to

Figure 3-2. Effect of segment inflation by raising the segment-lobar pressure gradient ($P_{ct}-P_{ao}$; cm H₂O; abscissa) on total collateral resistance [R_{coll} ; cm H₂O/(ml/sec); ordinate], top panel; intrasegmental airway resistance [R_s ; cm H₂O/(ml/sec); ordinate], middle panel, and intersegmental airway resistance [R_i ; cm H₂O/(ml/sec), ordinate], bottom panel, at five transpulmonary pressures ($P_{ao} = 2-6$ cm H₂O). The lobe was inflated with air while the segment was inflated with helium, air, or sulfurhexafluoride (SF₆).

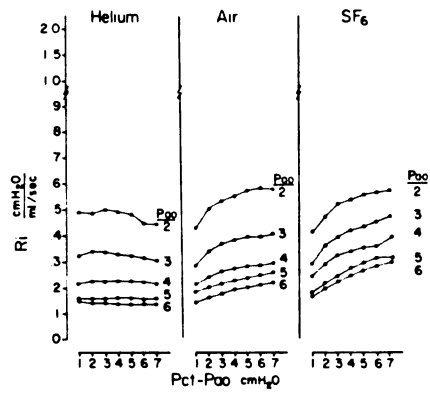
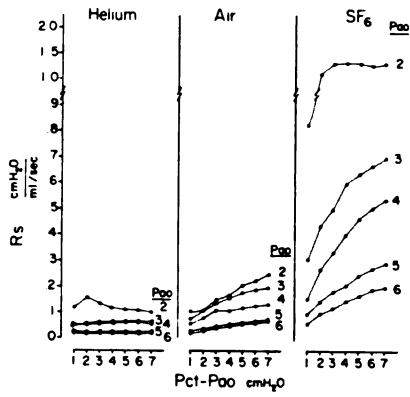
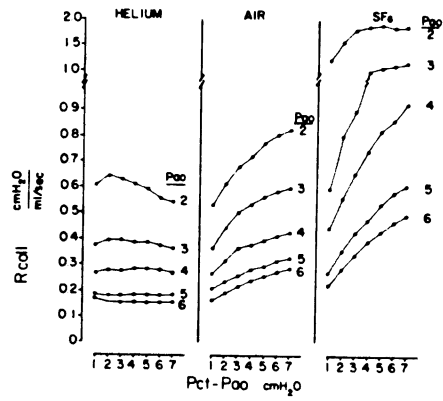


Figure 3-2

Figure 3-3. Same data as Figure 3-2 showing the effect of transpulmonary pressure (P_{ao} ; cm H_2O ; abscissa) on total collateral resistance [R_{coll} ; cm H_2O /(ml/sec), ordinate], top panel; intrasegmental airway resistance [R_s ; cm H_2O /(ml/sec), ordinate], middle panel; and intersegmental airway resistance [R_i ; cm H_2O /(ml/sec), ordinate], bottom panel; as the segment-lobar pressure gradient was held constant at seven values ($P_{ct}-P_{ao} = 1-7$ cm H_2O). The lobe was inflated with air while the segment was inflated with helium, air, or sulfurhexafluoride (SF_6).

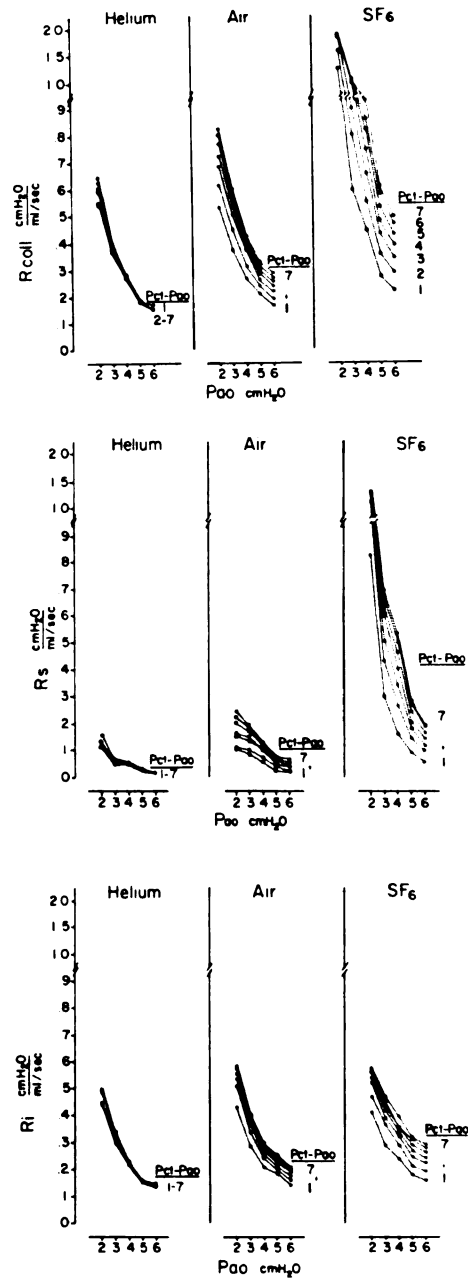


Figure 3-3

Table 3-2. Intrasegmental airway resistance (R_s) expressed as a fraction of collateral resistance (R_{coll}) (R_s/R_{coll} , $\bar{x} \pm SEM$) as the segment was inflated to a segment-lobar pressure difference ($Pct-Pao$) = 1-7 cm H₂O at transpulmonary pressure (Pao) = 2-6 cm H₂O in the left caudal lobes of excised dogs' lungs.

	Pct-Pao	Helium	Air	SF ₆
Pao = 2	1	.18 ± .09	.16 ± .05	.49 ± .11
	2	.20 ± .09	.16 ± .04	.59 ± .11
	3	.20 ± .06	.20 ± .04	.64 ± .08
	4	.18 ± .05	.20 ± .04	.64 ± .10
	5	.18 ± .04	.22 ± .05	.64 ± .09
	6	.18 ± .04	.23 ± .05	.65 ± .09
	7	.17 ± .04	.24 ± .06	.66 ± .09
Pao 3	1	.13 ± .02	.20 ± .04	.45 ± .10
	2	.14 ± .02	.21 ± .05	.47 ± .09
	3	.15 ± .02	.23 ± .05	.50 ± .09
	4	.15 ± .02	.24 ± .04	.52 ± .09
	5	.16 ± .03	.25 ± .06	.55 ± .09
	6	.16 ± .03	.25 ± .06	.56 ± .09
	7	.16 ± .03	.26 ± .07	.56 ± .09
Pao 4	1	.17 ± .05	.19 ± .04	.42 ± .08
	2	.18 ± .05	.21 ± .04	.46 ± .08
	3	.19 ± .06	.25 ± .06	.50 ± .08
	4	.19 ± .06	.23 ± .06	.52 ± .09
	5	.20 ± .05	.24 ± .06	.54 ± .09
	6	.21 ± .05	.24 ± .07	.56 ± .09
	7	.19 ± .04	.25 ± .07	.56 ± .09
Pao 5	1	.13 ± .03	.11 ± .03	.40 ± .06
	2	.12 ± .02	.14 ± .03	.41 ± .06
	3	.12 ± .02	.16 ± .03	.43 ± .06
	4	.13 ± .02	.18 ± .04	.46 ± .06
	5	.13 ± .02	.18 ± .04	.47 ± .06
	6	.14 ± .02	.19 ± .05	.48 ± .06
	7	.14 ± .02	.20 ± .05	.48 ± .07
Pao 6	1	.11 ± .02	.10 ± .03	.24 ± .07
	2	.10 ± .01	.13 ± .03	.30 ± .08
	3	.10 ± .01	.17 ± .03	.32 ± .08
	4	.10 ± .01	.18 ± .04	.34 ± .09
	5	.11 ± .01	.20 ± .04	.36 ± .09
	6	.11 ± .01	.21 ± .04	.39 ± .10
	7	.12 ± .02	.22 ± .05	.39 ± .10

Figure 3-4. The logarithm of the normalized pressure drop ($\log P_n$; ordinate) is shown as a function of the logarithm of Reynolds' number ($\log Re$; abscissa) and is referred to as a Moody diagram (Figure 1-6). In each of the five panels transpulmonary pressure (Pao) was held constant at 2-6 cm H₂O while the segment was inflated with helium (circles), air (triangles), or sulfurhexafluoride (SF₆; squares) by raising the segment-lobar pressure gradient to seven values (Pct-Pao = 1-7 cm H₂O). The reference airway dimensions are those of the wedged catheter tip. The dashed line has slope = -1, representing laminar flow.

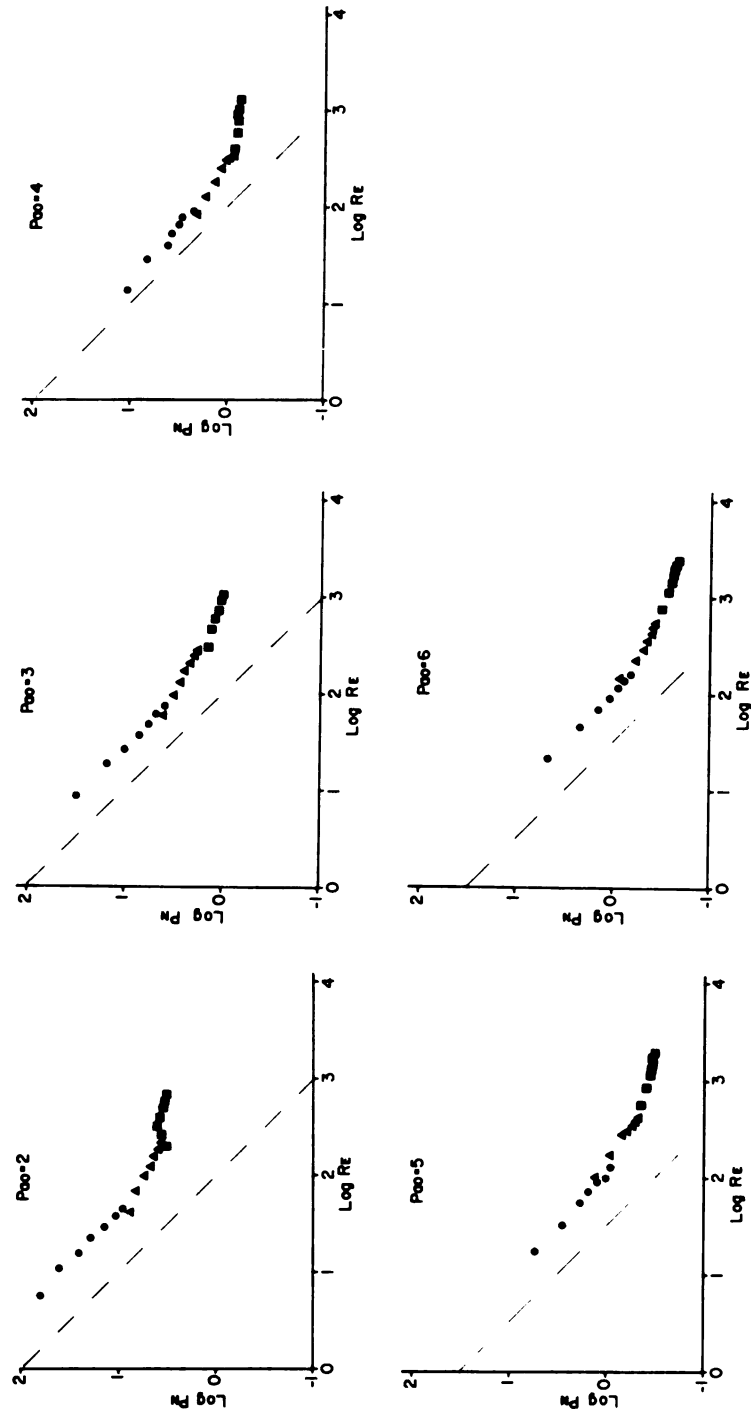


Figure 3-4

turbulent flow. The Re at which the slopes deviated from -1 increased as Pao increased: at Pao = 2 cm H₂O this change occurred at Re = 45 (Log Re = 1.65) whereas at Pao = 6 cm H₂O the change occurred at Re = 150 (Log Re = 2.18).

Data from Figure 3-5 are the same as those in Figures 3-4 with Log Pn plotted as a function of Log Re. Each panel shows data points when the segment was inflated to a constant Pct-Pao with He (circles), air (triangles), and SF₆ (squares). Data obtained at each Pao (2, 3, 4, 5, and 6 cm H₂O) are connected by lines. Laminar and transitional flow were present when Pct-Pao = 1-3 cm H₂O, but transitional and turbulent flow were present at Pct-Pao = 4-7 cm H₂O. Furthermore, at constant Pct-Pao, raising Pao resulted in multiple curves and not in a single curve as occurred when Pct-Pao was raised at constant Pao (Figure 3-4).

Discussion

Segment volume was increased in this study by raising either Pao or Pct-Pao. To distinguish between these two methods of raising segment volume, I refer to "segment inflation" as raising Pct-Pao at constant Pao, and "lobar inflation" as raising Pao at a constant Pct-Pao. I have confirmed my previous observation that segment inflation and lobar inflation have opposing effects on Rcoll (Chapter II) (2), and I have attempted to determine the mechanism of this effect. One of my hypotheses is that Rcoll is the sum of the resistances of two populations of airways in series: intrasegmental airway resistance (Rs) contributed by airways lying in the body of the segment and

Figure 3-5. The logarithm of the normalized pressure drop ($\log P_n$; ordinate) is shown as a function of the logarithm of Reynolds' number ($\log Re$; abscissa) and is referred to as a Moody diagram (Figure 1-6). In each of the seven panels segment inflation (Pct-Pao; cm H₂O) was held constant while transpulmonary pressures (Pao) increased from 2-6 cm H₂O. Lines connecting the points represent constant Pao when the segment was inflated with helium (circles), air (triangles), or sulfurhexafluoride (SF₆; squares). The reference airway dimensions are those of the wedged catheter tip. Dashed line has slope = -1, representing laminar flow.

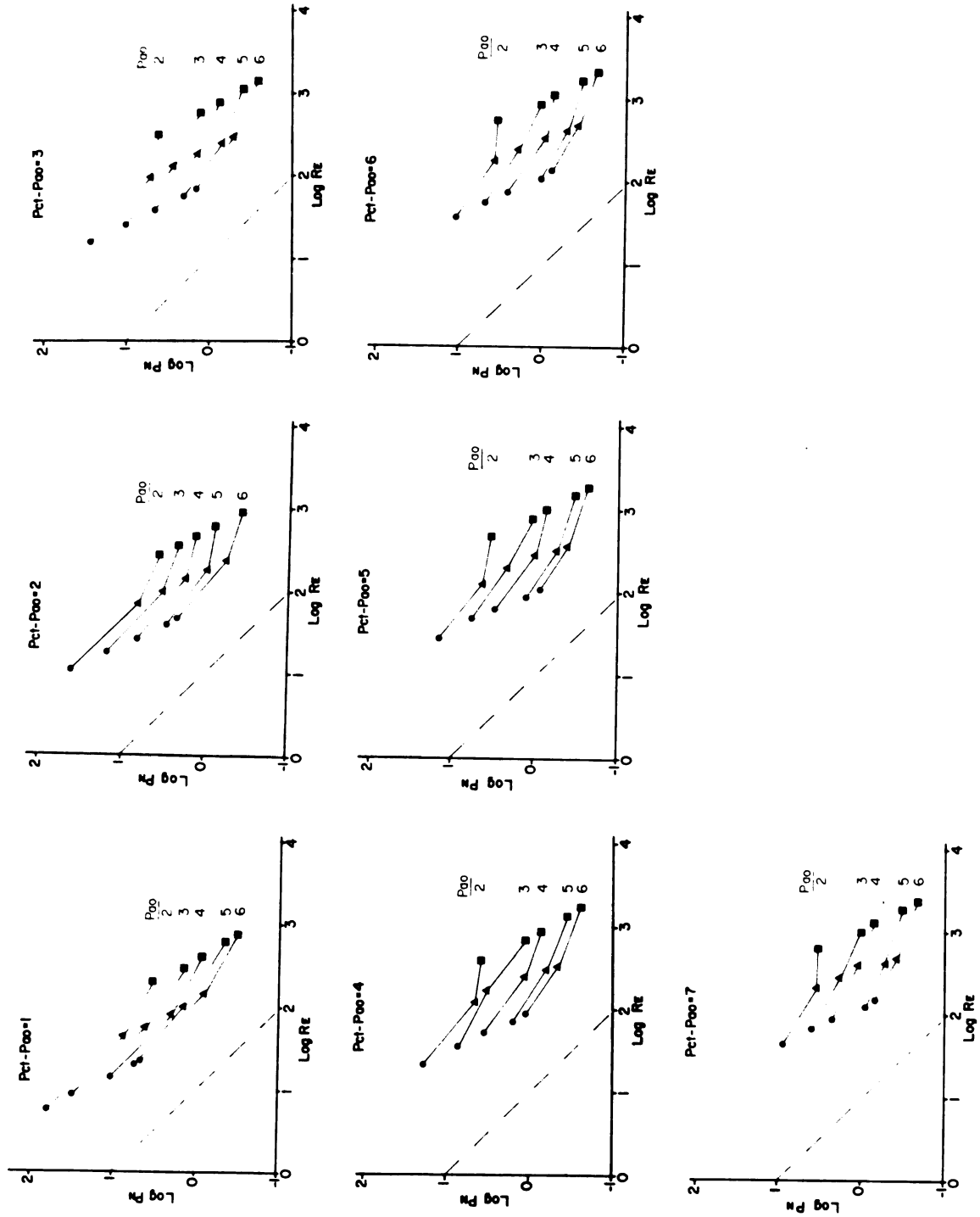


Figure 3-5

intersegmental airway resistance (R_i) contributed by airways coursing through the segment-lobar interface. Accordingly, segment inflation dilates intrasegmental airways and decreases R_s while this inflation distorts intersegmental airways and increases R_i . These opposing effects would tend to minimize any change in R_{coll} . In this study I used a pleural capsule to partition R_{coll} into R_s and R_i , and I made the following assumptions: (1) pressure is uniformly distributed throughout the pleural surface alveoli of the segment (this is supported by the negligible pressure gradient between two capsules glued to different points on the segmental pleural surface, Figure 3-1); (2) capsule pressure (P_s) represents the pressure in the most distal intrasegmental airway in which flow occurs; (3) \dot{V}_{coll} is uniformly distributed throughout the segment; and (4) the distribution of \dot{V}_{coll} within the segment remains constant during segment inflation or lobar inflation.

Irrespective of the gas used, segment inflation caused the same directional changes in R_{coll} , R_s , and R_i , not the opposing changes in R_s and R_i predicted by my hypothesis. Since lobar inflation decreases airway resistance (5, 6), I expected both segment inflation and lobar inflation would dilate intrasegmental airways and decrease R_s . Although R_s was decreased by lobar inflation (Figure 3-3), R_s surprisingly was not decreased by segment inflation (Figure 3-2) even when helium minimized nonlaminar flow caused by the higher \dot{V}_{coll} . This observation suggests that lobar inflation and segment inflation may have different effects on intrasegmental airway geometry. Bronchograms of a segment in a homogeneously inflated lobe and of a segment inflated nonhomogeneously demonstrate that intrasegmental airways dilate under both

conditions (7, 12). When the lobe is inflated homogeneously (i.e., when lobar distending pressure is uniform throughout the lobe, including the segment), the segment changes shape from a short fat cone to a long thin cone as intrasegmental airways lengthen and branching angles decrease (12). During segment inflation, however, the segment becomes more spherical, and branching angles appear to increase. In the present study, the increased branching angles occurring during segment inflation would tend to promote nonlaminar flow (9) and override any decrease in R_s resulting from airway dilation. In contrast, if the geometrical changes occurring during inflation in the present study are similar to those occurring during homogeneous lobar inflation (7, 12), the decreased branching angles would contribute to the measured decrease in R_s .

Examination of the fraction of R_{coll} comprised by R_s (R_s/R_{coll} , Table 3-2) supports nonlaminar gas flow in intrasegmental airways as one cause of the increase in R_{coll} during segment inflation. A comparison of R_s/R_{coll} data during air and He inflation reveals that at each P_{ao} , R_s/R_{coll} with air and R_s/R_{coll} with helium are similar at low $P_{ct}-P_{ao}$ and progressively diverge as $P_{ct}-P_{ao}$ increases. This is due to the trend of R_s-R_{coll} with air to increase during segment inflation, indicating a shift in the distribution of R_{coll} from R_i to R_s , whereas R_s/R_{coll} with helium remains constant. This correlates with the observation in Figure 3-2 that air and He R_{coll} are similar at low $P_{ct}-P_{ao}$, but R_{coll} with air exceeds R_{coll} with helium at high $P_{ct}-P_{ao}$. At low $P_{ct}-P_{ao}$, \dot{V}_{coll} is low and, Moody plots shown in

Figure 3-4 indicate that flow is laminar throughout the segment with both air and He. The Pct-Pao pressure loss is thus viscous dependent, and since the viscosities of air and He are similar, the absolute magnitudes and the distribution of their respective resistances are similar. At high Pct-Pao, however, \dot{V}_{coll} is high, so flow with air is probably nonlaminar, and resistance is density dependent. Thus, R_{coll} with air exceeds R_{coll} with helium. The greater nonlaminar flow occurring with air increases R_s and therefore increases R_s/R_{coll} with air. The increase in R_s as turbulence develops is evident from data when SF_6 was used as the inflating gas (Table 3-4). Even at Pct-Pao = 1 cm H_2O , R_s/R_{coll} with SF_6 is much greater than R_s/R_{coll} with air, and as Pct-Pao increases, R_s/R_{coll} with SF_6 increases even further.

Whereas segment inflation with SF_6 increased R_s/R_{coll} , lobar inflation with SF_6 shifted the distribution of R_{coll} from R_s toward R_i . Although \dot{V}_{coll} and thus R_e increased during both modes of segment inflation, the possible differences in segment geometry suggested earlier (i.e., branching angles increasing during segment inflation but decreasing lobar inflation) may cause increasing nonlaminar flow in the intrasegmental airways during segment inflation, thereby increasing R_s , and decreasing nonlaminar flow during lobar inflation, thereby decreasing R_s .

Analysis of data in Table 3-2 reveals that during segment inflation with SF_6 , R_s exceeds R_i , but during segment inflation with air and helium, R_i greatly exceeds R_s . This indicates that when flow is transitional to turbulent, R_{coll} is principally determined by



intrasegmental airways, but when flow is laminar to transitional, R_{coll} is principally determined by intersegmental airways.

I used a Moody analysis (8) to more specifically characterize the flow regime in the sublobar segment. During segment inflation flow was always laminar with helium, transitional with air, and transitional or turbulent with SF_6 (Figure 3-4). Interestingly, segment inflation resulted in all data points on one smooth curve, indicating that at any given P_{ao} , P_n was solely a function of Re . If segment airway diameter increased during segment inflation, the curve for each consecutively higher P_{ct} - P_{ao} would be shifted in a parallel direction downward and to the right. Since this shift did not occur with segment inflation, several inferences may be made. First, the dimensions of the segment airways may have remained constant during segment inflation, explaining why R_{coll} did not change when nonlaminar flow was minimized (see He curves in Figure 3-3). Second, R_{coll} may have been determined primarily by a high resistance population of airways whose dimensions were fixed, and secondarily by one or more populations of low resistance airways whose dimensions may have varied during segment inflation. The change in R_{coll} resulting from the dimensional changes in this secondary population of airways would not have been measured since their contribution to total R_{coll} would have been small. According to the data in Table 3-2 for air and He (where R_s/R_{coll} is small), R_s might represent the low resistance airways, and R_i might represent the high resistance airways.

In contrast to the data shown in Figure 3-4 obtained during segment inflation (where all points at constant P_{ao} lay on one smooth curve), Figure 3-5 shows that lobar inflation to five different P_{ao} resulted in five separate curves, indicating that P_n was a function of R_e and one or more other variables. The curves in Figure 3-5 were constructed assuming airway diameter and cross sectional area were equal to the dimensions of the wedged catheter tip. However, data in Figure 3-3 show that lobar inflation decreases R_{coll} , probably by dilation of intra- and intersegmental airways since R_i and R_s also decrease. This airway dilation was not accounted for in the curves in Figure 3-5 and may be the reason why these data do not fall on a single curve. If the spread of these curves is due solely to the unaccounted for changes in segment airway diameter occurring during lobar inflation, then compensation for these diameter changes should result in approximation of these curves into a single smooth curve. If, in contrast, other variables in addition to diameter changes cause the spread of these curves, then no amount of compensation for diameter changes would lead to a single smooth curve.

I tried several methods to account for segment airway diameter changes which might occur during lobar inflation. First, I assumed that segment airway diameter changed with the cube root of lobar volume (4). Values of lobar volume and compliance from excised dogs' lungs were obtained from data reported by Frank (1). The diameter of the segment airway at $P_{ao} = 30 \text{ cm H}_2\text{O}$ was assumed to be the diameter of the catheter tip (4 mm) since this is the P_{ao} at which the catheter

was wedged in the airway. As the lobe was deflated from $P_{ao} = 30$ cm H_2O , segment airway diameter was scaled to the cube of lobar volume, and the results of this recalculation are shown in Figure 3-6. Clearly, the data do not approximate a single curve, although closer approximation is evident when compared to the data shown in Figure 3-5.

I next assumed that segment airway diameter is scaled to transpulmonary pressure in the manner described by Hughes et al. (4) for excised dogs' lungs. The results of this recalculation are shown in Figure 3-7. Again, the data do not approximate a single curve, although closer approximation is evident when compared to data in Figure 3-5.

Since segment airway diameter does not scale either with the cube root of lobar volume or with P_{ao} during lobar inflation, I then determined if a single power function would relate lobar volume to segment airway diameter during lobar inflation. If this single power function exists, and if P_n is solely a function of R_e , then all the data shown in each panel of Figure 3-5 should fall on a single curve. In contrast, if multiple power functions are required to unite these separate curves into one single curve, then one or more variables other than segment airway diameter would be necessary to explain the relationship between P_n and R_e . Using the data in Figure 3-5, I adjusted the value of segment airway diameter in such a way as to approximate the curves as closely as possible. I then calculated the power function relating lobar volume to the adjusted diameter.

Figure 3-6. Effect of scaling segment airway diameter to cube root of lobar volume on data in the Moody diagrams illustrated in Figure 3-5. In each of the seven panels, segment inflation (Pct-Pao; cm H₂O) was held constant while transpulmonary pressure (Pao) was increased to Pao = 2-6 cm H₂O. Lines connecting the points represent constant Pao when the segment was inflated with helium (circles), air (triangles), or sulfurhexafluoride (SF₆; squares). Dashed line is slope = -1, representing laminar flow.

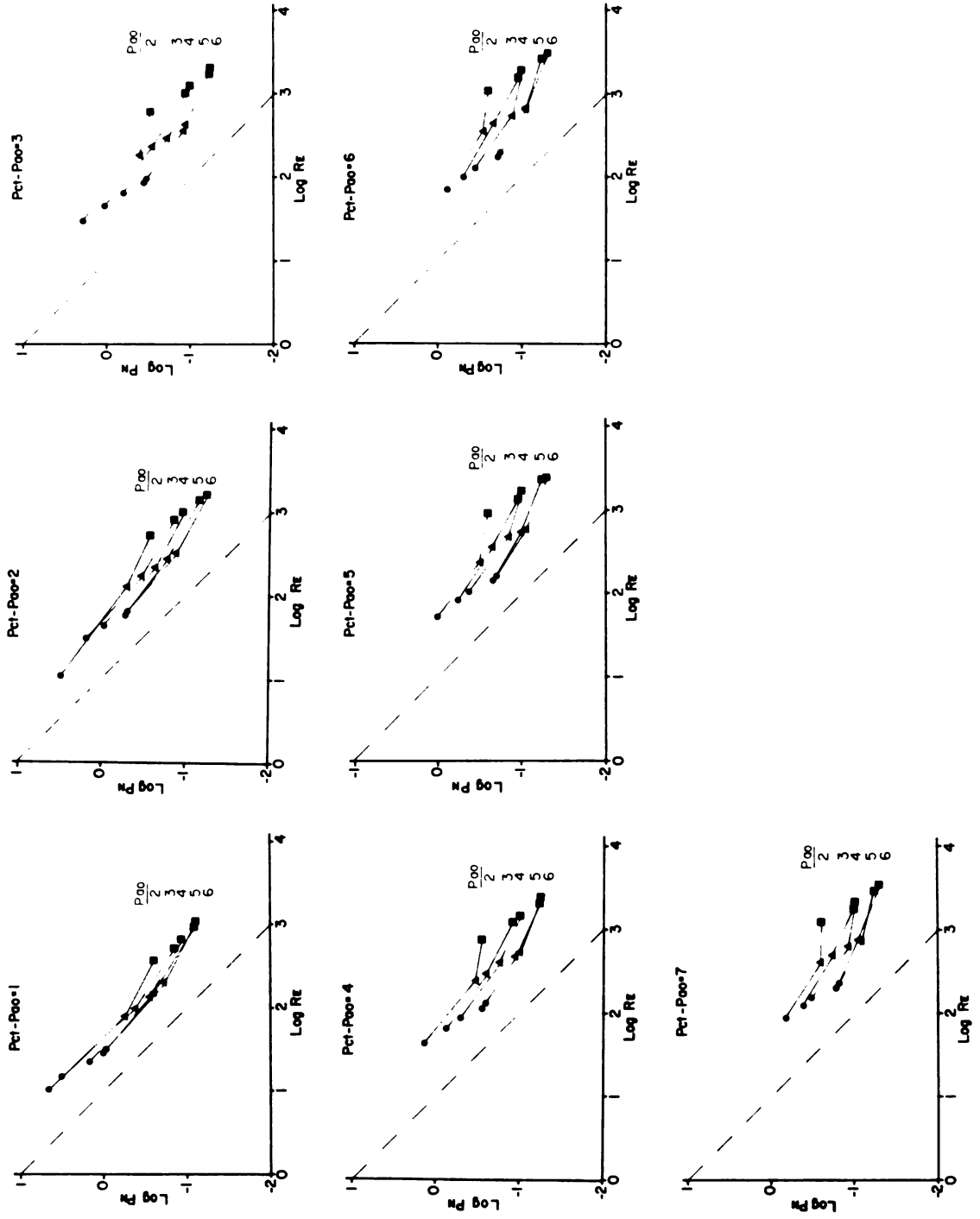


Figure 3-6

Figure 3-7. Effect of scaling segment airway diameter to transpulmonary pressure (Pao) on data in the Moody diagrams illustrated in Figure 3-5. In each of the seven panels, segment inflation (Pct-Pao; cm H₂O) was held constant while Pao was increased to 2-6 cm H₂O. Lines connecting the points represent constant Pao when the segment was inflated with helium (circles), air (triangles), or sulfurhexafluoride (SF₆; squares). Dashed line is slope = -1, representing laminar flow.

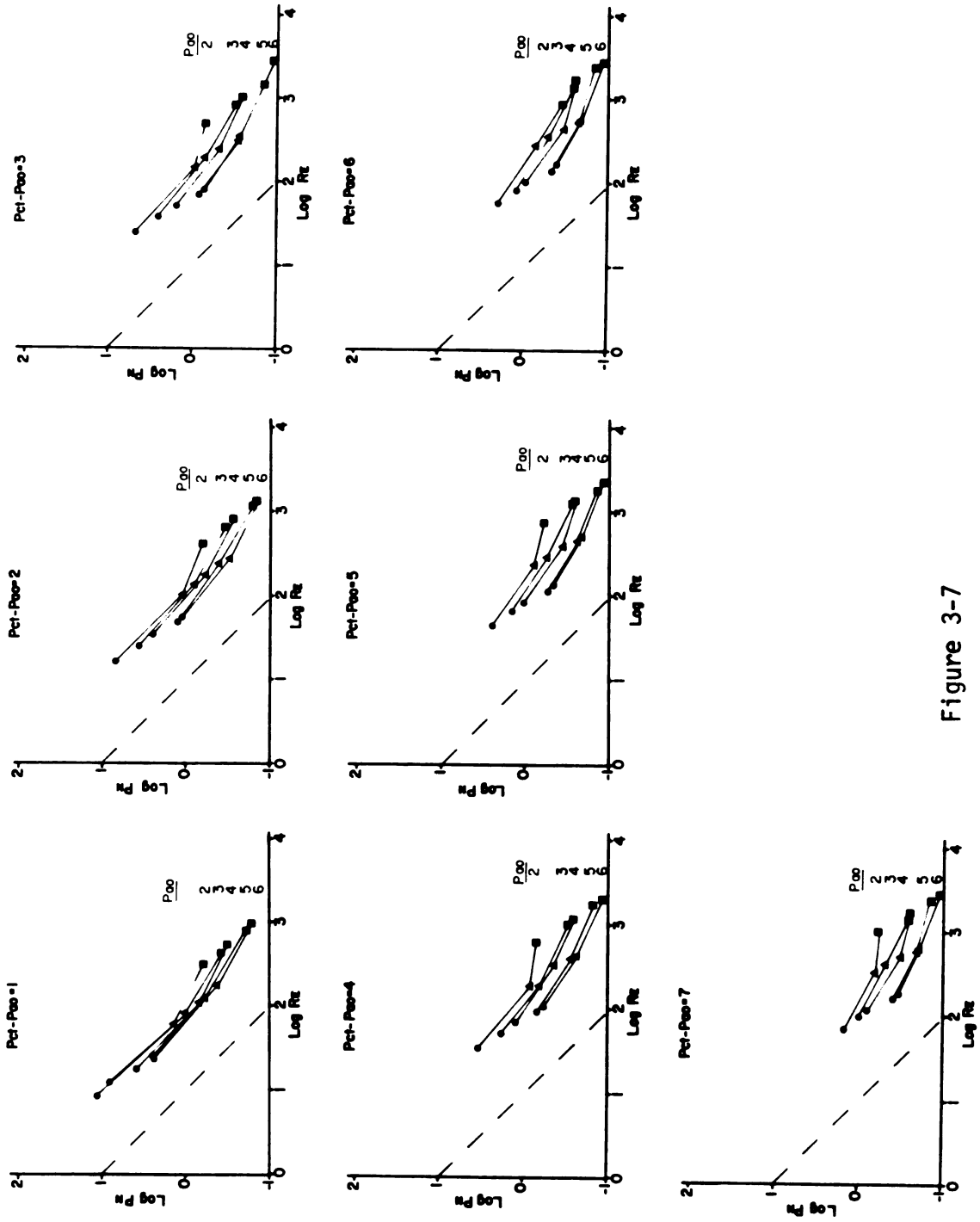


Figure 3-7

I found that at each Pct-Pao, a range of power functions was required to approximate the curves during lobar inflation (see Appendix B). Perhaps all segment airways do not experience the same proportional dimensional changes during lobar inflation. For example, if segment inflation decreases intersegmental airway diameter due to distortion of these airways at the segment-lobar interface (2), the resultant changes in intersegmental airway diameter would be unaccounted for in these computations. In contrast, P_n may be a function of one or more variables in addition to airway diameter and Re .

In conclusion, I have characterized the gas flow regime in a nonhomogeneously inflated sublobar lung segment during a variety of measurement conditions. I have shown that R_{coll} is increased by segment inflation and decreased by lobar inflation. Although non-laminar gas flow accounts for the increase in R_{coll} during segment inflation, I cannot explain why segment inflation fails to decrease R_{coll} in the absence of nonlaminar flow. Perhaps an increase in branching angles of intrasegmental airways or airway distortion at the segment-lobar interface during segment inflation contributes to this paradox.

Several investigators have compared R_{coll} and airway resistance to estimate if a segment in a healthy lung is ventilated primarily by collateral channels or airways, but one of the inherent methodological problems in these comparisons is that R_{coll} is measured during segment inflation while airway resistance is measured during homogeneous lobar inflation. If segment inflation increases R_{coll} , then the comparisons

will overestimate the difference between R_{coll} and airway resistance. Collateral resistance can be estimated under homogeneous conditions (i.e., when $P_{ct}-P_{ao} = 0 \text{ cm H}_2\text{O}$) by using data in Figure 3-2 and extrapolating the curves at each P_{ao} to the ordinate. Assuming the segment occupies 5 percent of the lung, I estimated lobar R_{coll} during homogeneous lobar inflation. Figure 3-8 compares these values of homogeneous R_{coll} to total lung resistance, peripheral airway resistance, and central airway resistance in open chested vagally intact dogs' lungs (5), and to total lung resistance in vagally denervated dogs' lungs (6). Homogeneous R_{coll} is substantially higher than the other resistances at all lung volumes and decreases to a greater extent as the lung is inflated, suggesting that a segment in the healthy lung is ventilated primarily by airways rather than collateral channels.



Figure 3-8. Comparison of the effect of raising lobar volume [plotted as percent vital capacity (VC); abscissa] on the following five resistances (cm H₂O/LPS, where LPS = liters per second): homogeneous collateral resistance [R_{coll} (homogeneous) obtained by extrapolating the curves at each P_{ao} in the center panel of Figure 3-2 to the ordinate]; total lung resistance (R_L) and central (R_c) and peripheral (R_p) airway resistance in vagally intact dogs as reported by Macklem and Mead (5); and R_L in vagotomized dogs as reported by Macklem et al. (6).

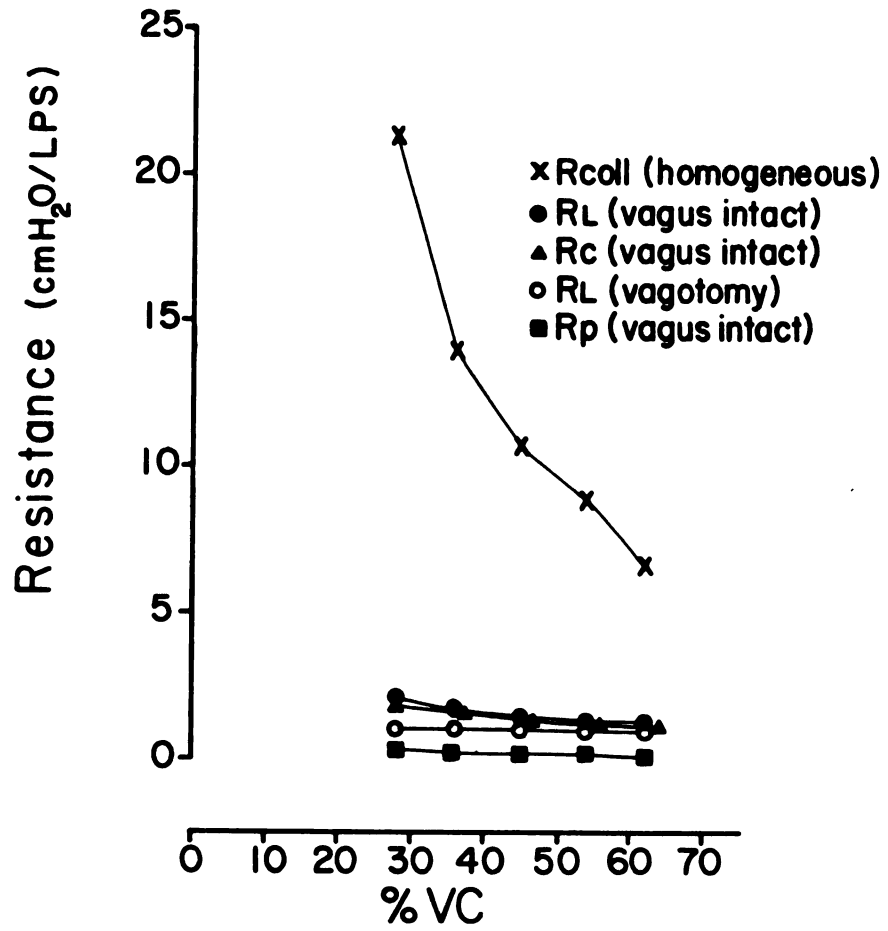


Figure 3-8

LIST OF REFERENCES

Chapter III

1. Frank, N. R. A comparison of static volume-pressure relations of excised pulmonary lobes of dogs. J. Appl. Physiol. 18: 274-278, 1963.
2. Fuller, S. D. and N. E. Robinson. The effect of regional inhomogeneity on collateral airway resistance. (Accepted, J. Appl. Physiol.: Respirat. Environ. Exercise Physiol.)
3. Hilpert, P. Collaterale ventilation Habilitations-schrift, Ans. der Medizinischen (Ph.D. Thesis). Tubingen, W. Germany: Universitatsklinik, 1970.
4. Hughes, J. M. B., F. G. Hoppin, Jr., and J. Mead. Effect of lung inflation on bronchial length and diameter in excised lungs. J. Appl. Physiol. 32: 25-35, 1972.
5. Macklem, P. T. and J. Mead. Resistance of central and peripheral airways measured by a retrograde catheter. J. Appl. Physiol. 22: 395-401, 1967.
6. Macklem, P. T., A. J. Woolcock, J. C. Hogg, J. A. Nadel, and N. J. Wilson. Partition of pulmonary resistance in the dog. J. Appl. Physiol. 26: 798-805, 1969.
7. Menkes, H., G. Gamsu, R. Schroter, and P. T. Macklem. Interdependence of lung units in isolated dog lungs. J. Appl. Physiol. 32: 675-680, 1972.
8. Moody, L. F. Friction factors for pipe flow. Trans. ASME 66: 671-678, 1944.
9. Olson, D. E., G. A. Dart, and G. F. Filley. Pressure drop and fluid flow regime of air inspired into the human lung. J. Appl. Physiol. 28: 482-494, 1970.
10. Sasaki, H. T. Takishima, and M. Nakamura. Collateral resistance at alveolar level in excised dog lungs. J. Appl. Physiol.: Respirat. Environ. Exercise Physiol. 48: 982-990, 1980.

11. Steel, R. G. D. and J. H. Torrie. Principles and Procedures of Statistics. New York: McGraw-Hill, 1960, pp. 110-111.
12. Sylvester, J. T., H. A. Menkes, and F. Stitik. Lung volume and interdependence in the pig. *J. Appl. Physiol.* 38: 395-401, 1975.

CHAPTER IV

PATHWAYS CONNECTING OBSTRUCTED AND NONOBSTRUCTED SUBLOBAR REGIONS IN THE DOG LUNG

Introduction

Inhomogeneous inflation of a sublobar lung segment within a lobe likely creates an interface of tissue distortion between the segment and the lobe. Airways penetrating the interface may also be distorted and contribute to the increased collateral airway resistance (R_{coll}) measured during inhomogeneity (3). Little is known about the arrangement of airways at the interface, however, and how this arrangement not only influences measurements of R_{coll} but also determines the flow route followed by gas leaving an obstructed segment.

A common diagram of the lung suggests that gas leaving an obstructed segment flows through collateral airways and is distributed diffusely throughout the remainder of the lobe (6). An unpublished but common observation does not support this model, however. I have observed that when gas containing no O_2 (e.g., sulfurhexafluoride, SF_6) flows into a catheter wedged in a subsegmental bronchus of an excised lung lobe, the obstructed segment's pleural surface, previously pink in color, turns blue while the lobar surface remains pink; substitution of 100 percent O_2 for SF_6 turns the segment the same homogeneous pink

color as in the lobe. Although this color change is likely do to desaturation and then oxygenation of hemoglobin in segmental capillary blood, this observation suggests that most of the gas leaving an obstructed segment does not enter the remaining lobe, requiring a quite different arrangement of collateral airways than in the model of Menkes and Traystman (6). Do collateral airways provide several different routes for collateral flow, or are there several types of airways in the interface which provide alternate routes for collateral flow? The purpose of this study is to define the arrangement of airways in the segment-lobar interface and the resulting flow route followed by gas exiting an obstructed sublobar lung segment.

Methods

Freshly excised left caudal lobes were obtained from mixed-breed dogs. The anatomy of the airways in the segment-lobar interface was examined in two series of experiments by making corrosion casts of individual (series one) and several adjacent (series two) sublobar segments. In a third series of studies, I measured the distribution of gas flowing out of an obstructed segment to estimate if gas follows the same flow route suggested by analysis of the resin casts.

Series One

Corrosion casts were made of individual subsegmental and bronchopulmonary segments. In five lobes a catheter with a flared tip (5 mm o.d.) was wedged in a subsegmental bronchus to isolate a subsegmental segment, and in five additional lobes a catheter was

ligated in a segmental bronchus to isolate a bronchopulmonary segment. The lobes were filled with water to reduce the occurrence of gas bubbles in the casts, following which they were laid horizontally in a water bath to minimize airway distortion.

Segment casts were prepared by slowly injecting Batson's solution (Polysciences, Warrington, Pennsylvania) into the segment catheters. After the compound hardened (approximately one hour), lung tissue was corroded away by submerging the specimens in concentrated potassium hydroxide for four to five days.

Series Two

Corrosion casts were made of adjacent subsegmental and adjacent bronchopulmonary segments. Catheters were wedged in three to four adjacent subsegmental segments in five lobes and ligated in three to four adjacent bronchopulmonary segments in an additional five lobes. All the injections occurred as the lobe lay horizontally in a water bath. Batson's solution was slowly injected simultaneously into the catheters wedged in each segment, and each segment contained a different color. The injection was discontinued when solution of mixed colors rapidly poured out of the lobar bronchus. Vinylite solution (Wards Natural Science Establishment, Rochester, New York) was similarly injected into the catheters ligated in bronchopulmonary segments. Following injection, the resins hardened, lung tissue was corroded away, and the parenchymal interface separating adjacent segments was dissected with the aid of a binocular dissecting microscope. Casts of acini were photographed by scanning photomacrography (2).

In pilot experiments, I noted that the interface separating adjacent subsegmental segments not only contained parenchymal tissue from each segment, but also contained large airways coursing between the segments. In contrast, the interface separating adjacent bronchopulmonary segments contained only parenchyma and did not contain large airways. I also found I could best demonstrate large airways using Batson's solution and parenchymal structures using Vinylite solution. Therefore, I used Batson's solution to inject adjacent subsegmental segments and Vinylite solution to inject adjacent bronchopulmonary segments.

Series Three: Distribution of Gas Leaving an Obstructed Segment

To estimate if gas follows a similar flow route suggested by the resin casts, I measured the distribution of gas exiting an obstructed segment. Excised left caudal lobes were obtained from 6 mixed breed dogs. Catheters (3.17 mm i.d.) were secured in the following segmental bronchi: superior, posterior, lateral, and the common bronchus supplying the medial and anterior segmental bronchi. These catheters completely obstructed the entire lobe, such that any gas entering or leaving the lobe did so through one or more of the four catheters. All catheters were of equal length and diameter. The lobe was suspended by the lobar bronchus in an airtight box, and the four catheters were attached to ports leading to the outside, each of which in turn were connected to port #1 of a 3-way connector (see Figure 4-1). Port #3 of the 3-way connector supplying one of the

Figure 4-1. Schematic diagram of excised left caudal lobe suspended by lobar bronchus (not shown) in an airtight box. Flared tip catheters were secured in segmental bronchi supplying the following bronchopulmonary segments: superior (S), posterior (P), lateral (L), and medial-anterior (M/A). The proximal ends of the four catheters were attached to ports leading to outside the box, and each port was attached to a 3-way connector. Three of the connectors were attached to gas collection bags, and the fourth connector was attached to a compressed air source and flowmeter. The lobe was inflated via a rheostat-controlled vacuum cleaner attached to a sixth port in the box. Transpulmonary pressure (Ptp; cm H₂O) was measured with a differential pressure transducer whose negative end measured box pressure and whose positive end was open to atmosphere.

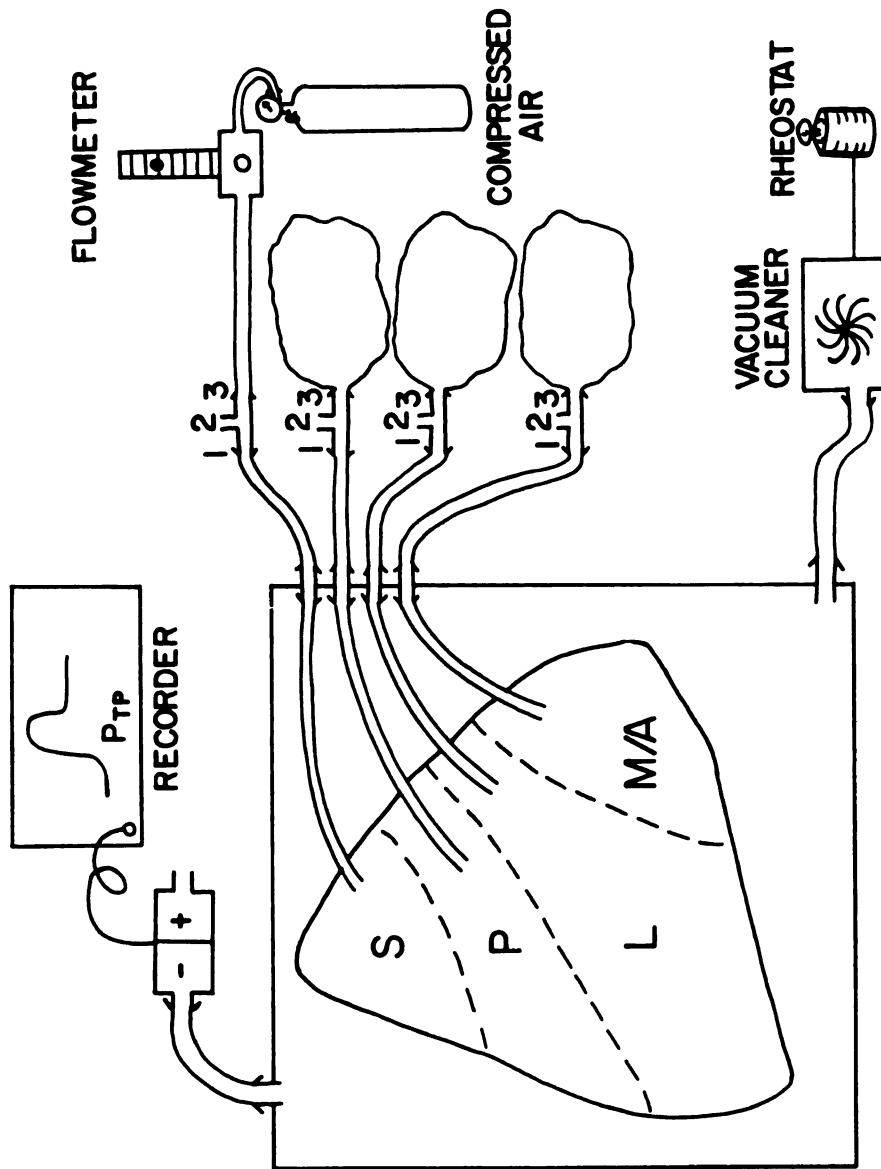


Figure 4-1

segments (henceforth called the "inflow segment") was attached to a compressed air source via a flowmeter, and port #3 of the connectors supplying the three remaining segments (henceforth called the "outflow segments") was attached to a 3.0 liter plastic bag for collection of air. The box was also attached to a vacuum cleaner and rheostat which allowed controlled reduction in box pressure for lobar inflation. Transpulmonary pressure (Ptp) was measured with a differential pressure transducer (PM131, Statham, Hato Rey, Puerto Rico) whose negative side measured box pressure and whose positive side was open to atmosphere. The pressure tracing was displayed on a photorecording oscilloscope (Electronics for Medicine, Model DR8, White Plains, New York).

Port #3 of all 3-way connectors was closed while port #2 remained open to atmosphere. The lobe was then slowly inflated to total lobe capacity (Ptp = 30 cm H₂O) and deflated to Ptp = 0 cm H₂O twice to remove atelectasis and provide a constant volume history. The lobe was fully inflated a third time and deflated to Ptp = 0 cm H₂O. This pressure was held constant while timed collections of gas were obtained. Port #2 of all 3-way connectors was closed, and port #3 was opened. Compressed air was delivered at a constant rate into the inflow segment. Air flowed out of the inflow segment and into the outflow segments to enter the collection bags. Flow was stopped after one minute, and the air volume in each collection bag was measured using a wedge spirometer (Med-Science Electronics, Inc., Model 570, St. Louis, Missouri) attached to an amplifier calibrated for volume at ambient temperature. These timed collections were performed using

inflow rates of one and two liters per minute and at Ptp of 0 and 5 cm H₂O to determine if inflow rate and Ptp influenced the distribution of outflow. Between each timed collection the lobe was reinflated to repeat the volume history as described above. This entire protocol was repeated four times, each time using a different segment for inflow while outflow was collected from the 3 remaining segments. The effect of inflow segment, inflow rate, and Ptp on the distribution of outflow was analyzed using a 3 x 2 x 2 factorial design analysis of variance (9). Differences between means of simple effects were tested with the Student-Newman-Keul's procedure and were considered significant at $p < .05$.

Results

Series One

Figure 4-2A illustrates the cast resulting when Batson's solution was injected into an individual bronchopulmonary segment. Note that the parenchymal surface is overlaid by a large airway branching into several generations, each sending smaller branches into the segment. Casts of individual subsegmental segments were similar in appearance (Figure 4-2B). When segments were located in the center region of the lobe rather than near a pleural surface, the segments were bounded by two parenchymal surfaces, each of which was overlaid by large airways with branches going into the segment.

Figure 4-2. Corrosion cast of individual bronchopulmonary segment (Figure 4-2A; red) and subsegmental segment (Figure 4-2B; white). Arrows point to large airways which overlay the segments' parenchymal surfaces and which send branches into the segments.



Figure 4-2B

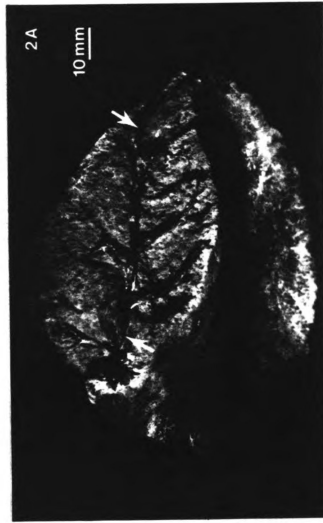


Figure 4-2A

Series Two

Figure 4-3A shows the cast obtained when three adjacent subsegmental segments were simultaneously injected with Batson's solution. Note the distinct separation of colors at the parenchymal interface between adjacent segments. Figure 4-3B illustrates the same specimen partially dissected to expose the airways in the interface region. Note that the large red airway coursing in the red-blue interface provides branches to both red and blue segments. This large airway originates from the bronchus supplying the blue segment. Within any interface there were several such airways which followed a similar branching pattern.

Figure 4-4A demonstrates the cast resulting when three adjacent bronchopulmonary segments were simultaneously injected with Vinylite. Note the distinct separation of colored resins at the interface. The interface was dissected, and a section of the interface was removed for further study. Red and blue nonrespiratory bronchioles, being branches of their respective segmental airways, supplied the acini of the interface section. Removal of the overlaying alveoli revealed many small airways passing between these adjacent bronchopulmonary segments. The airway walls has smooth outpouchings which were probably casts of alveoli, indicating the airways were respiratory bronchioles or alveolar ducts. Since the distinction of the latter is dependent on whether the airway walls are partially alveolated (i.e., respiratory bronchioles) or fully alveolated (i.e., alveolar ducts), and because potential filling defects in the casts usually make such

Figure 4-3A. Corrosion cast of three adjacent subsegmental segments. Arrows point to the well-defined interface separating the segments. The interface separating the red and blue segments was partially dissected to expose the underlying airways (Figure 4-3B).

Figure 4-3B. The large arrow points to a large airway, which I term an "interface" airway, coursing within and parallel to the red-blue interface and which provides branches (indicated by the small arrows) into both red and blue segments. There were several interface airways, following a similar branching pattern, within this interface.

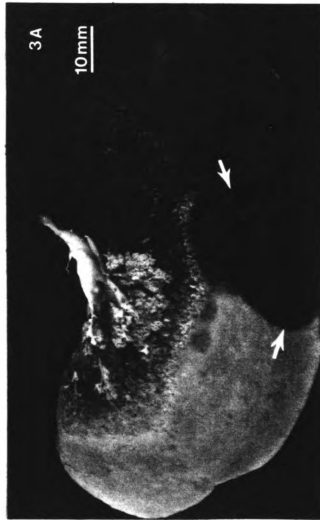
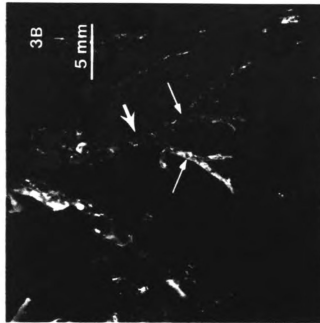
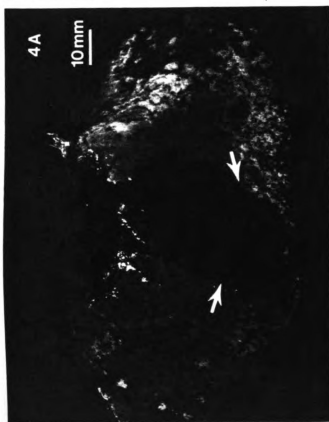
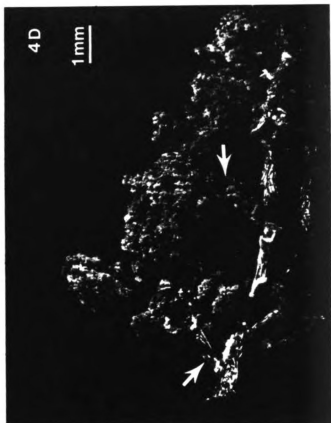
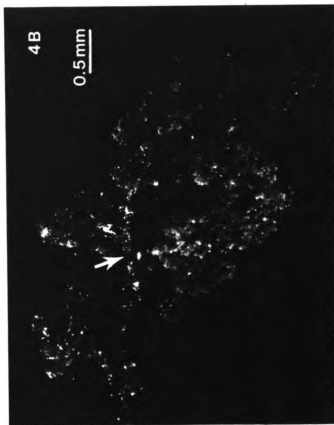


Figure 4-3B

Figure 4-3A

- Figure 4-4A. Corrosion cast of three adjacent bronchopulmonary segments. Arrows point to well-defined interface separating the segments. One interface was dissected to reveal the underlying airways (Figure 4-4B).
- Figure 4-4B. At the extreme left a blue nonrespiratory bronchiole branches into a blue respiratory bronchiole which further divides into red (arrow) and blue respiratory bronchioles. The airways and alveoli supplied by the red respiratory bronchiole interdigitate with similar structures supplied by the blue bronchiole.
- Figure 4-4C. A portion of the interface from another corrosion cast. A red non-respiratory bronchiole from a red segment provides respiratory bronchiole branches (arrows) which course into the neighboring blue segment to interdigitate with blue airways and alveoli.
- Figure 4-4D. A different view of the same specimen from Figure 4-4C. In the lower left, a respiratory bronchiole (arrow) crosses the interface to enter the blue segment and terminate as blue alveoli. In the center of the figure, two additional red respiratory bronchioles (arrow) cross the interface to interdigitate with blue alveoli.



a distinction impossible, I will refer to airways whose walls contain casts of alveoli as respiratory bronchioles. Figure 4-4B shows a blue nonrespiratory bronchiole branching into blue and red respiratory bronchioles. The airways and alveoli supplied by the red respiratory bronchiole (arrow) interdigitate with similar structures supplied by the blue respiratory bronchiole.

Figure 4-4C, taken from another specimen, demonstrates a red nonrespiratory bronchiole in the interface region branching into respiratory bronchioles (arrows) which course into the neighboring blue segment to interdigitate with blue airways and alveoli. Figure 4-4D is a different view of the same specimen. In the lower left, a red respiratory bronchiole (arrow) crosses the interface to enter the blue segment and terminate as blue alveoli. In the center of the figure, two additional red respiratory bronchioles (arrow) cross the interface to interdigitate with blue alveoli.

Series Three: Distribution of Gas Leaving an Obstructed Segment

Figure 4-5 indicates the distribution of gas flow in excised left caudal lobes as a function of inflow segment, inflow rate, and transpulmonary pressure. The segments are listed in the same order as they are arranged in the lobe (see Figure 4-1). In all cases, the majority of outflow from any segment was collected from the adjacent bronchopulmonary segments while only a modest volume was collected from more distant segments. When the inflow segment was either the superior or medial/anterior segment, raising Ptp distributed outflow

Figure 4-5. Distribution of outflow of gas leaving an obstructed bronchopulmonary segment (as a percent of total inflow volume, \bar{x} with SEM bars) as a function of inflow segment (underlined), inflow rate (low = 1 liter/minute, high = 2 liters/minute), and transpulmonary pressure (Ptp; cm H₂O) in six excised left caudal lobes. Inflow segment received 100 percent of total inflow volume. Segments listed in same order as they are arranged in the lobe (see Figure 4-1). Low flow = 1.0 LPM, high flow = 2.0 LPM. Stars indicate statistically significant differences ($p < .05$) between adjacent Ptp.

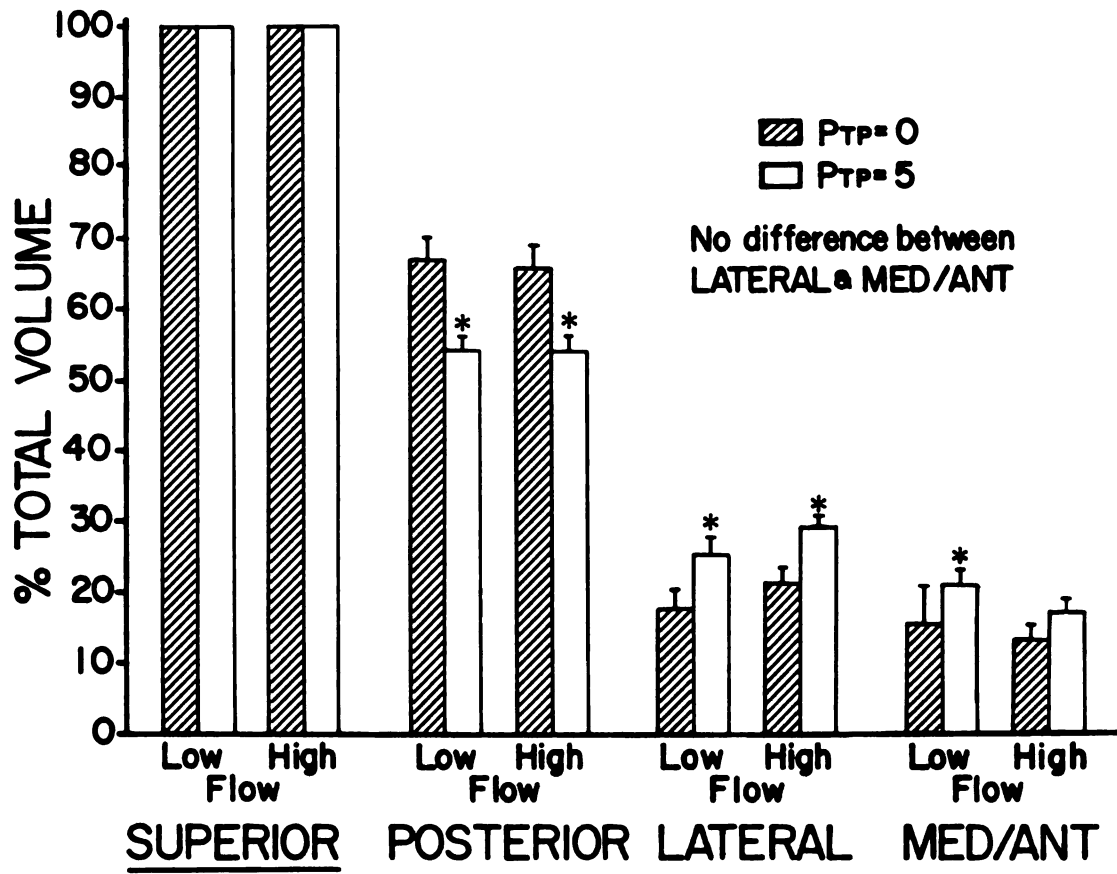


Figure 4-5

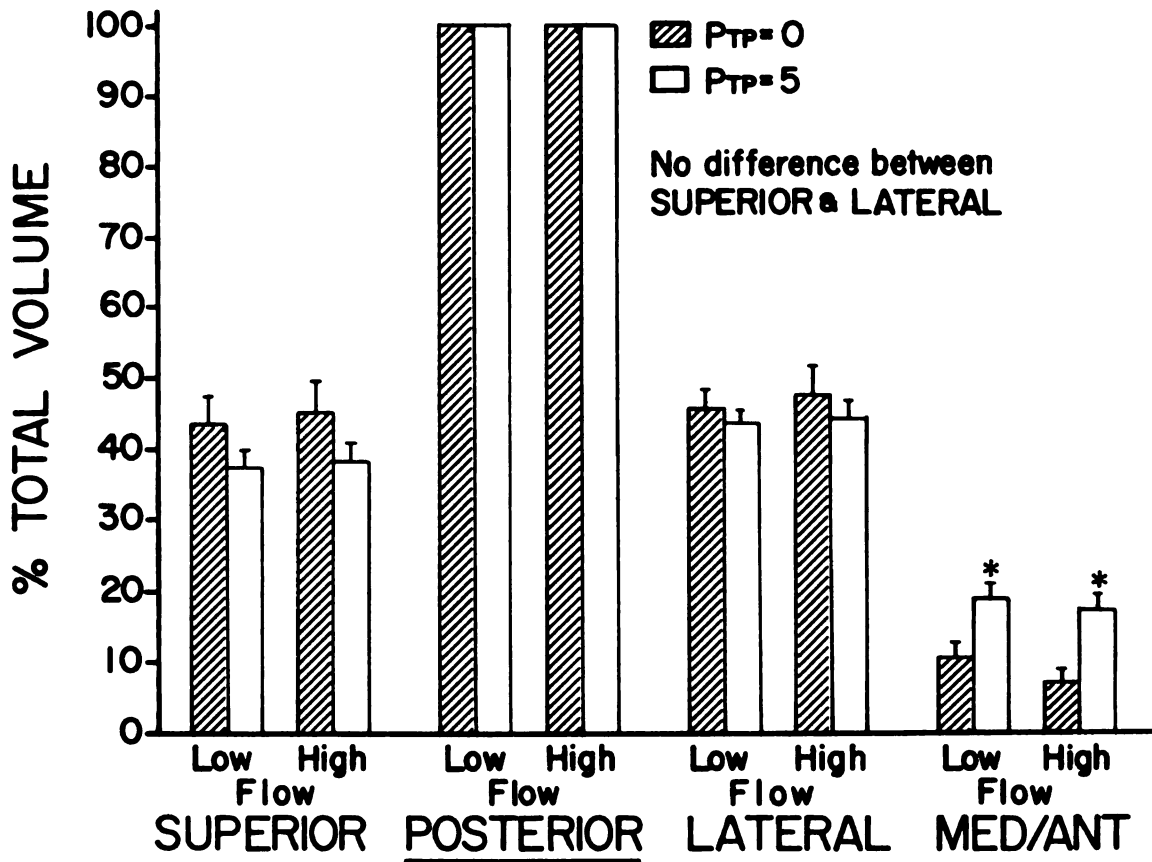


Figure 4-5

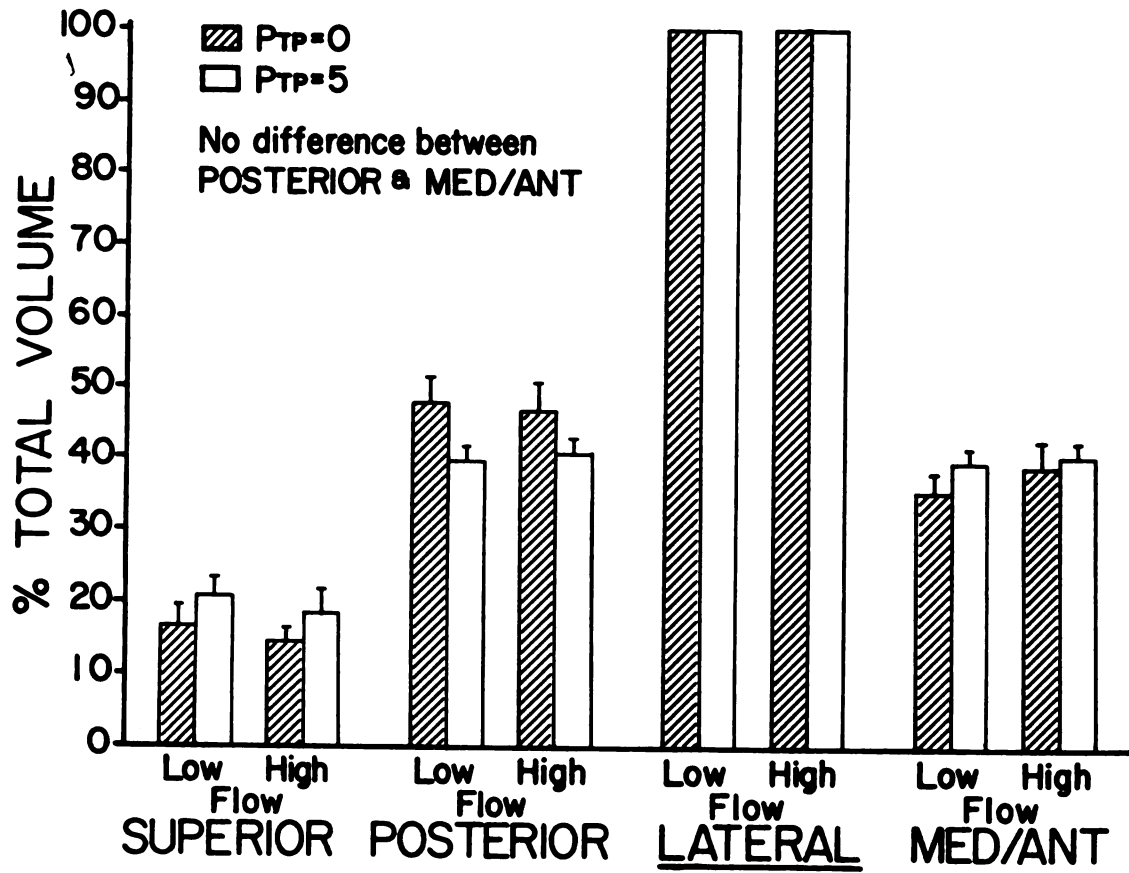


Figure 4-5

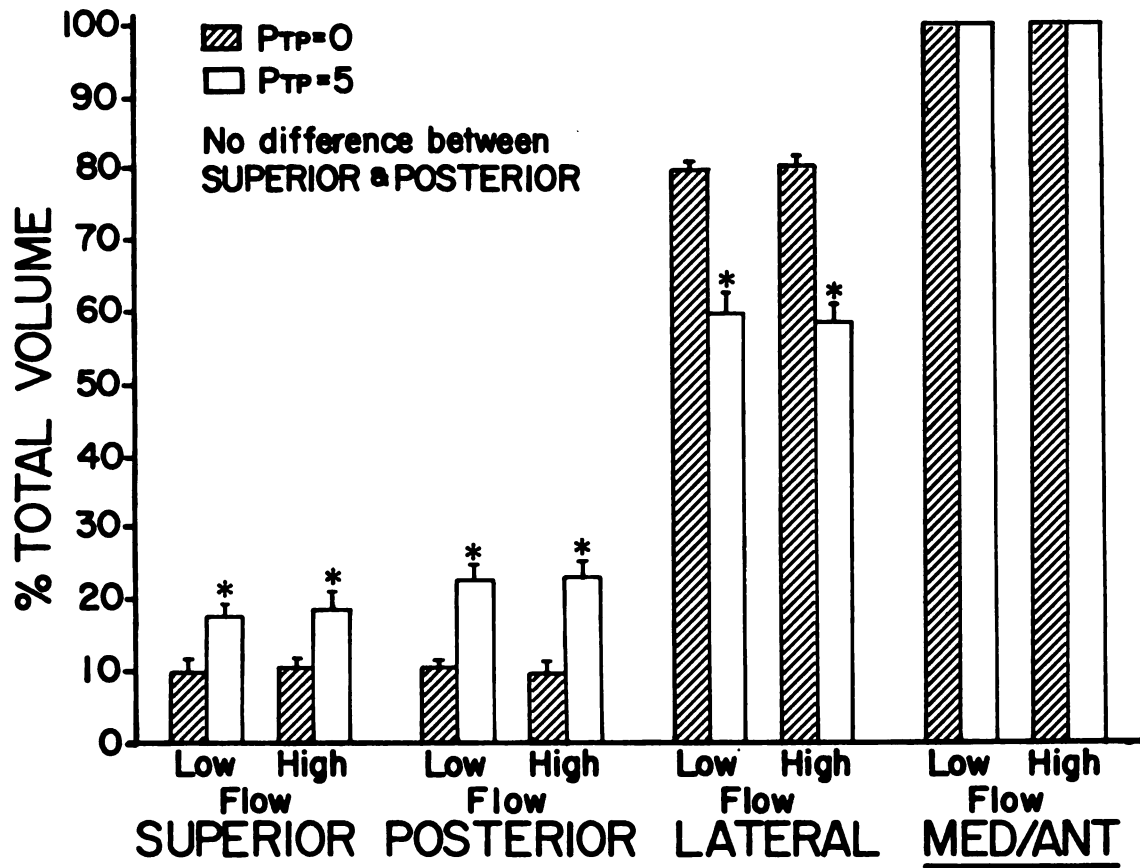


Figure 4-5

more uniformly to the outflow segments; at the higher Ptp, less volume was collected from the outflow segment nearest the inflow segment while more volume was collected from the more distant outflow segments. There was no effect of inflow rate on the distribution of outflow.

Further correlation of the similarity of the routes followed by gas and resin was obtained. A catheter was wedged in a subsegmental bronchus of several caudal lobes of excised dog lungs. The isolated segments were inflated with air, and their pleural borders were outlined with a marking pen. Resin was then injected into the wedged catheters as the lobe floated horizontally in a water bath, and the segments distended up to, but not beyond, the pleural borders outlined when the segments were gas filled. The resulting casts contained large airways overlaying the parenchymal surfaces which I believe likely served as exit routes for both gas and resin.

Discussion

This study was undertaken to define the arrangement of airways in the segment-lobar interface and the route followed by gas leaving an obstructed segment in the dog lung. Corrosion casts of single and adjacent segments demonstrate three possible routes. The first route is via the bronchus which overlays an individual segment's parenchymal surface and which sends branches into the segment (Figures 4-2 and 4-3). I call this bronchus an "interface airway" because it is found in the segment-lobar parenchymal interface. I propose the model in Figure 4-6 which demonstrates a possible course of resin flow through the individual segment and interface airway. Resin from the wedged catheter

- Figure 4-6. Model illustrating possible course of resin or gas flow through an obstructed segment and interface airway.
- A.** Resin enters the segment through a catheter wedged in a subsegmental bronchus and initially fills all the airways and alveoli originating from the bronchus (shaded area).
- B.** Resin continues to flow through collateral channels and into parenchymal tissue supplied by adjacent bronchi. This expands the segment's borders beyond their anatomic limits, and the expansion ceases when the nearest large airway (i.e., interface airway) is reached (shaded area). The resin enters the interface airway and flows retrograde to directly leave the lobe rather than flow across the interface through smaller, higher resistance branches to enter the lobe.

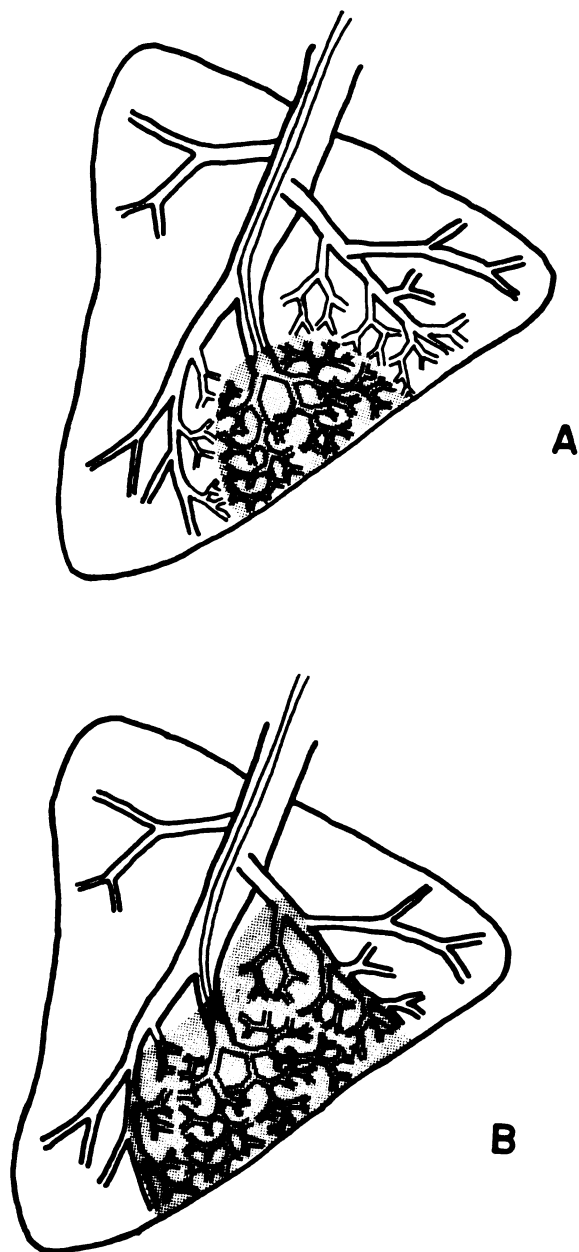


Figure 4-6

initially fills all the airways and alveoli originating from the bronchus containing the wedged catheter (shaded area, Figure 4-6A). Resin continues to flow through collateral channels and into parenchymal tissue supplied by adjacent bronchi. This expands the segment's borders beyond their anatomic limits, and the expansion ceases when the nearest large airway (i.e., interface airway) is reached (shaded area, Figure 4-6B). The resin enters this interface airway and flows retrograde to directly leave the lobe rather than flow across the interface airway through smaller, higher resistance branches to enter the lobe; these smaller branches form the second potential flow route. This model explains why after the segment filled, resin rapidly poured out of the lobar bronchus while the remaining lobe received no resin. In casts of individual subsegmental segments, the interface airway is either a branch of the bronchus containing the wedged catheter or a branch of a neighboring bronchus. In casts of individual bronchopulmonary segments, the interface airway is always a branch of a neighboring segmental bronchus. The size of the segment formed with a wedged catheter is therefore not determined by the anatomic limits of the segment but by the location of the nearest interface airway.

The third possible route followed by gas leaving an obstructed segment is likely between segment and lobar acini which interdigitate with one another at the interface. These interdigitating acini were clearly observed in the interface of Vinylite casts of adjacent bronchopulmonary segments (Figure 4-4). Examination of the interface reveals that at certain discrete points along the interface, respiratory

bronchioles from one segment penetrate the interface, enter the adjacent segment, and divide into alveoli and alveolar ducts [a pattern also described in the human lung (4, 7)]. These alveolar ducts may be connected to one another via collateral channels which I define as channels connecting acini originating from two separate airways. Potential collateral pathways in the dog lung are the interalveolar pore and interacinar duct (1, 4, 8). I failed to demonstrate the connections between interdigitating acini because casts of small groups of acini were too fragile for dissection.

It is possible that, similar to resin flow, most of the gas flowing out of an obstructed segment follows the large interface airway to directly exit the lobe rather than flowing through collateral channels to enter the lobe. This is suggested by the data in Figure 4-5 which illustrates that most of the gas exiting an obstructed bronchopulmonary segment was collected from the adjacent segments and that little gas was collected from the more distant segments. Furthermore, when a segment is inflated, a well defined boundary between the segment and the lobe is seen on the lobar pleural surface, and examination of the interface shows that the segment's boundaries expand up to, but not beyond, the nearest interface airway. If collateral channels were the major flow route, one would not expect the segment to expand beyond its anatomic limits (which it must do to reach the interface airway), and it would be a surprising coincidence for the interface airways to always be found directly beneath the segment's pleural boundary.

I recently reported that inhomogeneous inflation of a subsegmental segment with air increases R_{coll} (3), and I proposed that distortion of airways at the segment-lobe interface may contribute to this effect. The model in Figure 4-6 supports this concept of airway distortion. Such distortion may occur because the interface airway, being partially contained in the remaining lobe, would be held fixed as its branches move freely during segment inflation. Gas exiting the segment through the interface airway branches and interface airway would encounter a tortuous pathway with increased resistance, thus contributing to the increased R_{coll} . Also, a scanning electron micrograph (Figure 1-2) show parenchymal tissue distortion, probably resulting from the inflated segment bulging into the lobe while at the same time the interface is lengthened due to segment expansion. This would cause severe distortion of collateral channels and increase resistance to flow, contributing to increased R_{coll} .

LIST OF REFERENCES

Chapter IV

1. Boyden, E. A. The structure of the pulmonary acinus in a child of six years and eight months. Am. J. Anat. 132: 275-300, 1971.
2. Dale, D. Scanning photomacrography. Functional Photo. May/June 18-21, 1982.
3. Fuller, S. D. and N. E. Robinson. The effect of regional inhomogeneity on collateral airway resistance. (Accepted, J. Appl. Physiol.: Respirat. Environ. Exercise Physiol., 1984.
4. Henderson, R., K. Horsfield, and G. Cumming. Intersegmental collateral ventilation in the human lung. Resp. Physiol. 6: 128-134, 1968/1969.
5. Lambert, M. Accessory bronchiole-alveolar communications. J. Path. Bact. 70: 311-314, 1955.
6. Menkes, H. and R. J. Traystman. State of the art. Collateral Ventilation. Am. Rev. Resp. Dis. 116: 287-309, 1977.
7. Pumo, K. K. The morphology of the finer branches of the bronchial tree of the human lung. Dis. Chest. 46: 379-398, 1964.
8. Raskin, S. P. and P. G. Herman. Interacinar pathways in the human lungs. Am. Rev. Resp. Dis. 111: 489-495, 1975.
9. Steel, R. G. D. and J. H. Torrie. Principles and Procedures of Statistics. New York: McGraw-Hill, 1960, pp. 194-211.

CHAPTER V

DISCUSSION AND SUMMARY

The findings in Chapter II that segment inflation increases collateral resistance (R_{coll}) while lobar inflation decreases R_{coll} (Figures 2-1, 2-2, 2-3) appear conflicting. I expected R_{coll} to decrease during both modes of inflation because both segment and lobar inflation increase segment volume, and because airway resistance is inversely proportional to lung volume (2). To explain the effect of segment inflation on R_{coll} , I proposed two hypotheses: (1) segment inflation oppositely affects two populations of airways, such that the resistance through intrasegmental airways (R_s) decreases while the resistance through the intersegmental airways (R_i) increases, the net effect being determined by whether R_s or R_i changes more; (2) the high collateral flow rates resulting from segment inflation cause nonlaminar gas flow which increases R_{coll} . These hypotheses were tested in Chapter III where R_{coll} was partitioned into its R_s and R_i components. Segment inflation with air increased R_{coll} , R_s , and R_i and did not cause the opposing changes in R_s and R_i as predicted by the first hypothesis (Figure 3-2). In addition, the increase in R_{coll} , R_s , and R_i during segment inflation with air was accentuated by segment inflation with SF_6 and eliminated by segment inflation with helium, suggesting that nonlaminar flow occurred in the segment.

I concluded, for several reasons, that most of the nonlaminar flow occurred in intrasegmental airways. Firstly, R_s exceeded R_i during segment inflation with SF_6 (where, according to the Moody plots in Figure 3-4, flow was transitional to turbulent), but R_i exceeded R_s during segment inflation with helium (where flow was laminar) (Figure 3-2). Secondly, the fraction of R_{coll} attributable to RS (R_s/R_{coll}) increased as nonlaminar flow increased (by segment inflation with SF_6), but R_s/R_{coll} did not change during laminar flow when the segment was inflated with helium (Table 3-2).

Moody plots were constructed to more specifically characterize the flow regime in the segment. During segment inflation, the highest Reynolds' number (Re) at which laminar flow occurred ranged from 45 (at $P_{ao} = 2$ cm H_2O) to 150 (at $P_{ao} = 6$ cm H_2O) (Figure 3-4), suggesting that nonlaminar flow may occur in an obstructed segment during measurements of R_{coll} at Re far below the value of 2000 required for such flow in straight smooth tubes. In addition, the Moody plots for segment inflation (Figure 3-4) differed from those for lobar inflation (Figure 3-5). During segment inflation, all points in each plot lay on one smooth curve, so that P_n was solely a function of Re . Since an assumption of the Moody analysis is that airway dimensions are fixed as P_n and Re are varied, this finding indicates either that the dimensions of the segmental airways did not change during segment inflation, or that R_{coll} may be determined primarily by one or more populations of high resistance airways whose dimensions are fixed and secondarily by one or more populations of low resistance airways whose dimensions

may vary during segment inflation. In contrast, lobar inflation to five different transpulmonary pressures (P_{ao}) resulted in five separate curves, indicating that P_n was a function of Re plus one or more other variables. One of these variables is likely airway dimension since segment airways probably dilate during lobar inflation (references 5, 6, 7, and 12, Chapter 13). If this change in airway dimension could be compensated for in the Moody plots, the five separate curves in each plot should approximate a single curve. I attempted to compensate for the changes in airway diameter by scaling wedged airway diameter to the cube root for lobar volume and also to transpulmonary pressure as reported by Hughes et al. (1). The resultant compensated curves (Figures 3-6 and 3-7), although somewhat less separated than the noncompensated curves (Figure 3-5), still were not superimposed as in Figure 3-4. I then adjusted the value of segment airway diameter as needed to force the curves to approximate as closely as possible a single curve, and I calculated a power function relating lobar volume to diameter. In each Moody plot, a range of power functions was required to approximate the curves obtained during lobar inflation (Table A-1). Two conclusions may be made from the latter observation: (1) changes in wedged airway diameter may not reflect the dimensional changes in other intra- or intersegmental airways during lobar inflation. For example, if intersegmental airways are distorted by segment inflation, the resultant changes in intersegmental airways diameter would be unaccounted for in my computations. (2) Other variables in addition to airway diameter may contribute to the separation of the curves.

The arrangement of the airways in the segment-lobar interface was examined in Chapter IV. I identified two types of airways in the interface: (1) large airways (termed interface airways) coursing within and parallel to the interface and providing branches to both the segment and the lobe (Figure 4-3B); and (2) small airways (respiratory bronchioles and/or alveolar ducts) from the segment and the lobe interdigitating with one another where segment and lobar parenchyma abut (Figures 4-4B, 4-4C, and 4-4D). I suggested that segment and lobar acini may be connected by collateral pathways at points of interdigitation, but I was unable to demonstrate such pathways in the resin casts. On the basis of these findings, there are three possible flow routes for gas exiting an obstructed segment: (1) through the interface airway to flow directly out of the lobe; (2) through the interface airway and then interface airway branches to enter the lobe; (3) from segment acini to lobar acini at points of interdigitation to enter the remaining lobe. I hypothesized that gas flowed primarily through the interface airway to directly exit the lobe rather than flowing through the higher resistance interface airway branches or respiratory bronchioles to enter the lobe. To test this hypothesis, experiments were performed in which gas flowing into one bronchopulmonary segment was collected from the three remaining bronchopulmonary segments, and the volumes were measured to determine the distribution of gas flow exiting an obstructed segment. The majority of gas flow was distributed to the adjacent segments, and only a small amount was collected from the more distant segments (Figure 4-5), suggesting that the interface airway may have served as the primary flow route.

Distortion of the airways at the interface may be partly responsible for the failure of segment inflation to decrease R_{coll} in the absence of nonlaminar gas flow. Such distortion may occur because the interface airway, being partially contained in the remaining lobe, would be held fixed as its branches move freely during segment inflation. Gas exiting the segment first through the interface airway branches and then through the interface airway (Figure 4-6) would encounter a tortuous pathway which may increase resistance and promote nonlaminar flow. Furthermore, Figure 1-2 indicates there is parenchymal distortion at the interface which likely distorts the interdigitating respiratory bronchioles and collateral channels, causing an increase in their resistance. To relate this distortion to increased flow resistance, studies are required which quantify the geometrical changes undergone by the airways in the interface during segment inflation.

LIST OF REFERENCES

Chapter V

1. Hughes, J. M. B., F. G. Hoppin, Jr., and J. Mead. Effect of lung inflation on bronchial length and diameter in excised lungs. J. Appl. Physiol. 32: 25-35, 1972.
2. Macklem, P. T., A. J. Woolcock, J. C. Hogg, J. A. Nadel, and N. J. Wilson. Partitioning of pulmonary resistance in the dog. J. Appl. Physiol. 26: 798-805, 1969.

CHAPTER VI

CONCLUSIONS

1. Collateral resistance is lower in caudal lobes than in cranial lobes.
2. Collateral resistance is greater in intact than in excised lungs, and the difference is greater in the left cranial lobe than in the right caudal lobe.
3. Collateral resistance is influenced more by transpulmonary pressure than by segment pressure; i.e., collateral resistance is influenced more by the lobe than by the segment.
4. Collateral resistance is increased by segment inflation with air and decreased by lobar inflation.
5. Collateral resistance is increased more when segment-lobar inhomogeneity is created by segment deflation than by segment inflation.
6. The increase in collateral resistance during segment inflation with air is due to nonlaminar gas flow, but the reason why segment inflation fails to decrease collateral resistance is undetermined.
7. The hypothesis that segment inflation affects collateral resistance via directionally opposite changes in intrasegmental and intersegmental airway resistance is not supported.

8. The major site of collateral resistance measured during segment inflation is intersegmental airways when collateral flow is laminar and intrasegmental airways when flow is turbulent.
9. The critical Reynolds' number for nonlaminar gas flow in a sublobar segment in excised dogs' lungs during segment inflation is 45 at $P_{ao} = 2 \text{ cm H}_2\text{O}$ and 150 at $P_{ao} = 6 \text{ cm H}_2\text{O}$, far below the value of 2000 required for nonlaminar flow in straight smooth tubes.
10. Moody plots for segment inflation form a single smooth curve at each P_{ao} , indicating that P_n is solely a function of Re . This suggests that:
 - a. segment airways do not change dimension during segment inflation, or
 - b. collateral resistance may be determined primarily by one or more populations of high resistance airways whose resistance is fixed during segment inflation and secondarily by one or more populations of low resistance airways whose dimensions may vary during segment inflation.
11. Moody plots for lobar inflation form separate curves at each $P_{ct}-P_{ao}$, indicating that P_n is a function of Re plus one or more other variables. One of these variables is probably airway dimension.
12. During lobar inflation at a constant positive $P_{ct}-P_{ao}$ in excised dogs' lungs, segment airway diameter is not scaled to the cube root of lobar volume or to transpulmonary pressure.

13. Collateral resistance in excised dogs' lungs measured during homogeneous conditions (i.e., $P_{ct}-P_{ao} = 0$ cm H₂O) is substantially higher than total lung resistance, central airway resistance, or peripheral airway resistance in intact lungs and decreases to a greater extent than these other resistances as the lung is inflated.
14. When a segment is inflated by flowing gas into the segment through a wedged catheter, the segment expands beyond its anatomic limits until it reaches the nearest large airway (termed an interface airway).
15. There are three possible flow routes through which gas may exit an inflated segment:
 - a. through the interface airway to directly leave the lobe.
 - b. through the interface airway and then through interface airway branches to enter the lobe.
 - c. from segment acini to lobar acini through connections (likely collateral channels) at points of interdigitation.
16. Most of the gas exiting an obstructed bronchopulmonary segment can be collected from the adjacent bronchopulmonary segment(s), but only a small portion of the gas reaches the more distant segments.
17. Gas exiting an obstructed sublobar lung segment is distributed more uniformly throughout the lobe at higher transpulmonary pressures.

APPENDICES

APPENDIX A

MEAN (\pm SEM) VALUES OF COLLATERAL RESISTANCE
FOR CHAPTER II DATA

APPENDIX A

MEAN (\pm SEM) VALUES OF COLLATERAL RESISTANCE
FOR CHAPTER II DATA

Table A-1. Data points used in Figures 2-1, 2-2, and 2-3 in Chapter II showing collateral resistance [R_{coll} ; cm H₂O/(ml/sec); $\bar{x} \pm$ SEM] in left cranial and right caudal lobes in series one (excised lungs with the segment inflated relative to the lobe), series two (lungs of closed chest anesthetized dogs), and series three (excised lungs with the segment deflated relative to the lobe).

Pao (cm H ₂ O)	Series One							
	Pct-Pao (cm H ₂ O)							
	1	2	3	4	5	6	7	8
	<u>Left Cranial Lobe</u>							
2				.403 $\pm .114$.422 $\pm .114$.423 $\pm .108$.438 $\pm .120$.440 $\pm .120$
3			.336 $\pm .096$.343 $\pm .096$.350 $\pm .102$.372 $\pm .108$.386 $\pm .114$	
4		.268 $\pm .078$.292 $\pm .084$.312 $\pm .090$.330 $\pm .096$.342 $\pm .102$		
5	.209 $\pm .060$.235 $\pm .066$.262 $\pm .078$.289 $\pm .084$.304 $\pm .096$			
	<u>Right Caudal Lobe</u>							
2				.366 $\pm .090$.378 $\pm .090$.385 $\pm .090$.392 $\pm .084$.377 $\pm .084$
3			.281 $\pm .084$.296 $\pm .078$.309 $\pm .078$.299 $\pm .078$.322 $\pm .084$	
4		.226 $\pm .072$.242 $\pm .066$.259 $\pm .072$.263 $\pm .072$.270 $\pm .078$		
5	.175 $\pm .066$.193 $\pm .066$.212 $\pm .072$.238 $\pm .072$.247 $\pm .072$			

Table A-1--Continued

Series Two							
Pct-Pao (cm H ₂ O)							
Pao (cm H ₂ O)	1	2	3	4	5	6	7
<u>Left Cranial Lobe</u>							
5				.815 ±.174	.812 ±.174	.848 ±.186	.773 ±.150
6			.581 ±.114	.617 ±.126	.631 ±.132	.632 ±.126	
7		.422 ±.108	.449 ±.114	.468 ±.120	.488 ±.132		
8	.349 ±.090	.406 ±.108	.418 ±.102	.484 ±.108			
<u>Right Caudal Lobe</u>							
5				.371 ±.186	.364 ±.174	.416 ±.156	.333 ±.132
6			.247 ±.072	.286 ±.084	.296 ±.084	.296 ±.084	
7		.189 ±.054	.209 ±.048	.230 ±.054	.242 ±.060		
8	.140 ±.036	.160 ±.036	.185 ±.042	.211 ±.060			

Table A-1--Continued

Series Three					
Pct-Pao (cm H ₂ O)					
Pao (cm H ₂ O)	1	2	3	4	5
<u>Left Cranial Lobe</u>					
4	.250 ±.108	.435 ±.210	.581 ±.270		
5		.299 ±.120	.437 ±.186	.507 ±.222	
6			.350 ±.138	.430 ±.174	.521 ±.210
<u>Right Caudal Lobe</u>					
4	.500 ±.300	.662 ±.354	.845 ±.426		
5		.409 ±.162	.535 ±.204	.633 ±.246	
6			.372 ±.156	.412 ±.168	.484 ±.204

Collateral resistance ($\bar{x} \pm \text{SEM}$) from series one, two, and three experiments.

Pct = segment pressure (cm H₂O).

Pao = transpulmonary pressure (cm H₂O) in excised dogs' lungs (series one and three).

Ptp = transpulmonary pressure (cm H₂O) in lungs of closed chest anesthetized dogs (series two).

Pct-Pao = segment-lobar pressure difference (cm H₂O) in series one and two.

Pao-Pct = segment-lobar pressure difference (cm H₂O) in series three.

APPENDIX B

RELATIONSHIP OF SEGMENT AIRWAY DIAMETER TO LOBAR VOLUME
DURING LOBAR INFLATION FOR CHAPTER III DATA

APPENDIX B

RELATIONSHIP OF SEGMENT AIRWAY DIAMETER TO LOBAR VOLUME DURING LOBAR INFLATION FOR CHAPTER III DATA

If the separation of the curves shown in Figure 3-5 is due solely to the changes in segment airway diameter occurring during lobar inflation, then compensation for these diameter changes should lead to a singular relationship between P_n and Re . Although diameter is reported to be related to the cube root of lobar volume or to transpulmonary pressure during homogeneous lobar inflation (reference 4, Chapter III), data in Figures 3-6 and 3-7 indicate that such a relationship may not occur during lobar inflation (raising P_{ao} at a constant positive $P_{ct}-P_{ao}$). I determined if a single power function would relate lobar volume to segment airway diameter during lobar inflation, making P_n a single function of Re and indicating that the spread of the curves shown in Figure 3-5 was due to unaccounted for changes in segment airway diameter. In contrast, if multiple power functions are required to approximate these curves, then one or more variables other than segment airway diameter would be controlling influences on the relationship between P_n and Re .

In calculations required to produce Figures B-1 and B-2, I adjusted the value of segment airway diameter in such a way as to force the curves in Figure 3-5 to approximate a single curve. In Figure B-1, in the plot for $P_{ct}-P_{ao} = 1$, I adjusted the diameter to cause the $P_{ao} = 2-5$ curves to empirically approximate the $P_{ao} = 6$ curve. I

then used the diameters obtained to construct the Moody plots in Figure B-1. These plots indicate that the diameters used to approximate the curves for the Pct-Pao = 1 plot clearly do not apply to the Pct-Pao = 2-7 plots, as evidenced by the progressive spreading of the curves as Pct-Pao increases. In addition, Table B-1 shows that multiple power functions may be required to relate segment airway diameter to lobar volume.

In Figure B-2, I adjusted the value of segment airway diameter as described above to empirically approximate the curves for Pct-Pao = 7 from Figure 3-5. These diameters were used to construct the plots in Figure B-2. The data indicate that the diameters used to approximate the curves for the Pct-Pao = 7 plot do not apply to the Pct-Pao = 1.6 plots. Also, Table B-1 shows that multiple power functions may be required to relate segment airway diameter to lobar volume. These results indicate that during lobar inflation, P_n is a function of Re , airway diameter, and probably one or more other variables.

Figure B-1. Attempt to forcibly approximate the curves in each panel of Figure 3-5 into a single smooth curve. The logarithm of the normalized pressure drop (Log Pn; ordinate) is shown as a function of the logarithm of Reynolds' number (Log Re; abscissa). Each of the seven panels shows the relationship when segment inflation (Pct-Pao; cm H₂O) was held constant while transpulmonary pressure (Pao) increased from 2-6 cm H₂O. Lines connecting the points represent constant Pao when the segment was inflated with helium (circles), air (triangles), or sulfurhexafluoride (SF₆; squares). In the Pct-Pao = 1 plot in Figure 3-5, the value of segment airway diameter was adjusted to cause the Pao = 2-5 curves to empirically approximate the Pao = 6 curve. These diameters were used to construct all plots in this figure. Dashed line has slope = -1, representing laminar flow.

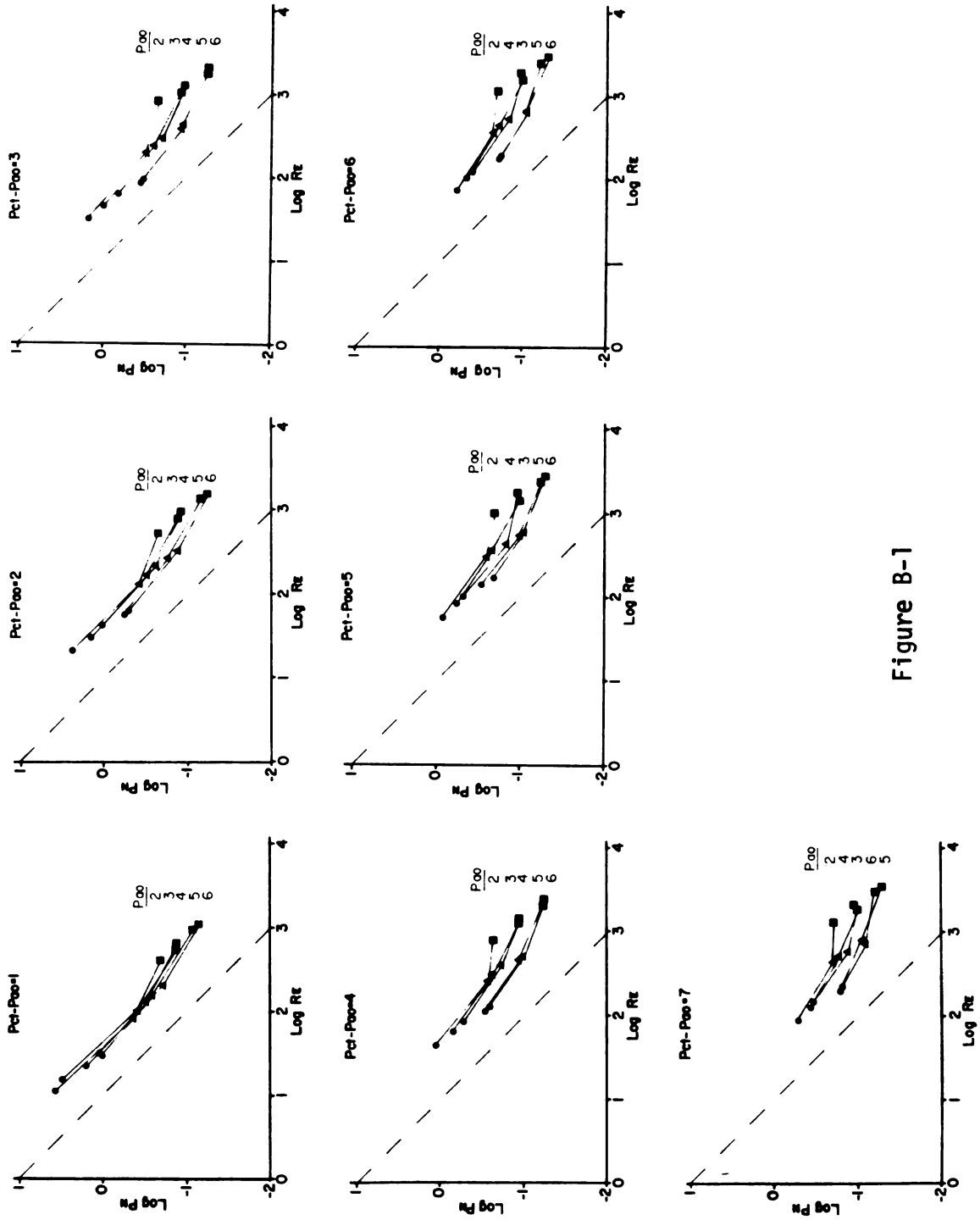


Figure B-1

Figure B-2. Attempt to forcibly approximate the curves in each panel of Figure 3-5 into a single smooth curve. The logarithm of the normalized pressure drop (Log Pn; ordinate) is shown as a function of the logarithm of Reynolds' number (Log Re; abscissa). Each of the seven panels shows the relationship when segment inflation (Pct-Pao; cm H₂O) was held constant while transpulmonary pressure (Pao) increased from 2-6 cm H₂O. Lines connecting the points represent constant Pao when the segment was inflated with helium (circles), air (triangles), or sulfurhexafluoride (SF₆; squares). In the Pct-Pao = 7 plot in Figure 3-5, the value of segment airway diameter was adjusted to cause the Pao = 2-5 curves to approximate the Pao = 6 curve. These diameters were used to construct all plots in the figure. Dashed line has slope = -1, representing laminar flow.

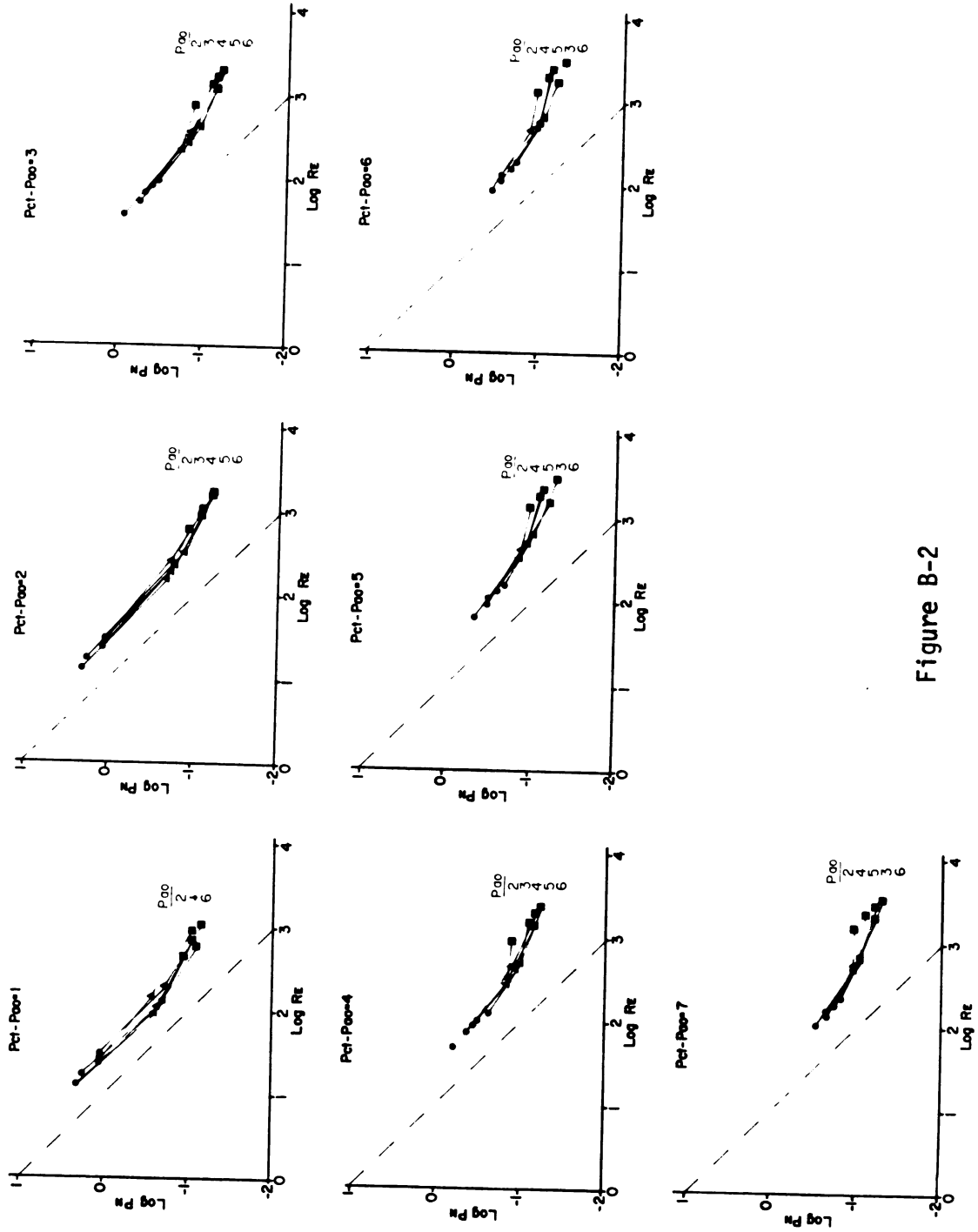


Figure B-2

Table B-1. Relationship of segment airway diameter to lobar volume when the curves in each panel of Figure 3-5 are forced to approximate a single curve.

P_{ao}^a	VL^b	$d(1)^c$	$x(1)^d$	$d(7)^e$	$x(7)^f$
2	28	1.96	0.56	1.70	0.67
3	36	2.22	0.58	1.96	0.71
4	45	2.48	0.60	2.28	0.70
5	54	2.60	0.69	2.68	0.64
6	62	2.78	0.76	2.78	0.76

^a P_{ao} = transpulmonary pressure (cm H₂O).

^b VL = lobar volume (percent vital capacity) obtained from data reported by Frank reference 1, Chapter III).

^c $d(1)$ = segment airway diameter (mm) required to approximate the $P_{ao} = 2-5$ curves in the Pct- $P_{ao} = 1$ panel of Figure 3-5 to the $P_{ao} = 6$ curve.

^d $x(1)$ = power function relating VL to d_1 according to the following example:

$$\frac{d(1) \text{ at } P_{ao} = 2}{d(1) \text{ at } P_{ao} = 6} = \left(\frac{VL \text{ at } P_{ao} = 2}{VL \text{ at } P_{ao} = 6} \right)^{x(1)}$$

^e $d(7)$ = segment airway diameter (mm) required to approximate the $P_{ao} = 2-5$ curves in the Pct- $P_{ao} = 7$ panel of Figure 3-5 to the $P_{ao} = 6$ curve.

^f $x(7)$ = power function relating VL to d_7 according to the following example:

$$\frac{d(7) \text{ at } P_{ao} = 2}{d(7) \text{ at } P_{ao} = 6} = \left(\frac{VL \text{ at } P_{ao} = 2}{VL \text{ at } P_{ao} = 6} \right)^{x(7)}$$